# Dual FGFR-targeting and pH-activable Ruthenium-Peptide Conjugates for targeted therapy of Breast Cancer

João Franco Machado[a,b], Marco Sá[a,Φ], Inês Pires[c,Φ], Miguel Tarita da Silva[b], Fernanda Marques[b,d], Jaime A. S. Coelho[a], Filipa Mendes[b,d], M. Fátima M. Piedade[e,f], Miguel Machuqueiro[c,e], María Angeles Jiménez[g], Maria Helena Garcia[a,e], João D. G. Correia[b,d]*,Tânia S. Morais[a,e]*

# Supporting information

**Table of contents**

Experimental section ..... 2
Materials and Methods ..... 2
Synthesis and characterization ..... 4
Synthesis of bipyridine ligands ..... 4
Synthesis of ruthenium organometallic complexes ..... 7
X-ray crystallography ..... 10
Stability in organic and aqueous medium ..... 12
Octanol-water partition coefficients (logP) ..... 12
Synthesis of peptides ..... 13
Synthesis of new pH-responsive ruthenium-peptide conjugates ..... 15
NMR conformational study ..... 16
*In vitro* Drug release ..... 17
Cytotoxicity Assays ..... 17
Computational methods ..... 18
Results and Discussion ..... 20
NMR conformation ..... 20
Cytotoxicity ..... 25
*In vitro* Drug release ..... 26
Density functional theory ..... 27
MD simulations ..... 31
NMR Spectra ..... 41
FT-IR Spectra ..... 54
UV-vis Spectra ..... 58
Stability of Ru complexes ..... 61
RP-HPLC chromatograms ..... 63
ESI-MS spectra ..... 66
References ..... 71

**Experimental section**

**Materials and Methods**

All chemicals and solvents were of analytical reagent grade and used without further purification unless dichloromethane, THF and *n*-hexane that were purified immediately before use with a MBraun SPS-800 solvent purification system. Starting materials [Ru($\eta^5$-$C_5H_4CO_2CH_2CH_3$)($PPh_3$)(2,2'-bipy)][$CF_3SO_3$] (**TM228**) and RuCp($PPh_3$)$_2$Cl were prepared as previously described.[84,85] All air-free manipulations were carried out under an atmosphere of dinitrogen using Schlenk techniques. NMR spectra were recorded in $(CD_3)_2CO$, $(CD_3)_2SO$, or $CDCl_3$ at probe temperature, on a Bruker Avance 400 spectrometer at 400.13 MHz ($^1$H NMR), 100.62 MHz (APT-$^{13}$C{$^1$H} NMR), or 161.97 MHz ($^{31}$P{$^1$H} NMR). Chemical shifts (δ) are reported in parts per million (ppm), downfield from solvent peaks considering internal $Me_4Si$ at 0.00 ppm ($^1$H and $^{13}$C NMR spectra) or external 85% $H_3PO_4$ ($^{31}$P NMR spectra). All NMR resonances were unambiguously assigned considering complementary 2D experiments (COSY, HSQC, and HMBC). FT-IR spectra were collected in KBr pellets at room temperature, on a Shimadzu IRAffinity-1 spectrophotometer (4000 – 400 cm$^{-1}$). Only the most significant bands are cited in the text. UV-vis spectra were acquired in dichloromethane at room temperature, on a Jasco V-560 spectrometer (233 – 900 nm) using quartz cuvettes with a 1 cm optical path. Elemental analyses were performed at Laboratório de Análises, Instituto Superior Técnico on a Fisons Instruments EA1108 system. Data acquisition, integration, and handling were accomplished with the software package EAGER-200 (Carlo Erba Instruments). ESI-MS spectra were collected in acetonitrile at room temperature, on a Bruker HCT ESI/QITMS spectrometer (100 – 3000 m/z) at positive ionization mode. High Resolution Mass spectra were recorded in a Dionex Ultimate 3000 UHPLC+ system equipped with a Multiple-Wavelength detector, using an imChem Surf C18 TriF 100A 3 µm 100x2,1mm column connected to Thermo Scientific Q Exactive hybrid quadrupole-Orbitrap mass spectrometer (Thermo Scientific™ Q Exactive™ Plus). Semi-preparative RP-HPLC experiments were performed at room temperature on a system composed of a Waters 2535 pump coupled to a Uniflows DG-3210 degasser and a Waters 2998 UV-vis diode-array detector (200 – 600 nm), using method 4, 6 - 10 (Table S1). Analytical RP-HPLC control analyses were carried out at room temperature on a system composed of a PerkinElmer Series 200 pump coupled to a PerkinElmer Series 200 degasser and a PerkinElmer Series 200 UV-vis detector (220 nm), using methods 1-3, 5, 11 (Table S1).

**Table S1.** Methods used in the analytical (1-3, 5-11) or semi-preparative (4, 6- 10) RP-HPLC assays.

| Method | Column/ precolumn | Flow (mL/min) | Mobile phases | Binary gradient |
|---|---|---|---|---|
| 1 | C18(2) [a] | 0.5 | **A:** 10 mM $NH_4HCO_3$ in $H_2O$, pH = 8<br>**B:** $CH_3CN$ | 0-3 min: 10 % B; 3-5 min: 10-70 % B; 5-10 min: 70 % B; 10-20 min: 70-90 % B; 20-25 min: 90 % B; 25-27 min: 90-10% B; 27-30 min: 10 % B |
| 2 | C18(2) [a] | 0.5 | **A:** 10 mM $NH_4HCO_3$ in $H_2O$, pH = 8<br>**B:** $CH_3CN$ | 0-3 min: 10 % B; 3-5 min: 10-70 % B; 5-10 min: 70 % B; 10-20 min: 70-90 % B; 20-30 min: 90 % B; 30-32 min: 90-10% B; 32-35 min: 10 % B |
| 3 | C18(2) [a] | 0.7 | **A:** 10 mM $NH_4HCO_3$ in $H_2O$, pH = 8<br>**B:** $CH_3CN$ | 0-3 min: 10% B; 3-5 min: 10-70% B; 5-10 min: 70% B; 10-15 min: 70-80% B; 15-20 min: 80% B; 20-25 min: 80-90% B; 25-28 min: 90% B; 28-30 min: 90-10% B; 30-40 min: 10% B |
| 4 | C18 [b] | 2 | **C:** 0.1 % TFA in $H_2O$<br>**D:** 0.1 % TFA in $CH_3CN$ | 0-5 min: 10 % D; 5-35 min: 10-100 % D; 35-38 min: 100 % D; 38-40 min: 100-10 % D; 40-45 min: 10 % D |
| 5 | C18 [c] | 1 | **C:** 0.1 % TFA in $H_2O$<br>**D:** 0.1 % TFA in $CH_3CN$ | 0-5 min: 10 % D; 5-20 min: 10-100 % D; 20-25 min: 100 % D; 25-27 min: 100-10 % D; 27-30 min: 10 % D |
| 6 | C18 [b] | 2 | **C:** 0.1 % TFA in $H_2O$<br>**D:** 0.1 % TFA in $CH_3CN$ | 0-5 min: 10 % D; 5-30 min: 10-40 % D; 30-45 min: 40 % D; 45-50 min: 40-100 % D; 50-53 min: 100 % D, 53-55 min: 100-10 % D, 55-60 min: 10 % D |
| 7 | C18(2) [d] | 3 | **A:** 10 mM $NH_4HCO_3$ in $H_2O$, pH = 8<br>**B:** $CH_3CN$ | 0-3 min: 10 % B; 3-5 min: 10-70 % B; 5-10 min: 70 % B; 10-20 min: 70-90 % B; 20-25 min: 90 % B; 25-27 min: 90-10 % B; 27-30 min: 10 % B |
| 8 | C18(2) [d] | 3 | **A:** 10 mM $NH_4HCO_3$ in $H_2O$, pH = 8<br>**B:** $CH_3CN$ | 0-3 min: 10 % B; 3-5 min: 10-70 % B; 5-10 min: 70 % B; 10-20 min: 70-90 % B; 20-30 min: 90 % B; 30-32 min: 90-10 % B; 32-35 min: 10 % B |
| 9 | C18(2) [d] | 3 | **A:** 10 mM $NH_4HCO_3$ in $H_2O$, pH = 8<br>**B:** $CH_3CN$ | 0-3 min: 10% B; 3-5 min: 10-70% B; 5-10 min: 70% B; 10-15 min: 70-80% B; 15-20 min: 80% B; 20-25 min: 80-90% B; 25-28 min: 90% B; 28-30 min: 90-10% B; 30-40 min: 10% B |
| 10 | C18(2) [d] | 3 | **A:** 10 mM $NH_4HCO_3$ in $H_2O$, pH = 8<br>**B:** $CH_3CN$ | 0-3 min: 10% B; 3-5 min: 10-70% B; 5-10 min: 70% B; 10-20 min: 70-90% B; 20-25 min: 90% B; 25-30 min: 90-95% B; 30-40 min: 95% B; 40-42 min: 95-10% B; 42-45 min: 10% B |
| 11 | C18(2) [a] | 0.7 | **A:** 10 mM $NH_4HCO_3$ in $H_2O$, pH = 8<br>**B:** $CH_3CN$ | 0-3 min: 10 % B; 3-5 min: 10-70 % B; 5-10 min: 70 % B; 10-25 min: 70-95 % B; 25-35 min: 95 % B; 35-37 min: 95-10 % B; 37-40 min: 10 % B |

*[a] Phenomenex Luna 00F-4251-E0 column (15 cm × 4.6 mm, 3 µm) coupled to Phenomenex Security Guard AJ0-928 precolumn (4 mm × 3.0 mm). [b] Macherey-Nagel VP250/8 Nucleosil 100-7 column (25 cm × 8 mm, 7 µm) coupled to Macherey-Nagel VP30/8 Nucleosil 100-7 precolumn (3 cm × 8 mm, 7 µm); [c] Supelco Analytical 568223-U column (25 cm × 4.6 mm, 5 µm) coupled to Supelco 568273-U Discovery precolumn (2 cm × 4.0 mm, 5 µm); [d] Phenomenex Luna 00F-4253-N0 column (15 cm × 10 mm, 10 µm) coupled to Phenomenex Security Guard AJ0-7221 precolumn (1 cm × 10 mm).*

## Synthesis and characterization

### Synthesis of bipyridine ligands

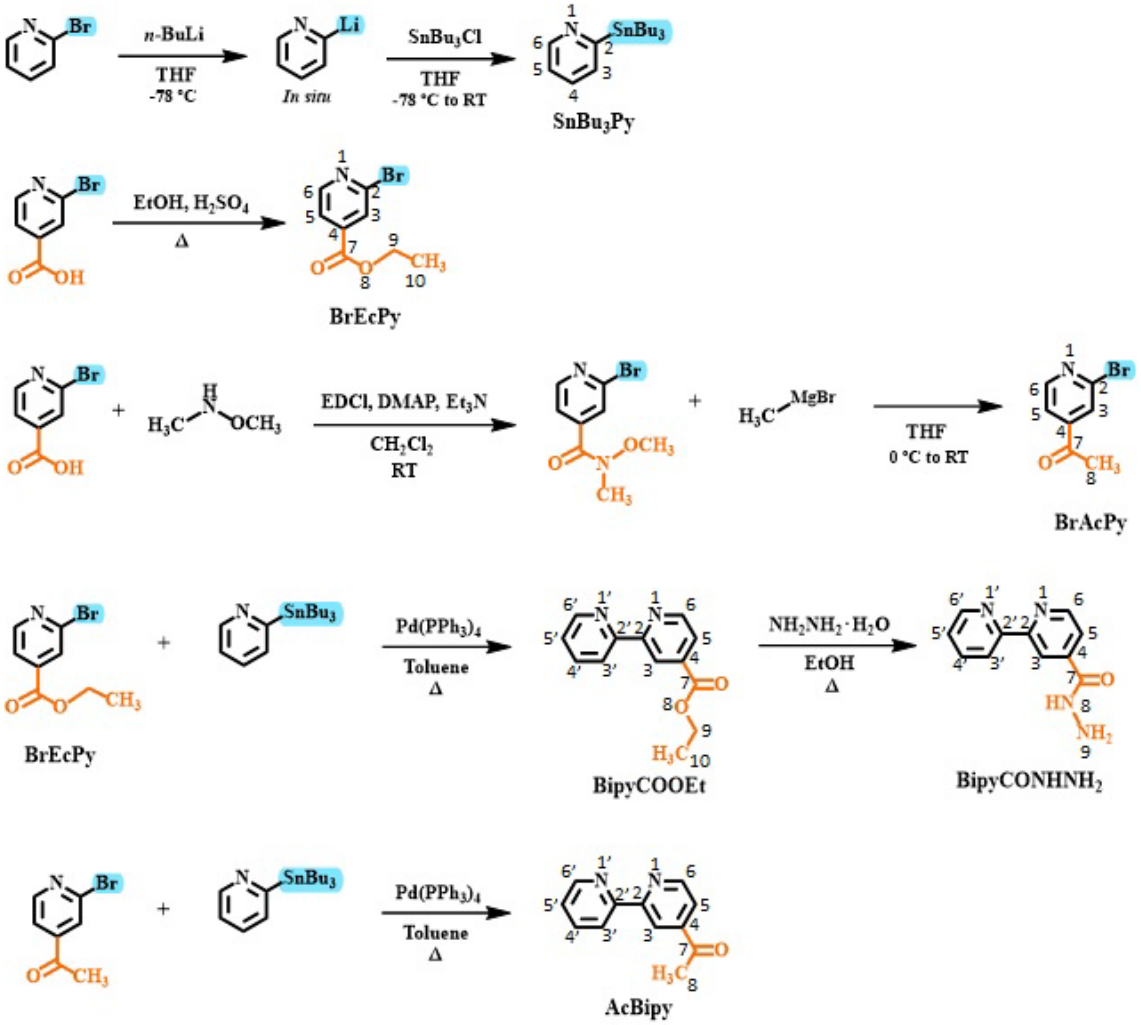


**Scheme S1.** Synthetic scheme for the monofunctionalized bipyridine ligands.

### 2-(Tributylstannyl)pyridine ($SnBu_3Py$)

$SnBu_3Py$ was prepared upon optimization of a previously reported procedure.[86] To a solution of 2-bromopyridine (0.35 mL, 3.7 mmol) in THF (10 mL), was slowly added BuLi (2.5 mL, 4.0 mmol) at 0 °C, getting a yellow color. The resulting mixture was stirred for 10 min at 0 °C, turning color to brown. At this point, Bu3SnCl (1.2 mL, 4. 4 mmol) was added at 0 °C and the mixture was allowed to warm slowly to room temperature and was stirred 1h, turning color to orange. The reaction was quenched with saturated aqueous $NH_4Cl$ solution (10 mL) and extracted with EtOAc (3 × 10 mL). The organic layers were collected, dried over MgSO4, filtered and the solvent evaporated under vacuum. The product was obtained as a brown oil (0.9 mL, 2.8 mmol) and used in the next step without any additional purification. Yield: 75%.

$^1$H NMR [$CDCl_3$, $Me_4Si$, 400.13 MHz] δ/ppm: 8.71 [d, 1, $H_6$, $^3J_{HH}$ = 5.68 Hz]; 7.46 [t, 1, $H_5$, $^3J_{HH}$ = 5.43 Hz]; 7.38 [d, 1, $H_3$, $^3J_{HH}$ = 7.45 Hz]; 7.09 [m, 1, $H_4$]; 1.54 [m, 6, $H_7$]; 1.26 [m, 12, $H_8$ + $H_9$]; 0.85 [t, 9, $H_{10}$, $^3J_{HH}$ = 7.33 Hz].

**2-Bromo-N-methyl-N-(methyloxy)-4-pyridinecarboxamide (BrMMPy)**

BrMMPy was prepared upon optimization of a previously reported procedure.[87] To a solution of 2-bromo-4-pyridinecarboxylic acid (1.0 g, 5.0 mmol) in dichloromethane (30 mL), was added EDCI (1.1 g, 6.8 mmol), N,O-Dimethylhydroxylamine (0.8 g, 8.0 mmol), DMAP (0.06 g, 0.5 mmol) and triethylamine (3 mL, 21.5 mmol). The resulting mixture was stirred for 20 h at room temperature. The mixture was diluted with water (20 mL) and extracted with dichloromethane (3 × 20 mL). The combined organic fraction was dried with $MgSO_4$, filtered and the solvent evaporated under vacuum. The product was purified by column chromatography, eluting with n-hexane/ ethyl acetate (1:1) to give a yellow oil (0.70 g, 2.9 mmol). Yield: 57%.

$^1$H NMR [$CDCl_3$, $Me_4Si$, 400.13 MHz] $\delta$/ppm: 8.45 [d, 1, $H_6$, $^3J_{HH}$ = 5.01 Hz]; 7.72 [s, 1, $H_3$]; 7.48 [dd, 1, $H_5$, $^3J_{HH}$ = 5.04 Hz and 1.43 Hz]; 3.55 [s, 3, $H_{10}$]; 3.37 [s, 3, $H_{11}$].

**2-Bromo-4-acetylpyridine (BrAcPy)**

BrAcPy was prepared upon optimization of a previously reported procedure.[87] To a solution of BrMMPy (0.44 g, 1.8 mmol) in THF (20 mL), was slowly added $CH_3MgBr$ (3 M in *n*-hexane, 1.0 mL, 3.0 mmol) at 0 °C. The resulting mixture was stirred for 20 h at room temperature, turning colour to yellow. The reaction was quenched with saturated aqueous $NH_4Cl$ solution (20 mL) and extracted with EtOAc (3 × 20 mL). The combined organic fraction was dried with $MgSO_4$, filtered and the solvent evaporated under vacuum. The product was purified by column chromatography, eluting with n-hexane/ ethyl acetate (1:1) to give a yellow powder (0.29 g, 1.4 mmol). Yield: 79 %.

$^1$H NMR [$CDCl_3$, $Me_4Si$, 400.13 MHz] $\delta$/ppm: 8.56 [d, 1, $H_6$, $^3J_{HH}$ = 5.05 Hz]; 7.92 [s, 1, $H_3$]; 7.69 [dd, 1, $H_5$, $^3J_{HH}$ = 5.12 Hz and 1.58 Hz]; 2.62 [s, 3, $H_8$].

**2-Bromo-4-ethyl carboxylate pyridine (BrEcPy)**

BrEcPy was prepared upon optimization of a previously reported procedure.[88] To a solution of 2-bromopyridine-4-carboxylic acid (1.0 g, 5 mmol) in ethanol (5 mL), was added conc. $H_2SO_4$ (0.8 mL, 15 eq.). The resulting mixture was heated under reflux for 4 h. After cooling to room temperature, the mixture was hydrolyzed with a saturated aqueous $NaHCO_3$ solution (20 mL) and extracted with EtOAc (3 × 20 mL). The combined organic fraction was dried with $MgSO_4$, filtered and the solvent evaporated under vacuum. The product was obtained as a white powder (0.79 g, 3.4 mmol). Yield: 68%.

$^1$H NMR [$CDCl_3$, $Me_4Si$, 400.13 MHz] $\delta$/ppm: 8.52 [d, 1, $H_6$ $^3J_{HH}$ = 4.92 Hz]; 8.04 [s, 1, $H_3$] ; 7.80 [d, 1, $H_5$, $^3J_{HH}$ = 5.04 Hz]; 4.42 [q, 2, $H_9$, $^3J_{HH}$ = 7.08 Hz] ; 1.41 [t, 3, $H_{10}$, $^3J_{HH}$ = 7.04].

**ethyl 2,2'-bipyridine-4-carboxylate (BipyCOOEt)**

To a solution of $SnBu_3Py$ (0.9 mL, 2.9 mmol) in toluene (30 mL), was added BrEcPy (0.48 g, 2.1 mmol) and $Pd(PPh_3)_4$ (0.10 g, 0.1 mmol). The resulting mixture was heated at 100 °C for 94h. The reaction was quenched with water (30 mL), extracted with EtOAc (3 × 20 mL). The combined organic fraction was dried with $MgSO_4$, filtered and the solvent evaporated under vacuum. The product was purified by column chromatography, eluting with n-hexane/ ethyl acetate (gradient - 0-1 min: 0% EtOAc; 1-25 min: 0-30% EtOAc), to give a yellow powder (0.14 g, 0.6 mmol). Yield: 30 %.

$^1$H NMR [$CDCl_3$, $Me_4Si$, 400.13 MHz] $\delta$/ppm: 8.92 [s, 1, $H_3$]; 8.82 [d, 1, $H_6$, $^3J_{HH}$ = 4.92 Hz]; 8.73 [d, 1, $H_{6'}$, $^3J_{HH}$ =3.16 Hz]; 8.41 [d, 1, $H_{3'}$, $^3J_{HH}$ = 9.12 Hz]; 7.88 [d, 1, $H_5$, $^3J_{HH}$ = 4.92 Hz]; 7.83 [t, 1, $H_{4'}$,

$^{3}J_{HH}$ = 7.80 Hz]; 7.35 [m, 1, $H_{5'}$]; 4.45 [q, 2, $H_9$, $^{3}J_{HH}$ = 7.20 Hz]; 1.44 [t, 3, $H_{10}$]. APT-$^{13}C\{^{1}H\}$ NMR [$(CD_3)_2SO$, $Me_4Si$, 100.62 MHz] δ/ppm: 165.42 [$C_7$]; 157.42 [$C_2$]; 155.54 [$C_{2'}$]; 150.05 [$C_6$]; 149.49 [$C_{6'}$]; 139.01 [$C_4$]; 137.17 [$C_{4'}$]; 124.27 [$C_{5'}$]; 122.99 [$C_5$]; 121.41 [$C_{3'}$]; 120.50 [$C_3$]; 61.98 [$C_9$]; 14.42 [$C_{10}$]. UV-vis [dichloromethane, $\lambda_{max}$/nm ($\varepsilon$/$M^{-1}.cm^{-1}$)]: 303 ($3.16\times10^3$); 282 ($4.54\times10^3$); 247 (sh); 238 ($5.02\times10^3$).

**2,2'-bipyridine-4-carbohydrazide (BipyCONHNH$_2$)**

To a solution of BipyCOOEt (0.02 g, 0.09 mmol) in ethanol (4 mL), was added $NH_2NH_2{\cdot}H_2O$ (0.4 mL, 3.8 mmol). The resulting mixture was heated under reflux for 8 h. After cooling to room temperature, the white product was obtained by filtration (0.01 g, 0.09 mmol). Yield: 50%.

$^{1}H$ NMR [DMSO, $Me_4Si$, 400.13 MHz] δ/ppm: 10.25 [br, 1, $H_8$]; 8.79 [d, 1, $H_6$, $^{3}J_{HH}$ = 5.04 Hz]; 8.70 [m, 2, $H_3$ + $H_{6'}$]; 8.38 [d, 1, $H_{3'}$, $^{3}J_{HH}$ = 7.96 Hz]; 7.97 [t, 1, $H_{4'}$, $^{3}J_{HH}$ = 7.70 Hz]; 7.77 [d, 1, $H_5$, $^{3}J_{HH}$ = 5.04 Hz], 7.49 [t, 1, $H_{5'}$, $^{3}J_{HH}$ =4.64 Hz]; 4.64 [br, $H_9$]. APT-$^{13}C\{^{1}H\}$ NMR [DMSO, $Me_4Si$, 100.62 MHz] δ/ppm: 164.25 [$C_7$]; 156.27 [$C_2$]; 154.85 [$C_{2'}$]; 150.21 [$C_6$]; 149.67 [$C_{6'}$]; 141.84 [$C_4$]; 137.79 [$C_{4'}$]; 124.88 [$C_{5'}$]; 121.43 [$C_5$]; 120.93 [$C_{3'}$]; 118.28 [$C_3$]. HRMS (ESI-MS): m/z calcd for $C_{11}H_{10}N_4O$ $[M+H]^+$ = 215.0927, found = 215.0923. UV-vis [dichloromethane, $\lambda_{max}$/nm ($\varepsilon$/$M^{-1}.cm^{-1}$)]: 282 ($1.10\times10^4$); 248 (sh); 240 ($1.4\times10^4$).

**2,2'-bipyridine-4-acetyl (AcBipy)**

To a solution of $SnBu_3Py$ (1.0 mL, 3.0 mmol) in toluene (30 mL), was added BrAcPy (0.40 g, 2.0 mmol) and $Pd(PPh_3)_4$ (0.13 g, 0.11 mmol). The resulting mixture was heated at 100 °C for 3 days, turning color from yellow to red. The reaction was quenched with water (20 mL), extracted with dichloromethane (3 × 20 mL). The combined organic fraction was dried with $MgSO_4$, filtered and the solvent evaporated under vacuum. The product was purified by column chromatography, eluting with n-hexane/ ethyl acetate (1:1), to give a white powder (0.20 g, 1.0 mmol). Yield: 50 %.

$^{1}H$ NMR [$(CD_3)_2CO$, $Me_4Si$, 400.13 MHz] δ/ppm: 8.90 [s, 1, $H_3$]; 8.88 [d, 1, $H_6$, $^{3}J_{HH}$ = 4.95 Hz]; 8.73 [d, 1, $H_{6'}$, $^{3}J_{HH}$ = 4.56 Hz]; 8.50 [d, 1, $H_{3'}$, $^{3}J_{HH}$ = 7.56 Hz]; 7.96 [t, 1, $H_{4'}$, $^{3}J_{HH}$ = 7.74 Hz]; 7.87 [d, 1, $H_5$, $^{3}J_{HH}$ = 4.94 Hz]; 7.46 [m, 1, $H_{5'}$]; 2.72 [s, 3, $H_8$]. APT-$^{13}C\{^{1}H\}$ NMR [DMSO, $Me_4Si$, 100.62 MHz] δ/ppm: 198.00 [$C_7$]; 158.14 [$C_2$]; 156.04 [$C_{2'}$]; 151.23 [$C_6$]; 150.24 [$C_{6'}$]; 144.99 [$C_4$]; 137.95 [$C_{4'}$]; 125.24 [$C_{5'}$]; 122.18 [$C_5$]; 121.58 [$C_{3'}$]; 119.01 [$C_3$]; 26.98 [$C_8$]. HRMS (ESI-MS): m/z calcd for $C_{12}H_{10}N_2O$ $[M+H]^+$ = 199.0866, found = 199.0861. UV-vis [dichloromethane, $\lambda_{max}$/nm ($\varepsilon$/$M^{-1}.cm^{-1}$)]: 250 (sh), 281 ($1.18\times10^4$), 305 (sh).

**Synthesis of ruthenium organometallic complexes**

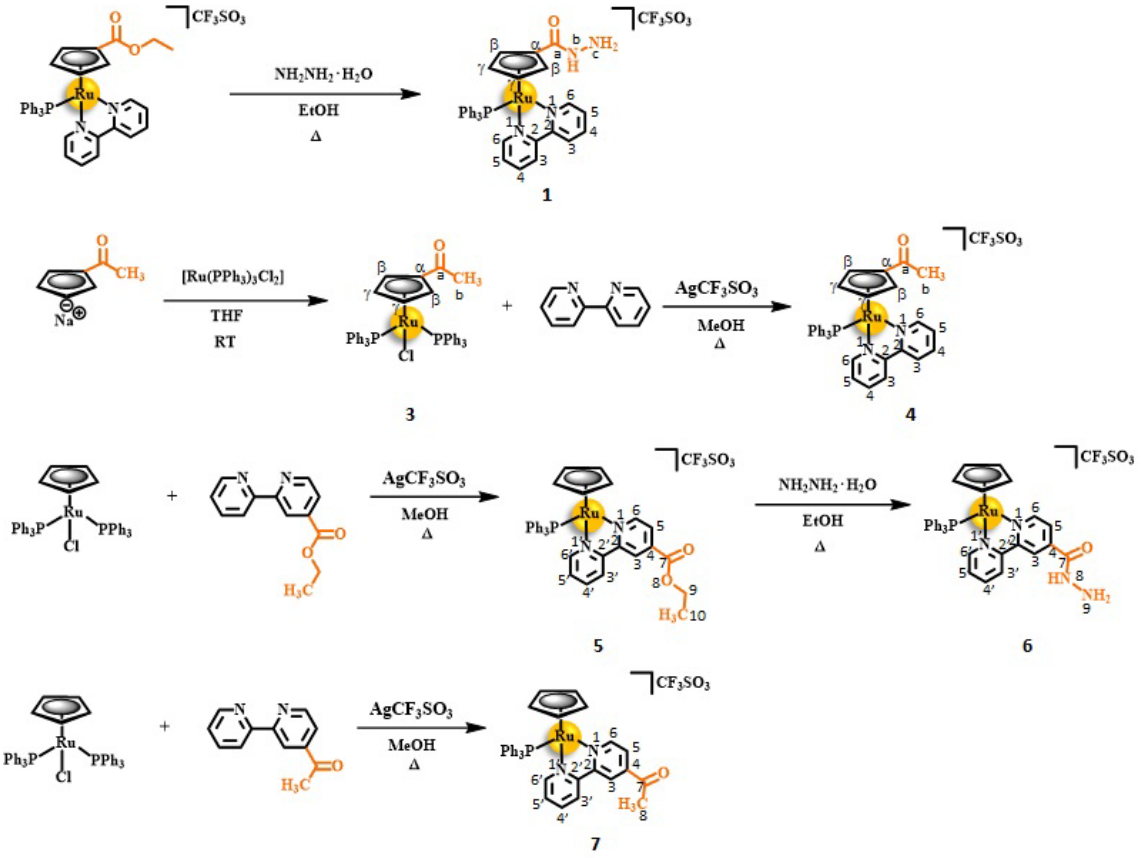


**Scheme S2.** Reaction schemes of the new Ru organometallic complexes

**[Ru(η$^5$-$C_5H_4CONHNH_2$)($PPh_3$)(2,2'-bipy)][$CF_3SO_3$] (1):**

To a solution of [Ru(η$^5$-$C_5H_4CO_2CH_2CH_3$)($PPh_3$)(2,2'-bipy)][$CF_3SO_3$] (0.20 g, 0.25 mmol) in ethanol (10 mL), was added $NH_2NH_2{\cdot}H_2O$ (80 % v/v, 1.8 mL, 37.5 mmol). The resulting mixture was heated under reflux for 5 h, turning from orange to red. The solvent was removed under vacuum. The residue was washed with diethyl ether (2 x 10 mL) and vacuum dried. The product was recrystallized by slow diffusion of methanol/diethyl ether, affording orange crystals (0.18 g, 0.23 mmol). Yield: 92 %.

$^1$H NMR [$(CD_3)_2SO$, $Me_4Si$, 400.13 MHz] δ/ppm: 9.28 [d, 2, $H_6$, $^3J_{HH}$ = 4.37 Hz]; 9.18 [br, 1, $H_b$]; 8.18 [d, 2, $H_3$, $^3J_{HH}$ = 7.77 Hz]; 7.87 [t, 2, $H_4$, $^3J_{HH}$ = 7.06 Hz]; 7.37 [m, 5, $H_5$ + $H_{para}(PPh_3)$]; 7.30 [m, 6, $H_{meta}(PPh_3)$]; 6.91 [t, 6, $H_{ortho}(PPh_3)$, $^3J_{HH}$ = 8.24 Hz]; 5.49 [br, 2, $H_\beta$]; 4.77 [br, 2, $H_\gamma$]; 4,12 [br, 2, $H_c$]. APT-$^{13}$C{$^1$H} NMR [$(CD_3)_2SO$, $Me_4Si$, 100.62 MHz] δ/ppm: 164.33 [$C_a$]; 155.66 [$C_6$]; 155.23 [$C_2$]; 136.62 [$C_4$]; 132.57 [d, $C_{ortho}(PPh_3)$, $^2J_{PC}$ = 10.95 Hz]; 130.69 [d, $C_{ipso}(PPh_3)$, $^1J_{PC}$ = 42.27 Hz]; 130.18 [br, $C_{para}(PPh_3)$]; 128.51 [d, $C_{meta}(PPh_3)$, $^3J_{PC}$ = 9.58 Hz]; 125.24 [$C_5$]; 123.37 [$C_3$]; 82.21 [$C_\alpha$]; 81.27 [$C_\beta$]; 77.09 [$C_\gamma$]. $^{31}$P{$^1$H} NMR [$(CD_3)_2SO$, 161.97 MHz] δ/ppm: 50.42 [s, $PPh_3$]. FT-IR [KBr, cm$^{-1}$]: 3318 ($\nu_{N-H}$, $CONHNH_2$), 3102-3058 ($\nu_{C-H}$, aromatic rings), 1641 ($\nu_{C=O}$, $CONHNH_2$), 1610-1608 ($\delta_{N-H}$, $CONHNH_2$), 1479-1382 ($\nu_{C=N}$ + $\nu_{C=C}$, aromatic rings), 1251 ($\nu CF_3SO_3$), 1226-698 ($\delta_{C-H}$, aromatic rings). Elemental analysis (%) found: C, 53.2; H, 3.9; N, 6.9; S, 4.0. Calc. for $C_{35}H_{30}RuF_3N_4O_4PS$ (791.75 g/mol): C, 53.1; H, 3.8; N, 7.1; S, 4.0. ESI-MS: m/z calcd for $C_{34}H_{30}RuN_4OP$ $[M]^+$ = 643.1,

found = 643.2. RP-HPLC: $t_R$ = 26.1 min (method 1, Table S1). UV-vis [dichloromethane, $\lambda_{max}$/nm ($\varepsilon$/$M^{-1}.cm^{-1}$)]: 289 ($2.65\times10^4$); 345 (sh); 409 ($5.34\times10^3$); 455 (sh).

**Na($\eta^5$-$C_5H_4COCH_3$) (2):**

Na($\eta^5$-$C_5H_4COCH_3$) was prepared upon optimization of a previously reported procedure.[89] Freshly cracked cyclopentadiene (2.5 mL, 30 mmol) was added dropwise to a slurry of sodium sand (0.17 g, 7.5 mmol) in tetrahydrofuran (15 mL) at 0 °C. The mixture was stirred at room temperature until all the sodium had reacted, turning from a colourless to a slightly pink solution. Upon addition of methyl acetate (2.4 mL, 30 mmol), the resulting mixture was refluxed for 2 h, acquiring red colour. The solvent was removed under vacuum, and the residue was washed successively with diethyl ether (10 mL) until the filtrate was clear. The product was vacuum dried, affording a white powder (0.73 g, 5.6 mmol). Yield: 74 %.

**[Ru($\eta^5$-$C_5H_4COCH_3$)($PPh_3$)$_2$Cl] (3):**

To a stirring solution of Na($\eta^5$-$C_5H_4COCH_3$) (0.55 g, 4.2 mmol) in tetrahydrofuran (20 mL) was added [Ru($PPh_3$)$_3Cl_2$] (3.2 g, 3.3 mmol). The resulting mixture was stirred overnight at room temperature, producing an orange precipitate. The residue was washed with tetrahydrofuran/diethyl ether (1:1, 2 x 10 mL) and vacuum dried. The product was recrystallized by slow diffusion of dichloromethane/*n*-hexane, affording burgundy crystals (1.78 g, 2.3 mmol). Yield: 70 %.

$^1$H NMR [$CDCl_3$, $Me_4Si$, 400.13 MHz] $\delta$/ppm: 7.36 [m, 12, $H_{ortho}(PPh_3)$]; 7.23 [t, 6, $H_{para}(PPh_3)$, $^3J_{HH}$ = 6.73 Hz]; 7.12 [m, 12, $H_{meta}(PPh_3)$]; 5.12 [br, 2, $H_\beta$]; 3.62 [br, 2, $H_\gamma$]; 2.21 [s, 3, $H_b$]. APT-$^{13}C\{^1H\}$ NMR [$CDCl_3$, $Me_4Si$, 100.62 MHz] $\delta$/ppm: 197.18 [$C_a$]; 137.31 [t, $C_{ipso}(PPh_3)$, $^1J_{PC}$ = 21.04 Hz]; 134.00 [t, $C_{ortho}(PPh_3)$, $^2J_{PC}$ = 4.86 Hz]; 129.11 [br, $C_{para}(PPh_3)$]; 127.61 [t, $C_{meta}(PPh_3)$, $^3J_{PC}$ = 4.53 Hz]; 88.13 [$C_\alpha$]; 86.71 [$C_\beta$]; 79.08 [$C_\gamma$]; 29.57 [$C_b$]. $^{31}P\{^1H\}$ NMR [$CDCl_3$, 161.97 MHz] $\delta$/ppm: 37.36 [s, $PPh_3$]. FT-IR [KBr, $cm^{-1}$]: 3101-3047 ($\nu_{C-H}$, aromatic rings), 2858 ($\nu_{C-H}$, $COCH_3$), 1680 ($\nu_{C=O}$, $COCH_3$), 1481-1354 ($\nu_{C=C}$, aromatic rings + $\delta_{C-H}$, $COCH_3$), 1273-692 ($\delta_{C-H}$, aromatic rings). Elemental analysis (%) found: C, 67.3; H, 4.9. Calc. for $C_{43}H_{37}RuClOP_2$ (768.24 g/mol): C, 67.2; H, 4.9. UV-vis [dichloromethane, $\lambda_{max}$/nm ($\varepsilon$/$M^{-1}.cm^{-1}$)]: 290 (sh); 394 ($2.70\times10^3$).

**[Ru($\eta^5$-$C_5H_4COCH_3$)($PPh_3$)(2,2'-bipy)][$CF_3SO_3$] (4):**

To a stirring solution of [Ru($\eta^5$-$C_5H_4COCH_3$)($PPh_3$)$_2$Cl] (0.38 g, 0.5 mmol) and $AgCF_3SO_3$ (0.13 g, 0.5 mmol) in methanol (20 mL), was added 2,2'-bipy (0.08 g, 0.5 mmol). The resulting mixture was heated under reflux for 4 h, turning from orange to red. Upon cannula filtration, the solvent was removed under vacuum. The residue was washed with *n*-hexane (2 x 10 mL) and vacuum dried. The product was recrystallized by slow diffusion of dichloromethane/diethyl ether, affording orange crystals (0.26 g, 0.34 mmol). Yield: 68 %.

$^1$H NMR [$(CD_3)_2CO$, $Me_4Si$, 400.13 MHz] $\delta$/ppm: 9.42 [d, 2, $H_6$, $^3J_{HH}$ = 4.51 Hz]; 8.23 [d, 2, $H_3$, $^3J_{HH}$ = 7.60 Hz]; 7.98 [m, 2, $H_4$]; 7.45 [m, 5, $H_5$ + $H_{para}(PPh_3)$]; 7.35 [m, 6, $H_{meta}(PPh_3)$]; 7.12 [m, 6, $H_{ortho}(PPh_3)$]; 5.78 [br, 2, $H_\beta$]; 4.70 [br, 2, $H_\gamma$]; 1.66 [s, 3, $H_b$]. APT-$^{13}C\{^1H\}$ NMR [$(CD_3)_2CO$, $Me_4Si$, 100.62 MHz] $\delta$/ppm: 195.36 [$C_a$]; 157.11 [$C_6$]; 156.55 [$C_2$]; 137.99 [$C_4$]; 133.89 [d, $C_{ortho}(PPh_3)$, $^2J_{PC}$ = 10.81 Hz]; 131.86 [d, $C_{ipso}(PPh_3)$,$^1J_{PC}$ = 42.37 Hz]; 131.33 [br, $C_{para}(PPh_3)$]; 129.51 [d, $C_{meta}(PPh_3)$, $^3J_{PC}$ = 9.80 Hz]; 126.74 [$C_5$]; 124.45 [$C_3$]; 86.64 [$C_\alpha$]; 84.78 [$C_\beta$]; 77.84 [$C_\gamma$]; 27.11 [$C_b$]. $^{31}P\{^1H\}$ NMR [$(CD_3)_2CO$, 161.97 MHz] $\delta$/ppm: 49.67 [s, $PPh_3$]. FT-IR [KBr, $cm^{-1}$]: 3110-2998 ($\nu_{C-H}$, aromatic rings), 2921 ($\nu_{C-H}$, $COCH_3$), 1660 ($\nu_{C=O}$, $COCH_3$), 1479-1336 ($\nu_{C=N}$ + $\nu_{C=C}$, aromatic rings + $\delta_{C-H}$, $COCH_3$), 1259

($\nu CF_3SO_3$), 1222-700 ($\delta_{C\text{-}H}$, aromatic rings). Elemental analysis (%) found: C, 55.7; H, 3.5; N, 3.5; S, 4.0. Calc. for $C_{36}H_{30}RuF_3N_2O_4PS$ (775.74 g/mol): C, 55.7; H, 3.9; N, 3.6; S, 4.1. ESI-MS: m/z calcd for $C_{35}H_{30}RuN_2OP$ $[M]^+$ =627.1, found = 627.3. RP-HPLC: $t_R$ = 25.4 min (method 2). UV-vis [dichloromethane, $\lambda_{max}$/nm ($\varepsilon$/$M^{-1}.cm^{-1}$)]: 288 ($1.86\times10^4$); 350 (sh); 404 ($3.62\times10^3$); 450 (sh).

**[Ru($\eta^5$-$C_5H_5$)($PPh_3$)(BipyCOOEt)][$CF_3SO_3$] (5):**

To a stirring solution of [$RuCp(PPh_3)_2Cl$] (0.36 g; 0.5 mmol) and $AgCF_3SO_3$ (0.13 g, 0.5 mmol) in methanol (20 mL), was added BipyCOOEt (0.11 g; 0.5 mmol). The resulting mixture was heated under reflux for 4 h, turning from orange to red. Upon cannula filtration, the solvent was removed under vacuum. The residue was washed with *n*-hexane (2 x 10 mL) and vacuum dried. The product was recrystallized by slow diffusion of dichloromethane/diethyl ether, affording a red crystalline solid (0.34 g, 0.42 mmol). Yield: 88 %.

$^1$H NMR [$CDCl_3$, $Me_4Si$, 400.13 MHz] $\delta$/ppm: 9.54 [d, 1, $H_6$ $^3J_{HH}$ = 6.04 Hz]; 9.36 [d, 1, $H_{6'}$, $^3J_{HH}$ = 5,68 Hz]; 8.18 [s, 1, $H_3$]; 7.84 [d, 1, $H_{3'}$, $^3J_{HH}$ = 5.97 Hz]; 7.75 [m, 2, $H_5$ + $H_{4'}$]; 7.34 [m, 4, $H_{5'}$ + $H_{para}(PPh_3)$]; 7.26 [m, 6, $H_{meta}(PPh_3)$]; 6.98 [m, 6, $H_{ortho}(PPh_3)$; 4.81 [s, 5, Cp]; 4.44 [q, 2, $H_9$, $^3J_{HH}$ = 7.08 Hz]; 1.43 [t, 3, $H_{10}$, $^3J_{HH}$ = 7.04 Hz]. APT-$^{13}C\{^1H\}$ NMR [$CDCl_3$, $Me_4Si$, 100.62 MHz] $\delta$/ppm: 163.82 [$C_7$]; 156.96 [$C_6$]; 156.49 [$C_{6'}$]; 156.00 [$C_4$]; 154.77 [$C_{2'}$]; 136.57 [$C_2$]; 136.02 [$C_{4'}$]; 132.90 [d, $C_{ortho}(PPh_3)$, $^2J_{PC}$ = 10.97 Hz]; 130.77 [d, $C_{ipso}(PPh_3)$,$^1J_{PC}$ = 42.81 Hz]; 130.42 [d, $C_{para}(PPh_3)$, $^4J_{PC}$ = 2.19 Hz]; 128.74 [d, $C_{meta}(PPh_3)$, $^3J_{PC}$ = 9.88 Hz]; 125.85 [$C_{5'}$]; 123.84 [$C_5$]; 123.21 [$C_{3'}$]; 121.88 [$C_3$]; 79.45 [Cp]; 62.75 [$C_9$]; 14.30 [$C_{10}$]. $^{31}P\{^1H\}$ NMR [$CDCl_3$, 161.97 MHz] $\delta$/ppm: 50.49 [s, $PPh_3$]. FT-IR [KBr, $cm^{-1}$]: 3100-3000 ($\nu_{C\text{-}H}$, aromatic rings), 3000-2850 ($\nu_{C\text{-}H}$, COOEt), 1724 ($\nu_{C=O}$, COOEt), 1600-1500 ($\nu_{C=N}$ + $\nu_{C=C}$, aromatic rings + $\delta_{C\text{-}H}$), 1240 ($\nu CF_3SO_3$), 1220-700 ($\delta_{C\text{-}H}$, aromatic rings). Elemental analysis (%) found: C, 55.4; H, 3.8; N, 3.4; S 4.0. Calc. for $C_{37}H_{32}RuF_3N_2O_5PS$ (805,77 g/mol): C, 55.2; H, 4.0; N, 3.48; S, 3.98. UV-vis [dichloromethane, $\lambda_{max}$/nm ($\varepsilon$/$M^{-1}.cm^{-1}$)]: 307 ($1.73\times10^4$); 350 (sh); 439 ($5.19\times10^3$); 490 (sh).

**[Ru($\eta^5$-$C_5H_5$)($PPh_3$)(BipyCONHNH$_2$)][$CF_3SO_3$] (6):**

To a solution of [Ru($\eta^5$-$C_5H_5$)($PPh_3$)(BipyCOOEt)][$CF_3SO_3$] (0.34 g, 0.4 mmol) in ethanol (10 mL), was added $NH_2NH_2{\cdot}H_2O$ (80 % v/v, 0.28 mL, 4.6 mmol). The resulting mixture was heated under reflux for 4 h. The solvent was removed under vacuum. The residue was washed with diethyl ether (2 x 10 mL) and vacuum dried. The product was recrystallized by slow diffusion of methanol/diethyl ether, affording orange powder (0.25 g, 0.31 mmol). Yield: 75 %.

$^1$H NMR [$CDCl_3$, $Me_4Si$, 400.13 MHz] $\delta$/ppm: 9.21 [d, 1, $H_6$, $^3J_{HH}$ = 5.96 Hz]; 9.10 [d, 1, $H_{6'}$, $^3J_{HH}$ = 5,68 Hz]; 8.41 [s, 1, $H_3$]; 8.20 [d, 1, $H_{3'}$, $^3J_{HH}$ = 8.08 Hz]; 7.73 [m, 2, $H_5$ + $H_{4'}$]; 7.35 [m, 3, $H_{para}(PPh_3)$]; 7.24 [m, 6, $H_{meta}(PPh_3)$]; 7.17 [t, 1, $H_{5'}$, $^3J_{HH}$ = 7.20 Hz]; 6,94 [m, 6, $H_{ortho}(PPh_3)$; 4.70 [s, 5, Cp]. APT-$^{13}C\{^1H\}$ NMR [$CDCl_3$, $Me_4Si$, 100.62 MHz] $\delta$/ppm: 162.38 [$C_7$]; 155.99 [$C_4$]; 155.80 [$C_6$]; 155.63 [$C_{2'}$]; 155.34 [$C_{6'}$]; 139.73 [$C_2$]; 136.45 [$C_{4'}$]; 132.71 [d, $C_{ortho}(PPh_3)$, $^2J_{PC}$ = 10.98 Hz]; 131.02 [d, $C_{ipso}(PPh_3)$]; 130.62 [d, $C_{para}(PPh_3)$, $^4J_{PC}$ = 2.19 Hz]; 128.75 [d, $C_{meta}(PPh_3)$, $^3J_{PC}$ = 9.52 Hz]; 125.22 [$C_{5'}$]; 124.52 [$C_{3'}$]; 123.20 [$C_5$]; 120.65 [$C_3$]; 78.75 [Cp]. $^{31}P\{^1H\}$ NMR [$CDCl_3$, 161.97 MHz] $\delta$/ppm: 50.52 [s, $PPh_3$]. $^1$H NMR [$(CD_3)_2SO$, $Me_4Si$, 400.13 MHz] $\delta$/ppm: 10.19 [br, $H_8$]; 9.52 [d, 1, $H_6$, $^3J_{HH}$ = 5.96 Hz]; 9.38 [d, 1, $H_{6'}$, $^3J_{HH}$ = 5,68 Hz]; 8,43 [s, 1, $H_3$]; 8.17 [d, 1, $H_{3'}$, $^3J_{HH}$ = 8.24 Hz]; 7.89 [t, 1, $H_{4'}$, $^3J_{HH}$ = 7.80 Hz]; 7.60 [d, 1, $H_5$, $^3J_{HH}$ = 6.04 Hz]; 7.39 [m, 3, $H_{para}(PPh_3)$]; 7.35 [m, 1, $H_{5'}$]; 7.29 [m, 6, $H_{meta}(PPh_3)$]; 6.94 [m, 6, $H_{ortho}(PPh_3)$; 4.90 [s, 5, Cp]; 4.75 [br, $H_9$]. APT-$^{13}C\{^1H\}$ NMR [$(CD_3)_2SO$, $Me_4Si$, 100.62 MHz] $\delta$/ppm: 161.98 [$C_7$]; 156.39 [$C_6$]; 156.15[$C_{6'}$]; 155.49 [$C_4$]; 154.88 [$C_{2'}$]; 139.73 [$C_2$]; 136.32 [$C_{4'}$]; 132.60 [d, $C_{ortho}(PPh_3)$, $^2J_{PC}$ = 10.98 Hz]; 130.82 [d, $C_{ipso}(PPh_3)$, $^1J_{PC}$ = 41.71 Hz]; 130.14 [d, $C_{para}(PPh_3)$, $^4J_{PC}$ = 2.20 Hz]; 128.54 [d, $C_{meta}(PPh_3)$, $^3J_{PC}$ = 9.52 Hz]; 125.27 [$C_{5'}$]; 123.68

[$C_{3'}$]; 121.82 [$C_5$]; 120.29 [$C_3$]; 78.784 [Cp]. $^{31}P\{^1H\}$ NMR [$(CD_3)_2SO$, 161.97 MHz] $\delta$/ppm: 51.09 [s, $PPh_3$]. FT-IR [KBr, $cm^{-1}$]: 3400-3150 ($\nu_{N-H}$, $CONHNH_2$), 3100-3000 ($\nu_{C-H}$, aromatic rings), 1660 ($\nu_{C=O}$, $CONHNH_2$), 1600-1500 ($\nu_{C=N}$ + $\nu_{C=C}$, aromatic rings + $\delta_{C-H}$), 1230 ($\nu CF_3SO_3$), 1220-700 ($\delta_{C-H}$, aromatic rings). Elemental analysis (%) found: C, 52.9; H, 3.8; N, 6.9; S 4.0. Calc. for $C_{35}H_{30}RuF_3N_4O_4PS$ (791.75 g/mol): C, 53.1; H, 3.82; N, 7.08; S, 4.05. ESI-MS: m/z calcd for $C_{34}H_{30}RuN_4OP$ (643.12 u) $[M]^+$ = 643.2, found = 643.1 RP-HPLC: $t_R$ = 32.5 min (method 3). UV-vis [dichloromethane, $\lambda_{max}$/nm ($\varepsilon$/$M^{-1}.cm^{-1}$)]: 300 ($1.94\times10^4$); 341 (sh); 427 ($5.29\times10^3$); 475 (sh).

**[Ru($\eta^5$-$C_5H_5$)($PPh_3$)(AcBipy)][$CF_3SO_3$] (7):**

To a stirring solution of [$RuCp(PPh_3)_2Cl$] (0.36 g; 0.5 mmol) and $AgCF_3SO_3$ (0.13 g, 0.5 mmol) in methanol (20 mL), was added AcBipy (0.10 g; 0.5 mmol). The resulting mixture was heated under reflux for 3 h, turning from orange to dark red. Upon cannula filtration, the solvent was removed under vacuum. The residue was washed with *n*-hexane (2 x 10 mL) and vacuum dried. The product was recrystallized by slow diffusion of dichloromethane/diethyl ether, affording a red crystalline solid (0.33g, 0.42 mmol). Yield: 84 %.

$^1H$ NMR [$(CD_3)_2CO$, $Me_4Si$, 400.13 MHz] $\delta$/ppm: 9.75 [d, 1, $H_6$, $^3J_{HH}$ = 5.69 Hz]; 9.56 [d, 1, $H_{6'}$, $^3J_{HH}$ = 5.67 Hz]; 8.49 [s, 1, $H_{3'}$]; 8.41 [d, 1, $H_3$, $^3J_{HH}$ = 8.38 Hz]; 7.94 [t, 1, $H_{4'}$, $^3J_{HH}$ = 7.84 Hz]; 7.68 [d, 1, $H_5$, $^3J_{HH}$ = 6.06 Hz]; 7.42 [4, m, $H_{para}(PPh_3)$ + $H_{5'}$]; 7.33 [m, 6, $H_{meta}(PPh_3)$]; 7.13 [t, 6, $H_{orto}(PPh_3)$, $^3J_{HH}$ = 8.91 Hz]; 5.00 [s, 5, $H_{Cp}$]; 2.69 [s, 3, $H_8$]. APT-$^{13}C\{^1H\}$ NMR [$(CD_3)_2CO$, $Me_4Si$, 100.62 MHz] $\delta$/ppm: 196.40 [$C_7$]; 156.76 [d, $C_6$ $^1J_{NC}$ = 1.70 Hz]; 157.39 [$C_2$]; 157.19 [d, $C_{6'}$, $^1J_{NC}$ = 1.78 Hz]; 156.26 [$C_{2'}$]; 142.94 [$C_4$]; 137.13 [$C_{4'}$]; 133.82 [d, $C_{orto}(PPh_3)$, $^2J_{PC}$ = 11.03 Hz]; 131.91 [d, $C_{ipso}(PPh_3)$, $^1J_{PC}$ = 42.58 Hz]; 131.09 [d, $C_{para}(PPh_3)$, $^4J_{PC}$ = 2.15 Hz]; 129.44 [d, $C_{meta}(PPh_3)$, $^3J_{PC}$ = 9.72 Hz]; 126.24 [$C_{5'}$]; 124.89 [$C_{3'}$]; 122.86 [$C_5$]; 122.03 [$C_3$]; 80.06 [$C_{Cp}$]; 26.99 [$C_8$]. $^{31}P\{^1H\}$ NMR [$(CD_3)_2CO$, 161.97 MHz] $\delta$/ppm: 50.80 [s, $PPh_3$]. FT-IR [KBr, $cm^{-1}$]: 3106-3054 ($\nu_{C-H}$, aromatic rings), 2919 ($\nu_{C-H}$, -$COCH_3$), 1691 ($\nu_{C=O}$, -$COCH_3$), 1536-1363 ($\nu_{C=N}$ + $\nu_{C=C}$, aromatic rings + $\delta_{C-H}$, -$COCH_3$), 1263 ($\nu CF_3SO_3$), 1222-700 ($\delta_{C-H}$, aromatic rings). Elemental analysis (%) found: C, 55.5: H, 3.9; N, 3.5; S, 4.0. Calc. for $C_{36}H_{30}RuF_3N_2O_4PS$ (775.74 g/mol): C, 55.7; H, 3.9; N, 3.6; S, 4.1. ESI-MS: m/z calcd for $C_{35}H_{30}RuN_2OP$ (627,11 u) $[M]^+$ = 627.1, found = 627.3. UV-vis [dichloromethane, $\lambda_{max}$/nm ($\varepsilon$/$M^{-1}.cm^{-1}$)]: 265 (sh), 307 ($2{,}04\times10^4$), 355 (sh), 441 ($7{,}34\times10^3$), 505 (sh).

**X-ray crystallography**

Crystals of complexes **1**, **3**, and **4** suitable for X-ray diffraction studies were mounted on a loop with Fromblin protective oil. X-ray diffraction data were collected on a Bruker AXS-KAPPA APEX II diffractometer with graphite-monochromated radiation (Mo Ka, l = 0.71073 Å) at 150 K. Intensity data were corrected for Lorentz polarization effects. The X-ray generator was operated at 50 kV and 30 mA, and the X-ray data collection was monitored by the APEX program.[90] Empirical absorption correction using SABADS[91] was applied and data reduction was done with the SMART and SAINT programs. SHELXT2014[92] was used for structure solution, and SHELXL-2018[93] was used for full matrix least-squares refinement on $F^2$. Both programs are included in the package of programs WINGX-version 2020.2.[94] Non-hydrogen atoms were refined anisotropically. All the hydrogen atoms were inserted in the calculated positions and allowed to refine in the parent carbon atom. Compound 3 has a large void accessible in the unit cell that must be a disorder solvent molecule. Some disorder models have been attempted for various types of solvent molecules but none has been successful. The graphical representations were prepared using MERCURY4.2. A summary of the crystal data, structure solution and refinement parameters for the structures are given in Table S2.

**Table S2.** Data collection and structure refinement parameters for [Ru($\eta^5$-$C_5H_4CONHNH_2$)($PPh_3$)(2,2'-bipy)][$CF_3SO_3$] (**1**), [Ru($\eta^5$-$C_5H_4COCH_3$)($PPh_3$)$_2$Cl] (**3**) and [Ru($\eta^5$-$C_5H_4COCH_3$)($PPh_3$)(2,2'-bipy)][$CF_3SO_3$] (**4**)

| **Compound** | **1** | **3** | **4** |
|---|---|---|---|
| Empirical formula | $C_{35}H_{30}F_3N_4O_4PRuS$ | $C_{43}H_{39}ClOP_2Ru$ | $C_{36}H_{30}F_3N_2O_4PRuS$ |
| Formula weight | 791.73 | 768.18 | 775.72 |
| T (K) | 150(2) | 298(2) | 298(2) |
| Wavelength (Å) | 0.71073 | 0.71073 | 0.71073 |
| Crystal system | Monoclinic | Triclinic | Monoclinic |
| Space group | P 21/c | P -1 | P 21/n |
| a (Å) | 10.6705(6) | 10.5179(3) | 12.793(2) |
| b (Å) | 15.8832(11) | 11.2268(4) | 14.351(2) |
| c (Å) | 19.6104(12) | 19.1391(7) | 18.673(3) |
| $\alpha$ (°) | 90 | 85.0610(10) | 90 |
| β (°) | 92.973(2) | 75.2640(10) | 105.872(5) |
| γ (°) | 90 | 63.1770(10) | 90 |
| Volume (Å$^3$) | 3319.1(4) | 1949.41(12) | 3297.4(9) |
| Z | 4 | 2 | 4 |
| Calculated density (mg m$^{-3}$) | 1.584 | 1.309 | 1.563 |
| Absorption coefficient (mm$^{-1}$) | 0.647 | 0.584 | 0.648 |
| F (000) | 1608 | 788 | 1576 |
| θ Range for data collection (°) | 2.302 to 27.504 | 2.304 to 27.503 | 2.180 to 24.296 |
| Limiting indices | -13≤h≤3,<br>-18≤k≤20,<br>-25≤l≤25 | -12≤h≤13,<br>-14≤k≤14,<br>-24≤l≤24 | -14≤h≤14,<br>-16≤k≤16,<br>-21≤l≤21 |
| Reflections collected/unique | 30202 / 7612<br>[R(int) = 0.0557] | 48830 / 8897<br>[R(int) = 0.0361] | 53815 / 5318<br>[R(int) = 0.0874] |
| Completeness to θ (%) | 99.9 | 99.2 | 99.1 |
| Refinement method | Full-matrix least-squares on F^2 | | |
| Data/restraints/parameters | 7612 / 0 / 459 | 8897 / 0 / 433 | 5318 / 0 / 433 |
| Goodness-on-fit on $F^2$ | 1.009 | 0.936 | 1.134 |
| Final R indices [I > 2σ(I)] | R1 = 0.0358,<br>wR2 = 0.0859 | R1 = 0.0393,<br>wR2 = 0.1280 | R1 = 0.0507,<br>wR2 = 0.1274 |
| R indices (all data) | R1 = 0.0501,<br>wR2 = 0.0930 | R1 = 0.0460,<br>wR2 = 0.1344 | R1 = 0.0772,<br>wR2 = 0.1553 |
| Largest diff. peak and hole (eÅ)$^{-3}$ | 0.645 and -0.48 | 1.678 and -0.420 | 0.851 and -0.841 |

**Table S3.** Selected bond lengths and torsion angles for [Ru($\eta^5$-$C_5H_4CONHNH_2$)($PPh_3$)(2,2'-bipy)][$CF_3SO_3$] (**1**), [Ru($\eta^5$-$C_5H_4COCH_3$)($PPh_3$)$_2$Cl] (**3**) and [Ru($\eta^5$-$C_5H_4COCH_3$)($PPh_3$)(2,2'-bipy)][$CF_3SO_3$] (**4**)

| **1** | | **3** | | **4** | |
|---|---|---|---|---|---|
| *Bond lengths (Å)* | | | | | |
| Ru(1)–Cp[a] | 1.8326(2) | Ru(1)–Cp[a] | 1.8570(2) | Ru(1)–Cp[a] | 1.8399(5) |
| Ru(1)–P(1) | 2.3213(7) | Ru(1)–P(1) | 2.3292(7) | Ru(1)–P(1) | 2.3401(15) |
| Ru(1)–N(3) | 2.072(2) | Ru(1)–P(2) | 2.3154(8) | Ru(1)–N(1) | 2.082(4) |
| Ru(1)–N(4) | 2.078(2) | Ru(1)–Cl(1) | 2.4457(7) | Ru(1)–N(2) | 2.081(4) |
| C(6) –O(1) | 1.233(3) | C(6)–O(1) | 1.223(4) | C(6)–O(1) | 1.213(7) |
| C(6) –N(1) | 1.331(4) | C(6)–C(7) | 1.499(5) | C(6)–C(7) | 1.498(9) |
| N(1)–N(2) | 1.425(4) | | | | |
| *Angles (°)* | | | | | |
| Cp[a]–Ru(1)–P(1) | 129.267(19) | Cp[a]–Ru(1)–P(1) | 122.667(19) | Cp[a]–Ru(1)–P(1) | 128.74(4) |
| Cp[a]–Ru(1)–N(3) | 127.51(6) | Cp[a]–Ru(1)–P(2) | 121.39(19) | Cp[a]–Ru(1)–N(1) | 127.94(12) |
| Cp[a]–Ru(1)–N(4) | 128.21(6) | Cp[a]–Ru(1)–Cl(1) | 122.64(2) | Cp[a]–Ru(1)–N(2) | 130.16(13) |
| C(1)–C(6)–O(1) | 121.5(3) | C(1)–C(6)–O(1) | 120.5(3) | N(1)–Ru(1)–N(2) | 76.48(18) |
| P(1)–Ru(1)–N(3) | 89.97(6) | C(1)–C(6)–C(7) | 117.5(3) | C(1)–C(6)–C(7) | 116.2(6) |
| P(1)–Ru(1)–N(4) | 88.51(6) | O(1)–C(6)–C(7) | 122.0(3) | C(1)–C(6)–O(1) | 120.6(6) |
| N(3)–Ru(1)–N(4) | 77.12(8) | P(1)–Ru(1)–P(2) | 99.15(3) | O(1) –C(6)–C(7) | 123.3(6) |
| C(6)–N(1)–N(2) | 120.1(2) | P(1)–Ru(1)–Cl(1) | 93.24(3) | P(1)–Ru(1)–N(1) | 88.63(13) |
| O(1) –C(6)–N(1) | 120.7(3) | P(2)–Ru(1)–Cl(1) | 89.90(3) | P(1)–Ru(1)–N(2) | 88.11(13) |

**Stability in organic and aqueous medium**

The stability of complexes **1**, **4**, **6** and **7** was evaluated in 100% DMSO(the co-solvent used in biological assays) and 5%DMSO/DMEM (Dulbecco's Modified Eagle Medium) over 24 h by UV-vis spectroscopy on a Jasco V-560 spectrometer (260 – 900 nm), using quartz cuvettes with a 1 cm optical path, and in 20%DMSO/$D_2O$ by $^1$H NMR spectroscopy using a BrukerAvance400 spectrometer working on 400.13 MHz, over 48 h. For the UV-vis experiments, solutions of the complexes in dimethyl sulfoxide or 95 % cell culture medium DMEM+GlutaMAX-I : 5 % dimethyl sulfoxide were prepared at appropriate concentrations ($5.4\times10^{-5}$ – $8.1\times10^{-5}$ M) and analysed at t = 0 h, 0.25 h, 0.5 h, 0.75 h, 1 h, 2 h, 3 h, 4 h, 5 h, 6 h, and 24 h. In between measurements, the samples were kept at room temperature, and protected from light. The variation of the maximum absorbance over time was calculated for the most representative bands of each complex ($\pi\rightarrow\pi^*$ transitions and MLCT bands). For the NMR experiments: solutions of the four complexes in 80% $D_2O$/20% DMSO-$d_6$ were prepared at 2.0 mM and analyzed at t = 0 h, 1 h, 2 h, 3 h, 4 h, 5 h, 6 h, 24 h and 48 h. The samples were kept at room temperature and protected from light in between measurements. Upon competition of the assay, the spectra were analyzed regarding the number, chemical shift, integration, and multiplicity of each $^1$H resonances for each complex.

**Octanol-water partition coefficients (logP)**

The lipophilicity of complexes **1**, **4** 6 and **7** and [Ru($\eta^5$-$C_5H_5$)($PPh_3$)(2,2'-bipy)][$CF_3SO_3$] (**TM34**) was estimated by the shake-flask method.[95] Prior to the experiments, *n*-octanol and distilled water

were vigorously mixed for 24 h at room temperature, to promote solvent saturation of both phases. The phases were separated, and the compounds were dissolved in the organic phase to prepare solutions at 5.7 x $10^{-5}$ M to 4.0 x $10^{-4}$ M. The solutions were equilibrated with water for 4 h in a mechanical shaker, at a phase ratio of 2 mL/2 mL (*n*-octanol/water). Then, the aqueous and octanol layers were carefully separated by centrifugation (5000 rpm, 10 min) and the UV-vis absorption spectra of the complexes in the *n*-octanol phase were recorded. The concentration of each sample was determined by using the calibration curve in *n*-octanol. The partition coefficient values were calculated according to the following equation:

$$\log P_{oct/water} = \log\left(\frac{[complex]_{oct}}{[complex]_{water}}\right)$$

where $\log P_{oct/water}$ represents the octanol-water partition coefficient, $[complex]_{oct}$ represents the concentration of the complex in the *n*-octanol phase, and $[complex]_{water}$ represents the concentration of the complex in the water phase. All experiments were performed in triplicate.

**Synthesis of peptides**

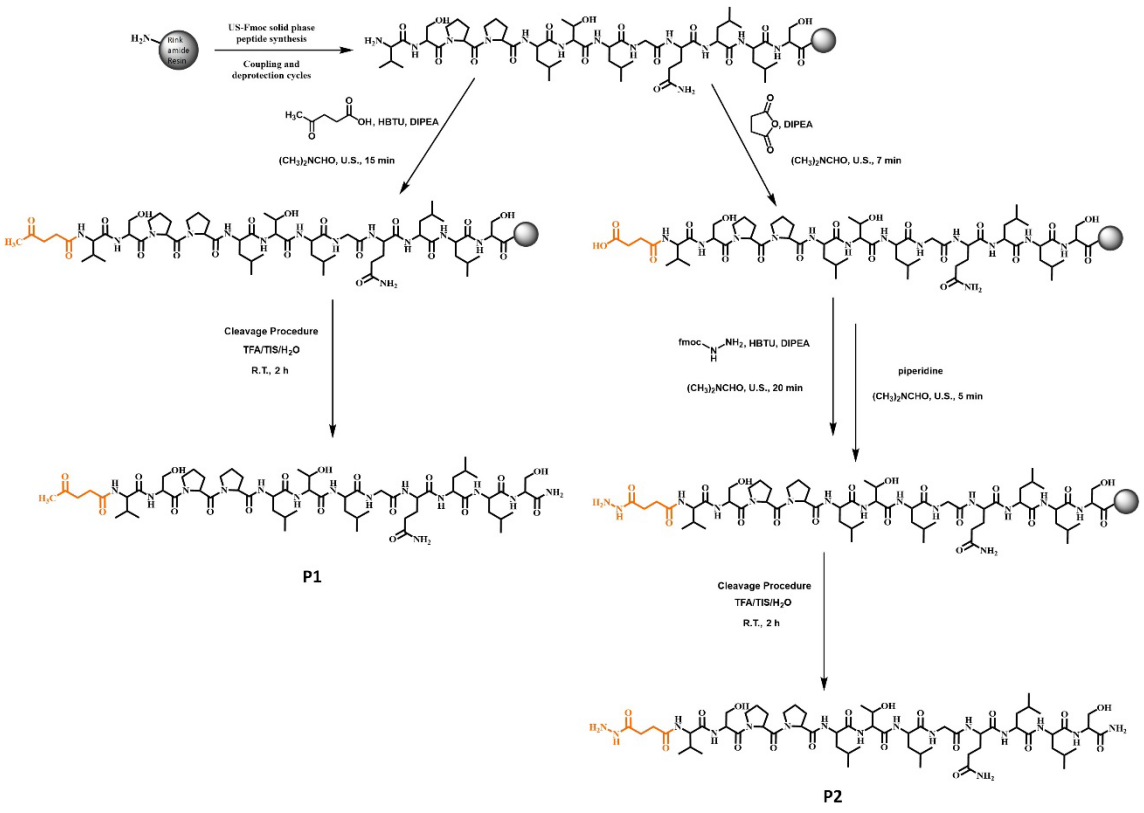


**Scheme S3.** Reaction schemes of the new peptides **P1** (left) and **P2** (right).

The peptides were prepared as *C*-terminal amides by ultrasound-assisted solid-phase peptide synthesis (US-SPPS)[96, 97] on a polypropylene reactor with an incorporated polyethylene frit and

removable cap (5 mL syringe, 25 µm pore, Multisyntech GmbH). The syntheses were carried out at 0.3 mmol scale on a Rink amide MBHA resin (100-200 mesh, molar substitution = 0.78 mmol/g), using standard 9-fluorenylmethyloxycarbonyl (Fmoc) L-amino acids with orthogonal sidechain protecting groups (*tert*-butyl for serine and threonine, trityl for glutamine). For the coupling of the 12 amino acids, it was used a 5-fold excess of the Fmoc-L-amino acids and *N,N,N',N'*-tetramethyl-*O*-(1*H*-benzotriazol-1-yl)uronium hexafluorophosphate (HBTU) in DMF, in the presence of 10-fold excess of *N*,*N*-diisopropylethylamine (DIPEA) for 5 to 25 min. Deprotection of Fmoc group from the *N*-terminal coupled amino acids was performed by treating the resin with a solution of piperidine in DMF (20 % v/v) for 5 min. Sonification during all coupling and deprotection steps was performed on an Elmasonic Elma S30H ultrasonic water bath (240 × 137 × 100 mm, 2.75 L) at a frequency of 37 KHz and controlled temperature at 30 ± 5 °C. The efficacy of each coupling and deprotection reaction was monitored by the colorimetric Kaiser test.[98] Upon final derivatization of the *N*-terminus with a ketone or a hydrazide spacing group in peptide P1 or P2, respectively (further details below), the peptides were fully deprotected and cleaved from the resin by reaction with a solution of trifluoroacetic acid/water/triisopropylsilane (95/2.5/2.5) during 2 h at room temperature (without sonification). Then, the peptides were precipitated with ice-cold diethyl ether, separated by centrifugation (5000 rpm, 10 min, 4 °C), purified by RP-HPLC, and lyophilized.

**$CH_3CO(CH_2)_2CONH$-VSPPLTLGQLLS-$CONH_2$ (P1)**

The VSPPLTLGQLLS peptide was prepared by US-SPPS as previously reported by us.[97] Upon conjugation of the last amino acid to the resin, the Fmoc group was removed as above described. Then, the resin was treated with a solution of a 5-fold excess of levulinic acid in DMF, in the presence of 5-fold excess of HBTU and a 10-fold excess of DIPEA for 15 min under sonication. Upon completing the synthesis, the peptide was full deprotected, cleaved from the resin, and precipitated as above described. The product was purified by RP-HPLC (method 4) and lyophilized overnight, affording a white powder. Purity: 99 %. ESI-MS: m/z calcd for $C_{61}H_{104}N_{14}O_{18}$ (1320.77 u) =1321.8 $[M+H]^+$; 661.4 $[M+2H]^{2+}$, found = 1322.2 $[M+H]^+$; 661.4 $[M+2H]^{2+}$. RP-HPLC: $t_R$ = 16.0 min (method 5); $t_R$ = 12.2 min (method 1).

**$NH_2NHCO(CH_2)_2CONH$-VSPPLTLGQLLS-$CONH_2$ (P2)**

The VSPPLTLGQLLS peptide was prepared by US-SPPS as previously reported by us.[97] Upon conjugation of the last amino acid to the resin, the Fmoc group was removed as above described. The resin was treated with an equimolar solution of succinic anhydride in DMF, in the presence of 2-fold excess of DIPEA for 7 min under sonication. Then, the resin was reacted with a solution of a 5-fold excess of 9-fluorenylmethyl carbazate in DMF, in the presence of 5-fold excess of HBTU and a 10-fold excess of DIPEA for 20 min under sonication. Upon completing the synthesis and removing the last Fmoc group, the peptide was full deprotected, cleaved from the resin, and precipitated as above described. The product was purified by RP-HPLC (method 6) and lyophilized overnight, affording a white powder. Purity: 98 %. ESI-MS: m/z calcd for $C_{60}H_{104}N_{16}O_{18}$ (1336.77 u) = 1337.8 $[M+H]^+$; 669.4 $[M+2H]^{2+}$, found =1338.2 $[M+H]^+$; 669.7 $[M+2H]^{2+}$. RP-HPLC: $t_R$ = 15.9 min (method 5); $t_R$ = 12.3 min (method 3).

**Synthesis of new pH-responsive ruthenium-peptide conjugates**

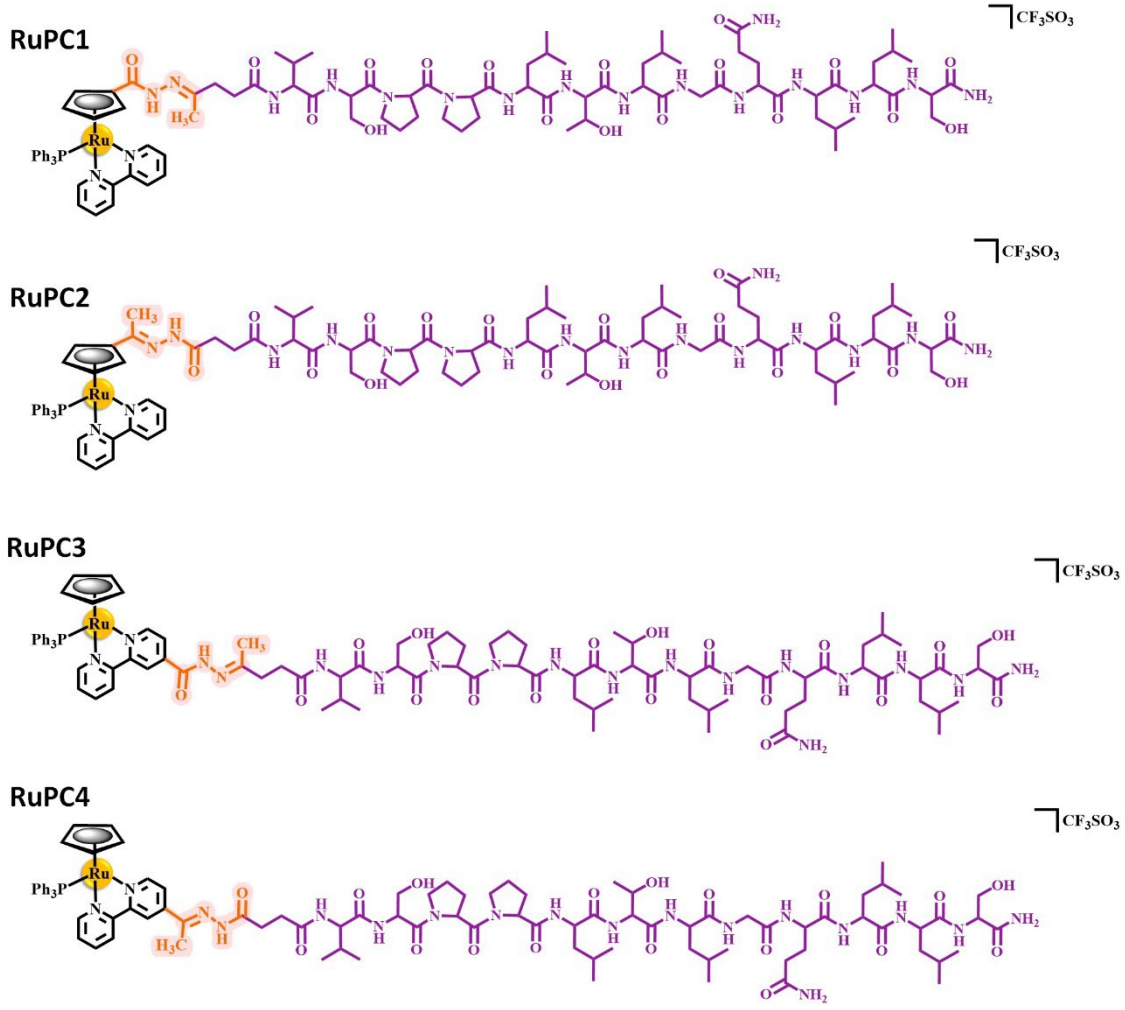


**Figure S1.** Chemical structures of Ruthenium-peptide conjugates

**(*E*,*Z*)-[Ru(η$^5$-$C_5H_4R$)($PPh_3$)(2,2'-bipy)][$CF_3SO_3$], R = $CONHNC(CH_3)(CH_2)_2CONH$-VSPPLTLGQLLS-$CONH_2$ (RuPC1):**

To a stirring solution of $CH_3CO(CH_2)_2CONH$-VSPPLTLGQLLS-$CONH_2$ (66 mg; 50 µmol) in 10 mL methanol, was added [Ru(η$^5$-$C_5H_4CONHNH_2$)($PPh_3$)(2,2'-bipy)][$CF_3SO_3$] (39 mg, 50 µmol) and trifluoroacetic acid (20 µL, 0.2 % v/v). The resulting mixture was stirred at room temperature for 20 h, acquiring dark orange colour. The solvent was removed under vacuum. The residue was

washed with diethyl ether (2 x 5 mL) and vacuum dried. The product was purified by RP-HPLC (method 7) and lyophilized overnight, affording an orange powder. Purity: 98 %. ESI-MS: m/z calcd for $C_{95}H_{132}RuPN_{18}O_{18}$ (1945.87 u) $[M+H]^{2+}$ = 973.4, found = 973.8. RP-HPLC: $t_R$ = 19.6 min (method 1).

**[Ru($\eta^5$-$C_5H_4R$)($PPh_3$)(2,2'-bipy)][$CF_3SO_3$], R = $C(CH_3)NNHCO(CH_2)_2$CONH-VSPPLTLGQLLS-$CONH_2$ (RuPC2):**

To a stirring solution of $NH_2NHCO(CH_2)_2$CONH-VSPPLTLGQLLS-$CONH_2$ (67 mg; 50 µmol) in 10 mL methanol, was added [Ru($\eta^5$-$C_5H_4COCH_3$)($PPh_3$)(2,2'-bipy)][$CF_3SO_3$] (39 mg, 50 µmol) and trifluoroacetic acid (20 µL, 0.2 % v/v). The resulting mixture was stirred at room temperature for 20 h, acquiring dark orange colour. The solvent was removed under vacuum. The residue was washed with diethyl ether (2 x 5 mL) and vacuum dried. The product was purified by RP-HPLC (method 7) and lyophilized overnight, affording an orange powder. Purity: 97 %. ESI-MS: m/z calcd for $C_{95}H_{132}RuPN_{18}O_{18}$ (1945.87 u) $[M+H]^{2+}$ = 973.4, found = 973.8. RP-HPLC: $t_R$ = 22.8 min (method 2).

**(*E*,*Z*)-[Ru($\eta^5$-$C_5H_5$)($PPh_3$)(2,2'-bipy-R)][$CF_3SO_3$], R = $CONHNC(CH_3)(CH_2)_2$CONH-VSPPLTLGQLLS-$CONH_2$ (RuPC3):**

To a stirring solution of $CH_3CO(CH_2)_2$CONH-VSPPLTLGQLLS-$CONH_2$ (60 mg; 45 µmol) in 10 mL methanol, was added [RuCp($PPh_3$)(bipy-$CONHNH_2$)][$CF_3SO_3$] (43 mg, 54 µmol) and trifluoroacetic acid (20 µL, 0.2 % v/v). The resulting mixture was stirred at room temperature for 22 h, acquiring red colour. The solvent was removed under vacuum. The residue was washed with diethyl ether (2 x 5 mL) and vacuum dried. The product was purified by RP-HPLC (method 8) and lyophilized overnight, affording a red powder. Purity: 91 %. ESI-MS: m/z calcd for $C_{95}H_{132}RuPN_{18}O_{18}$ (1945.87 u) $[M+H]^{2+}$ = 973.4, found = 973.9. RP-HPLC: $t_R$ = 19.3 min (method 3).

**(*E*,*Z*)-[Ru($\eta^5$-$C_5H_5$)($PPh_3$)(2,2'-bipy-R)][$CF_3SO_3$], R = $C(CH_3)NNHCO(CH_2)_2CON(H)$-VSPP LTLGQLLS-$CONH_2$ (RuPC4):**

To a stirring solution of $NH_2NHCO(CH_2)_2$CONH-VSPPLTLGQLLS-$CONH_2$ (67 mg; 50 µmol) in 10 mL methanol, was added [RuCp($PPh_3$)(AcBipy)][$CF_3SO_3$] (39 mg; 50 µmol) and trifluoroacetic acid (20 µL, 0.2 % v/v). The resulting mixture was stirred at room temperature for 20 h, acquiring red colour. The solvent was removed under vacuum. The residue was washed with diethyl ether (2 x 5 mL) and vacuum dried. The product was purified by RP-HPLC (method 9) and lyophilized overnight, affording a red powder. Purity: 96 %. ESI-MS: m/z calcd for $C_{95}H_{132}RuN_{18}O_{18}P$ (1945,87 u) $[M+H]^{2+}$ = 973.4, found = 973,8. RP-HPLC: $t_R$ = 19.4 min (method 10).

**NMR conformational study**

NMR sample preparation

NMR samples for peptide **P1** and conjugate **RuPC1** were prepared at approximately 1 mM concentration in aqueous solution ($H_2O/D_2O$ 9:1 v/v) at pH 7.4 containing 5 % deuterated DMSO. DMSO was necessary for solubility of the conjugate **RuPC1**. DSS was added as internal reference.

NMR spectra acquisition

NMR spectra were recorded on a Bruker AVNEO-600 spectrometer operating at a 600.13 MHz proton frequency and equipped with a cryoprobe. Calibration of probe temperature was done

using a methanol sample. As previously reported,[99] 1D and 2D spectra, i.e., total correlated spectroscopy (TOCSY), nuclear Overhauser enhancement spectroscopy (NOESY), and $^{1}H–^{13}C$ and $^{1}H$-$^{15}N$ heteronuclear single quantum coherence spectra (HSQC), were acquired using standard pulse sequences. $^{1}H$-$^{1}H$-TOCSY spectra were recorded at 20 and 60 ms mixing times, and $^{1}H$-$^{1}H$-NOESY spectra at 150 ms. $^{1}H–^{13}C$ and $^{1}H$-$^{15}N$-HSQC spectra were recorded at natural heteronuclear abundance. NMR spectra were acquired at 5°C. The TOPSPIN program (Bruker Biospin, Karlsruhe, Germany) was used to process NMR spectra. The $^{13}C$ and $^{15}N$ δ-values were indirectly referenced using the IUPAC-recommended $^{13}C/^{1}H$ and $^{15}N/^{1}H$ ratios.

NMR assignment

2D NMR spectra were analyzed using the NMRFAM-SPARKY software.[100] $^{1}H$, $^{13}C$ and $^{15}N$ chemical shifts for **P1** and conjugate **RuPC1** were assigned at 5°C following a standard sequential analysis[101] of 2D $^{1}H$-$^{1}H$-TOCSY, and $^{1}H$-$^{1}H$-NOESY spectra, that were examined in combination with the corresponding 2D $^{1}H–^{13}C$- and $^{1}H$-$^{15}N$-HSQC HSQC spectra. The assigned chemical shifts are listed in Tables S4 – S6. Helix populations were estimated from $^{1}H_a$ and $^{13}C_a$ chemical shifts as previously described.[102]

***In vitro* Drug release**

The ability of **RuPC1**, **RuPC2** and **RuPC3** to release the active ruthenium organometallic complex (**1**, **4** and **6**, respectively) in an aqueous solution at pH 6.8 and pH 7.4 was evaluated by analytical RP-HPLC on a system composed of a PerkinElmer Series 200 pump coupled to a PerkinElmer Series 200 degasser and a PerkinElmer Series 200 UV-vis detector (220 nm) using method 1, 2 or 3, respectively (Table S1). Solutions of the conjugates in 90 % phosphate buffer (10 mM in water, pH = 6.8 or 7.4) : 10 % acetonitrile were prepared at 0.5 mg/mL and analysed over a period of 50 h, with rigorous injections of 100 µL per measurement. In between analyses, the samples were kept at room temperature, and protected from light. For each measurement, the collected fractions were analysed by ESI-MS (positive ionization mode), on a Bruker HCT ESI/QITMS spectrometer (100 – 3000 m/z) using acetonitrile as solvent. The RP-HPLC chromatograms were normalised referring to the blank assays performed under the same experimental conditions. The absolute and relative values of the area under the curve (AUC) were determined for each compound detected by using the software package TotalChrom Navigator. The percentage of drug release was calculated according to the following equation:

$$\%DR_t = 100 - \left(\frac{AUC_t \times 100}{AUC_{t_0}}\right)$$

where $\%DR_t$ represents the amount of complex released (%) at a given time $t$; $AUC_t$ represents the absolute value of the area under the curve of the conjugate at time $t$; and $AUC_{t_0}$ represents the initial absolute value of the area under the curve of the conjugate at $t$ = 0 h.

**Cytotoxicity Assays**

The cytotoxicity of all conjugates, free complexes **1**, **4**, **6** and **7** and peptides **P1** and **P2** was evaluated in the human breast cancer cell lines MCF-7, MDA-MB-231, SK-BR-3, MDA-MB-134-VI (all from ATCC) and in normal human dermal fibroblasts HDF (Sigma-Aldrich). The assays were performed at pH 6.8 and 7.4 for all the breast cancer cell lines, and at pH 7.4 for the normal cell

line. The MCF-7, MDA-MB-231, SK-BR-3, and MDA-MB-134-VI cell lines were cultured in DMEM+Glutamax-I (Gibco) supplemented with 10 % fetal bovine serum (FBS) and 1 % antibiotics. The HDF cell line was cultured in fibroblasts growth medium (Sigma-Aldrich). All cells were maintained in a Heraeus incubator (37 °C) with a humidified atmosphere of 5 % $CO_2$. The cell viability was determined by the [3-(4,5-dimethylthiazol-2-yl)-2,5-diphenyltetrazolium bromide] (MTT) assay, which relies on the reduction of the yellow MTT to purple formazan by the mitochondrial dehydrogenases of metabolically viable cells. For the experiments, the cells were seeded in 96-well plates ($1\times10^4$ – $2\times10^4$ cells/200 µL medium) and allowed to adhere overnight. The compounds were previously dissolved in 83.1 % phosphate buffer (10 mM in water, pH = 6.8): 16.9 % dimethyl sulfoxide (DMSO) and/or 83.1 % phosphate buffer (10 mM in water, pH = 7.4): 16.9 % DMSO to prepare stock solutions at 1 – 2 mM, that were incubated at 37 °C during 48 h prior to the assays. The compounds were then diluted in the cell culture medium to obtain working solutions in the range of 0.1 – 50 µM. For all the tested solutions, the final concentration of DMSO in the medium did not exceed 1 %, and at this concentration no cytotoxic effect was observed in the cells. After incubating the cells with the working solutions for 48 h at 37 °C, the medium was removed and 200 µL of MTT solution in phosphate buffer saline (0.5 mg/mL) were added to each well. After 3 h of incubation at 37 °C, the solution was removed, and the purple formazan formed inside the cells was then dissolved in 200 µL of DMSO. The cell viability (expressed as a % of control) was evaluated by measuring the absorbance at 570 nm, in a multi-well spectrophotometer (PowerWave Xs, Bio-Tek Instruments, USA). The $IC_{50}$ values were calculated in GraphPad Prism 9.0. The results are shown as the mean ± standard deviation of two experiments performed with six technical replicates each.

Selectivity index values were calculated according to the following equation:

$$SI = \frac{IC_{50}\ (HDF_{7.4})}{IC_{50}\ (BC_{6.8})}$$

where $SI$ represents the selectivity index of a compound for a given breast cancer cell line over the normal HDF cell line; $IC_{50}\ (HDF_{7.4})$ represents the $IC_{50}$ value (µM) of that compound determined at pH 7.4 in the HDF cell line; and $IC_{50}\ (BC_{6.8})$ represents the $IC_{50}$ value (µM) of that compound determined at pH 6.8 in the breast cancer cell line understudy.

**Computational methods**

**Density Functional Theory**

Density functional theory (DFT) calculations were performed using the Gaussian 16 software package[103] and structural representations were generated with *CYLview*.[104] All the geometry optimizations were carried out using the hybrid meta-GGA functional M06-2X developed by Truhlar and co-workers[105] and a mixed basis set of SDD for ruthenium and 6 31G(d,p) for all other atoms. For ruthenium additional effective core potential was employed. All of the optimized geometries were verified by frequency computations as minima (zero imaginary frequencies). Single-point energy calculations on the optimized geometries were then evaluated using the same functional and a mixed basis set of SDD for ruthenium and the valence triple-zeta Def2 TZVPP for all other atoms. The free energy values presented along the SI were derived from the electronic energy values obtained at the M06-2X/def2-TZVPP,SDD(Ru)//M06-2X/6-

31G(d,p),SDD(Ru) level, and corrected by using the thermal and entropic corrections based on structural and vibration frequency data calculated at the M06-2X/6-31G(d,p),SDD(Ru) level.

**Molecular Dynamics**

**TM34** parameters were adopted from a previous study.[85] Complexes **1** and **4** were built by modifying the **TM34** using Pymol v. 2.5.[106] The topologies were obtained by submitting the substituted group (Cp) fragment to the Automated Topology Builder and Repository (ATB).[107] The optimized geometry and electrostatic potential (ESP) of each derivative were calculated with Gaussian 09[103] using the B3LYP functional[108 – 110] and the 6-31G** basis set[111] for all atoms except ruthenium, which used the Stuttgart/Dresden effective core potential basis set.[112] The atomic partial charges calculated by the ATB web server were substituted with those obtained from the RESP protocol.[85]

The simulations were carried out with GROMACS 2020.6[113] and GROMOS 54A7 force field, [114] using the SPC water model.[115] The starting configurations were obtained by placing the compound in the water phase (~6000 water molecules) of a previously equilibrated lipid bilayer of 128 1-palmitoyl-2-oleoyl-sn-glycero-3-phosphocholine (POPC) molecules. We used the Parrinello-Rahman barostat[116 - 117] to keep semi-isotropic pressure at 1.0 bar with a compressibility of $4.5 \times 10^{-5}$ $bar^{-1}$ with a coupling constant of 2 ps and v-rescale thermostat[118] to maintain 310 K in the system, with a coupling constant of 0.1 ps. Electrostatic interactions were treated with the Particle mesh Ewald (PME) method, with a Verlet scheme using 0.9 nm cutoff for rlist, rcoulomb and rvdw parameters.[119] All bonds of the compounds and membrane were constrained using the P-LINCS algorithm,[120] while for water molecules we used the SETTLE algorithm.[120]

To correct all unfavorable interactions between the multiple components of the system (complexes, lipids and water), we performed several steps of minimization and initiation protocols. The minimization consisted of 2 steps of the steepest descent algorithm without and with LINCS constraints on all bonds. The initiation protocol consisted also of 2 MD simulation steps. In the first step (50 ps), we generated all velocities in the system, while keeping a constant volume (NVT). Here, both membrane and compound were position-restrained (k = 1000 kJ $mol^{-1}$ $nm^{-2}$). In the second step (100 ps), we employed a semi-isotropic pressure coupling (NPT) on the system using the same solute position restraints as in the previous step. Five replicates of 1 µs were performed for each complex. Membrane insertion equilibrium was reached after 200 ns, except for replicate 3 of complex **1** which was considered equilibrated only after 350.

Unrestrained MD methods only allow us to sample conformations attainable within the limited simulation time available. With enhanced sampling methods, such as Umbrella Sampling (US),[122] we can force the compound to sample very unfavorable regions of the membrane. This is done by applying a pulling bias potential (pull code) along the z-axis (membrane normal vector), holding the compound at a specific distance to the center of the membrane (defined as our reference point). In this scheme, the distance to the membrane center is sliced in umbrellas and a starting conformation is assigned to each one of them. We used Steered MD (sMD) to generate those starting configurations of the different systems. In sMD, the compounds were placed at the water phase and slowly pulled to the membrane center using a force constant of 1000 kJ $mol^{-1}$ $nm^{-2}$ and a pulling rate of 0.05 nm/ns. Both in sMD and the US simulations, the pulling was performed on the ruthenium atom of the complexes and the reference was the last

atoms of each lipid tail, at the membrane center. The system was divided into 38 umbrellas, each corresponding to a certain insertion depth from 0.0 to 3.7 nm (0.1 nm step) measured from the membrane center (Figure S10). We observed that, in one simulation of umbrella 0.0, the compound established an unexpected contact with the opposite lipid monolayer. Since it may have been promoted by our sMD protocol, we just substituted its initial conformation with the one used in umbrella 0.1 and allowed the system to quickly equilibrate. We performed 3 replicates of 200 ns for all complexes in each of those 38 umbrellas and considered the systems to be equilibrated after 50 ns, disregarding the initial segments.

MD membrane insertion analysis was calculated using as reference the average z positions of phosphorous atoms of the interacting lipid monolayer. Independent of the monolayer, we considered that the water phase corresponds to positive values while the lipid membrane interior has negative values. The quantification of the local deformation in the lipid monolayer was calculated using the MembIT tool[123] as the difference between average monolayer bulk thickness (phosphate groups located >1.5 nm away from the compound) and average local monolayer thickness (phosphate groups within 0.5 nm). Angle analysis was performed using GROMACS 2020.6 gangle analysis tool.[113] We defined the reference vector as the membrane normal, and the vector between the ruthenium atom and the phosphorus atom from the triphenylphosphine group. The tumbling property was calculated using the previous angles and by creating 3 angle sectors ([0,60]=q1, [60,120]=q2 and [120,180]=q3) to count how many times the complexes shift from q1 to q3 or from q3 to q1, which corresponds to half a tumbling. The potential of mean force (PMF) profiles were calculated with the weighted histogram analysis method (WHAM),[124] which is part of the GROMACS 2020.6 package.[113] The membrane permeability coefficients were calculated with the Inhomogeneous Solubility-Diffusion Model (ISDM) using the PMF profile.[119, 125-127] The permeability coefficients error values were calculated using the Jackknife method.[128,129] This leave-one-out strategy groups our three replicates in pairs (1-2, 1-3, 2-3) and estimates the error associated with using the information from the complete sampling.

All graphics and images were created using gnuplot[130] and PyMOL.[107]

**Results and Discussion**

## NMR conformational study

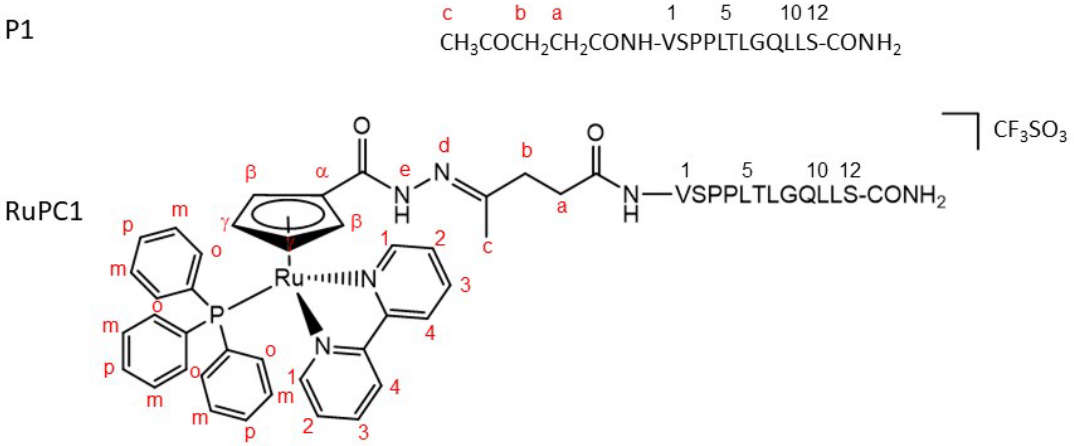


**Figure S2.** Sequences of peptide **P1** and conjugate **RuPC1**. Atoms for the conjugate moiety are labelled and residue numbers are indicated for the peptide moiety.

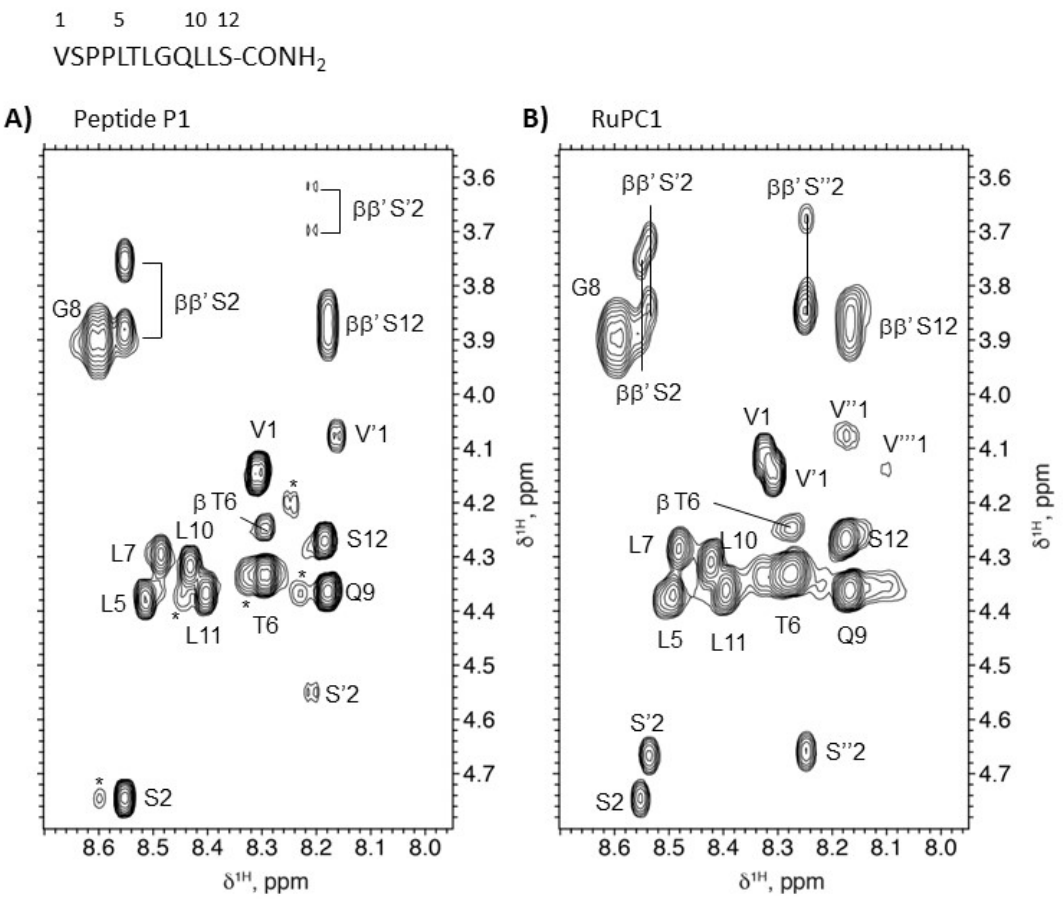


**Figure S3.** 2D $^{1}H$-$^{1}H$-TOCSY spectra for (**A**) **P1** and (**B**) **RuPC1** in aqueous solution ($H_2O/D_2O$ 9:1 v/v) at pH 7.4 containing 5 % deuterated DMSO at 5°C. Cross-peaks between $^{1}H_{\alpha}$ and $^{1}H_N$ amide protons are labeled. Some cross-peaks between $^{1}H_{\beta}$ and $^{1}H_N$ amide protons are also seen. Assigned minor species in **P1** are indicated as V'1 and S'2. Unassigned cross-peaks for minor species in **P1** are indicated by asterisks. The second major species in **RuPC1** is indicated by V'1 and S'2, and the minor species as V''1, V'''1 and S''2. Peptide sequence indicating residue numbering is shown at the top.

**Table S4.** $^{1}H$, $^{13}C$ and $^{15}N$ chemical shifts (ppm, from DSS) for **P1** in aqueous solution ($H_2O/D_2O$ 9:1 v/v) at pH 7.4 containing 5 % deuterated DMSO and at 5°C. Chemical shifts assigned for Val 1 and Ser 2 of a minor species (either *cis* Pro 3 or *cis* Pro 4) are shown in italics.

| Residue | $^{1}H_N$ | $^{15}N$ | $^{1}H_\alpha$ | $^{13}C_\alpha$ | $^{1}H_\beta$ | $^{13}C_\beta$ | Other |
|---|---|---|---|---|---|---|---|
| $CH_3CO$ a | --- | --- | 2.20 | 31.9 | | | |
| $CH_2$-$CH_2$ b,c | --- | --- | 2.52, 2.57 | 31.8 | 2.85,2.85 | 40.7 | |
| Val 1 | 8.31 | 123.5 | 4.14 | 62.0 | 2.07 | 32.9 | $^{1}H_\gamma$ 0.93; $^{13}C_\gamma$ 20.3; $^{1}H_{\gamma'}$ 0.93; $^{13}C_{\gamma'}$ 21.1 |
| Val'1 | *8.16* | --- | *4.08* | --- | | | *$^{1}H_\gamma$ 0.93; $^{1}H_{\gamma'}$ 0.93* |
| Ser 2 | 8.55 | 121.9 | 4.74 | 56.6 | 3.75,3.88 | 63.1 | |
| Ser'2 | *8.21* | --- | *4.55* | --- | *3.62,3.70* | --- | |
| Pro 3 | --- | --- | 4.70 | 61.7 | 1.90,2.35 | 30.9 | $^{1}H_{\gamma\gamma'}$ 2.02,2.05; $^{13}C_\gamma$ 27.4; $^{1}H_{\delta\delta'}$ 3.70,3.86; $^{13}C_\delta$ 50.7 |
| Pro 4 | --- | --- | 4.42 | 62.9 | 1.89,2.29 | 32.0 | $^{1}H_{\gamma\gamma'}$ 2.03,2.03; $^{13}C_\gamma$ 27.4; $^{1}H_{\delta\delta'}$ 3.64,3.82; $^{13}C_\delta$ 50.4 |
| Leu 5 | 8.51 | 122.7 | 4.38 | 55.3 | 1.55,1.65 | 42.4 | $^{1}H_\gamma$ 1.65; $^{13}C_\gamma$ 27.0; $^{1}H_\delta$ 0.88; $^{1}H_{\delta'}$ 0.93 |
| Thr 6 | 8.29 | 115.2 | 4.33 | 61.5 | 4.27 | 70.1 | $^{1}H_{\gamma2}$ 1.20; $^{13}C_{\gamma2}$ 21.7; $^{1}H_{\gamma1}$ 5.84 |
| Leu 7 | 8.49 | 124.5 | 4.29 | 56.0 | 1.62,1.66 | 42.4 | $^{1}H_\gamma$ 1.65; $^{13}C_\gamma$ 27.0; $^{1}H_\delta$ 0.88; $^{1}H_{\delta'}$ 0.93 |
| Gly 8 | 8.60 | 109.3 | 3.90 | 45.6 | | | |
| Gln 9 | 8.18 | 120.1 | 4.27 | 56.1 | 2.06,2.06 | 29.6 | $^{1}H_{\gamma\gamma'}$ 2.34,2.34; $^{13}C_\gamma$ 34.0; $^{1}H_{\varepsilon\varepsilon'}$ 6.95,7.77; $^{15}N_\varepsilon$ 112.8 |
| Leu 10 | 8.43 | 123.5 | 4.32 | 55.6 | 1.61,1.69 | 42.2 | $^{1}H_\gamma$ 1.68; $^{13}C_\gamma$ 27.1; $^{1}H_\delta$ 0.88; $^{1}H_{\delta'}$ 0.93 |
| Leu 11 | 8.40 | 122.7 | 4.37 | 55.3 | 1.60,1.69 | 42.2 | $^{1}H_\gamma$ 1.68; $^{13}C_\gamma$ 27.1; $^{1}H_\delta$ 0.88; $^{1}H_{\delta'}$ 0.93 |
| Ser 12 | 8.18 | 116.5 | 4.36 | 58.3 | 3.85,3.90 | 63.8 | |
| $CONH_2$ | 7.28,7.56 | 109.0 | | | | | |

**Table S5.** $^{1}H$, $^{13}C$ and $^{15}N$ chemical shifts (ppm, from DSS) for **RuPC1** in aqueous solution ($H_2O/D_2O$ 9:1 v/v) at pH 7.4 containing 5 % deuterated DMSO and at 5°C. Chemical shifts corresponding to the two major species (X and X') and to the minor species (X'' and X''') are listed. "nd" stands for not determined.

| Residue | $^{1}H_N$ | $^{15}N$ | $^{1}H_\alpha$ | $^{13}C_\alpha$ | $^{1}H_\beta$ | $^{13}C_\beta$ | Other |
|---|---|---|---|---|---|---|---|
| $CH_3CN$ a | --- | --- | 2.21 | 31.9 | | | |
| $CH_3CN$ a' | | | 2.40 | 32.9 | | | |
| $CH_2$-$CH_2$ b-c | --- | --- | 2.51, 2.57 | 31.7 | 2.86,2.86 | 40.7 | |
| $CH_2$-$CH_2$ b'-c' | | | 2.54, 2.60 | 34.3 | 2.55,2.55 | 36.4 | |
| Val 1 | 8.31 | 123.5 | 4.14 | 62.0 | 2.07 | 32.9 | $^{1}H_\gamma$ 0.93; $^{13}C_\gamma$ 20.2; $^{1}H_{\gamma'}$ 0.93; $^{13}C_{\gamma'}$ 21.2 |
| Val' 1 | 8.32 | --- | 4.11 | 62.0 | 2.00 | 32.9 | $^{1}H_\gamma$ 0.86; $^{13}C_\gamma$ 20.3; $^{1}H_{\gamma'}$ 0.87; $^{13}C_{\gamma'}$ 21.1 |
| Val''1 | *8.17* | --- | *4.07* | --- | | | |
| Val'''1 | *8.10* | --- | *4.14* | --- | | | |
| Ser 2 | 8.55 | 121.9 | 4.75 | 56.6 | 3.75,3.88 | 63.1 | |
| Ser'2 | 8.54 | --- | 4.67 | 56.6 | 3.72,3.83 | | |
| Ser''2 | *8.25* | --- | *4.66* | --- | *3.68,3.85* | --- | |
| Pro 3 | --- | --- | 4.69 | 61.7 | 1.89,2.35 | 30.9 | $^{1}H_{\gamma\gamma'}$ 2.02,2.05; $^{13}C_\gamma$ 27.4; $^{1}H_{\delta\delta'}$ 3.71,3.85; $^{13}C_\delta$ 50.7 |
| Pro'3 | --- | --- | 4.65 | 61.6 | 1.88,2.32 | nd | $^{1}H_{\gamma\gamma'}$ 1.99,2.02; $^{13}C_\gamma$ nd $^{1}H_{\delta\delta'}$ 3.66,3.80; $^{13}C_\delta$ 50.7 |
| Pro''3 | --- | --- | *4.55* | | 1.85,2.25 | | |
| Pro 4 | --- | --- | 4.41 | 62.9 | 1.88,2.27 | 32.0 | $^{1}H_{\gamma\gamma'}$ 2.00,2.00; $^{13}C_\gamma$ 27.4; $^{1}H_{\delta\delta'}$ 3.64,3.80; $^{13}C_\delta$ 50.4 |
| Pro'4 | --- | --- | 4.39 | nd | 1.88,2.26 | nd | $^{1}H_{\gamma\gamma'}$ 2.00,2.00; $^{13}C_\gamma$ nd $^{1}H_{\delta\delta'}$ 3.60,3.77; $^{13}C_\delta$ 50.4 |
| Pro''4 | --- | --- | | | | | $^{1}H_{\delta\delta'}$ 3.57,3.75 |
| Leu 5 | 8.50 | 122.6 | 4.37 | 55.3 | 1.54,1.65 | 42.4 | $^{1}H_\gamma$ 1.63; $^{13}C_\gamma$ 27.0; $^{1}H_\delta$ 0.87; $^{1}H_{\delta'}$ 0.92 |
| Thr 6 | 8.28 | 115.1 | 4.33 | 61.4 | 4.25 | 70.1 | $^{1}H_{\gamma2}$ 1.20; $^{13}C_{\gamma2}$ 21.7 |
| Leu 7 | 8.48 | 124.4 | 4.29 | 56.0 | 1.62,1.66 | 42.2 | $^{1}H_\gamma$ 1.65; $^{13}C_\gamma$ 27.0; $^{1}H_\delta$ 0.87; $^{1}H_{\delta'}$ 0.92 |
| Gly 8 | 8.60 | 109.3 | 3.90 | 45.6 | | | |
| Gln 9 | 8.18 | 120.1 | 4.27 | 56.1 | 2.06,2.06 | 29.6 | $^{1}H_{\gamma\gamma'}$ 2.33,2.33; $^{13}C_\gamma$ 34.0; $^{1}H_{\varepsilon\varepsilon'}$ 6.95,7.77; $^{15}N_\varepsilon$ 112.7 |
| Leu 10 | 8.42 | 123.4 | 4.31 | 55.6 | 1.61,1.69 | 42.2 | $^{1}H_\gamma$ 1.67; $^{13}C_\gamma$ 27.0; $^{1}H_\delta$ 0.88; $^{1}H_{\delta'}$ 0.93 |
| Leu 11 | 8.40 | 122.7 | 4.36 | 55.3 | 1.60,1.69 | 42.2 | $^{1}H_\gamma$ 1.67; $^{13}C_\gamma$ 27.0; $^{1}H_\delta$ 0.87; $^{1}H_{\delta'}$ 0.92 |
| Ser 12 | 8.17 | 116.5 | 4.36 | 58.3 | 3.85,3.90 | 63.9 | |
| $CONH_2$ | 7.28,7.56 | 109.0 | | | | | |

**Table S6.** $^{1}H$ and $^{13}C$ chemical shifts (ppm, from DSS) for the conjugate moiety of **RuPC4** in aqueous solution ($H_2O/D_2O$ 9:1 v/v) at pH 7.4 containing 5 % deuterated DMSO and at 5°C.

| | | | | |
|---|---|---|---|---|
| **Bipy** | H1 | 9.28 | C1 | 158.1 |
| | H2 | 7.31 | C2 | 128.2 |
| | H3 | 7.81 | C3 | 139.5 |
| | H4 | 7.91 | C4 | 126.1 |
| **Bipy'** | H1 | 9.24 | C1 | 148.0 |
| | H2 | 7.31 | C2 | 128.2 |
| | H3 | 7.81 | C3 | 139.5 |
| | H4 | 7.91 | C4 | 126.1 |
| **Cp** | Hβ | 5.47 | Cβ | 85.6 |
| | Hγ | 5.62 | Cγ | 86.9 |
| **PPh3** | Horto | 7.04 | Corto | 135.7 |
| | Hmeta | 7.26 | Cmeta | 131.3 |
| | Hpara | 7.41 | Cpara | 133.2 |

**Table S7.** Chemical shift differences between the $^{13}C_\beta$ and $^{13}C_\gamma$ ($\Delta^{\beta\gamma} = \delta^{C\beta} - \delta^{C\gamma}$, ppm) of Pro residues in the major species observed for **P1** and **RuPC1** in aqueous solution ($H_2O/D_2O$ 9:1 v/v) at pH 7.4 containing 5 % deuterated DMSO at 5°C.

| **P1** | | | | **RuPC1** | | | |
|---|---|---|---|---|---|---|---|
| **Residue** | **$\delta^{C\beta}$, ppm** | **$\delta^{C\gamma}$, ppm** | **$\Delta^{\beta\gamma}$, ppm** | **Residue** | **$\delta^{C\beta}$, ppm** | **$\delta^{C\gamma}$, ppm** | **$\Delta^{\beta\gamma}$, ppm** |
| Pro 3 | 30.9 | 27.4 | 3.5 | Pro 3 | 30.9 | 27.4 | 3.5 |
| Pro 4 | 32.0 | 27.4 | 4.6 | Pro 4 | 32.0 | 27.4 | 4.6 |

**Table S8.** Averaged $\Delta\delta_{H\alpha}$ and $\Delta\delta_{C\alpha}$ values and estimated helix percentages for the major species of P3C and RuPC4 in aqueous solution ($H_2O/D_2O$ 9:1 v/v) at pH 7.4 containing 5 % deuterated DMSO and at 5°C. Percentage of helical structure was estimated from these values. [a] Error correspond to the standard deviation.

| **Peptide** | **Helical residues** | **$\Delta\delta_{H\alpha}$, ppm** | **% helix** | **$\Delta\delta_{C\alpha}$, ppm** | **% helix** | **Averaged % helix[a]** |
|---|---|---|---|---|---|---|
| **P1** | 7-9 | -0.05 | 13 | 0.56 | 18 | 16±3 |
| **RuPC1** | 7-9 | -0.06 | 14 | 0.56 | 18 | 16±2 |

**Cytotoxicity**

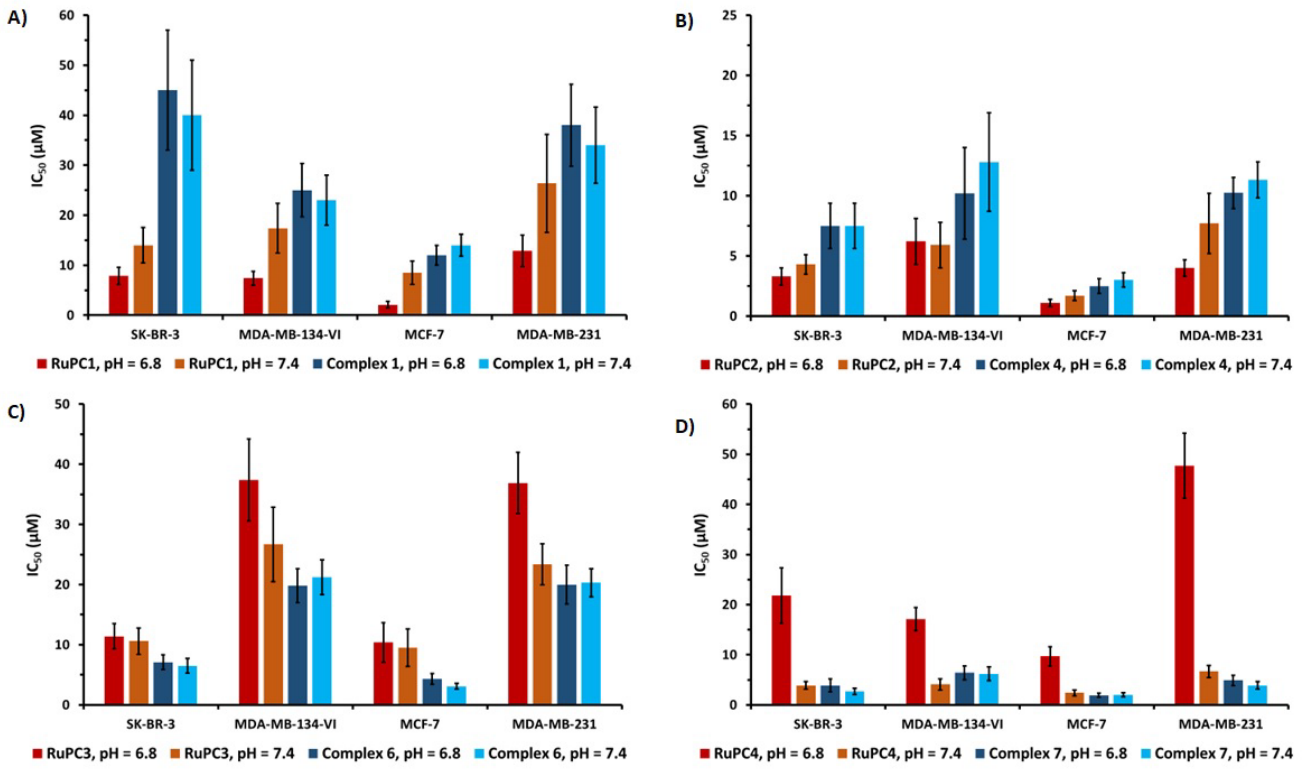


**Figure S4.** Cytotoxic activity expressed as IC50 values (μM) of (**A**) **RuPC1** and **complex 1**, (**B**) **RuPC2** and **complex 4**, (**C**) **RuPC3** and **complex 6**, (**D**) **RuPC4** and **complex 7**, the breast cancer cell lines SK-BR-3, MDA-MB-134-VI, MCF-7, and MDA-MB-231, after 48 h incubation determined upon previous incubation of the compounds in aqueous solutions at pH 6.8 and pH 7.4 for 48 h.

## *In vitro* Drug release

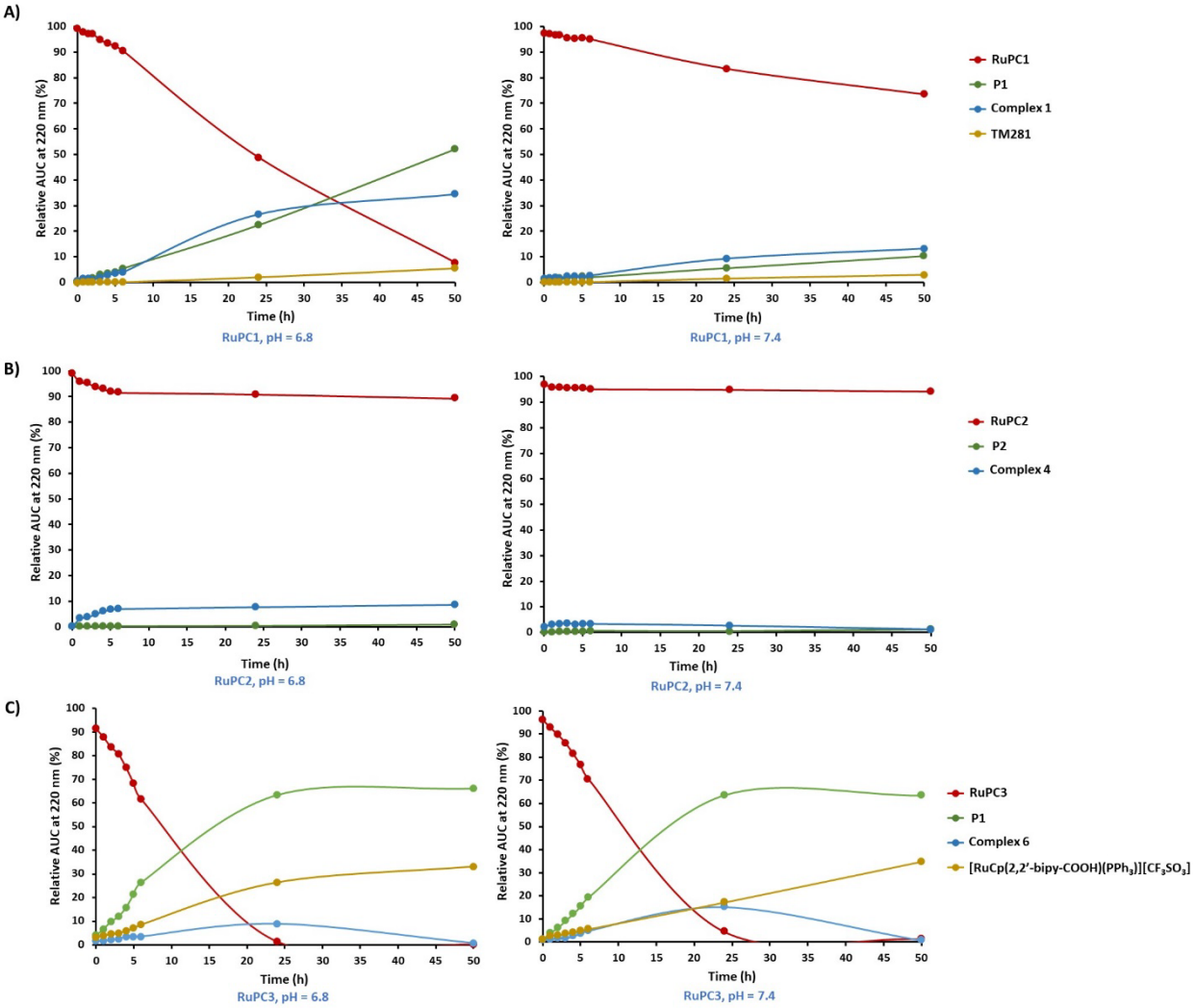


**Figure S5.** Relative area under the curve (AUC) *vs.* time detected at 220 nm (bottom) for **RuPC1 (A)**, **RuPC2 (B)** and **RuPC3 (C)** in phosphate buffer solutions at pH 6.8 (tumour microenvironment) and pH 7.4 (bloodstream/healthy tissues) over time.

## Density functional theory

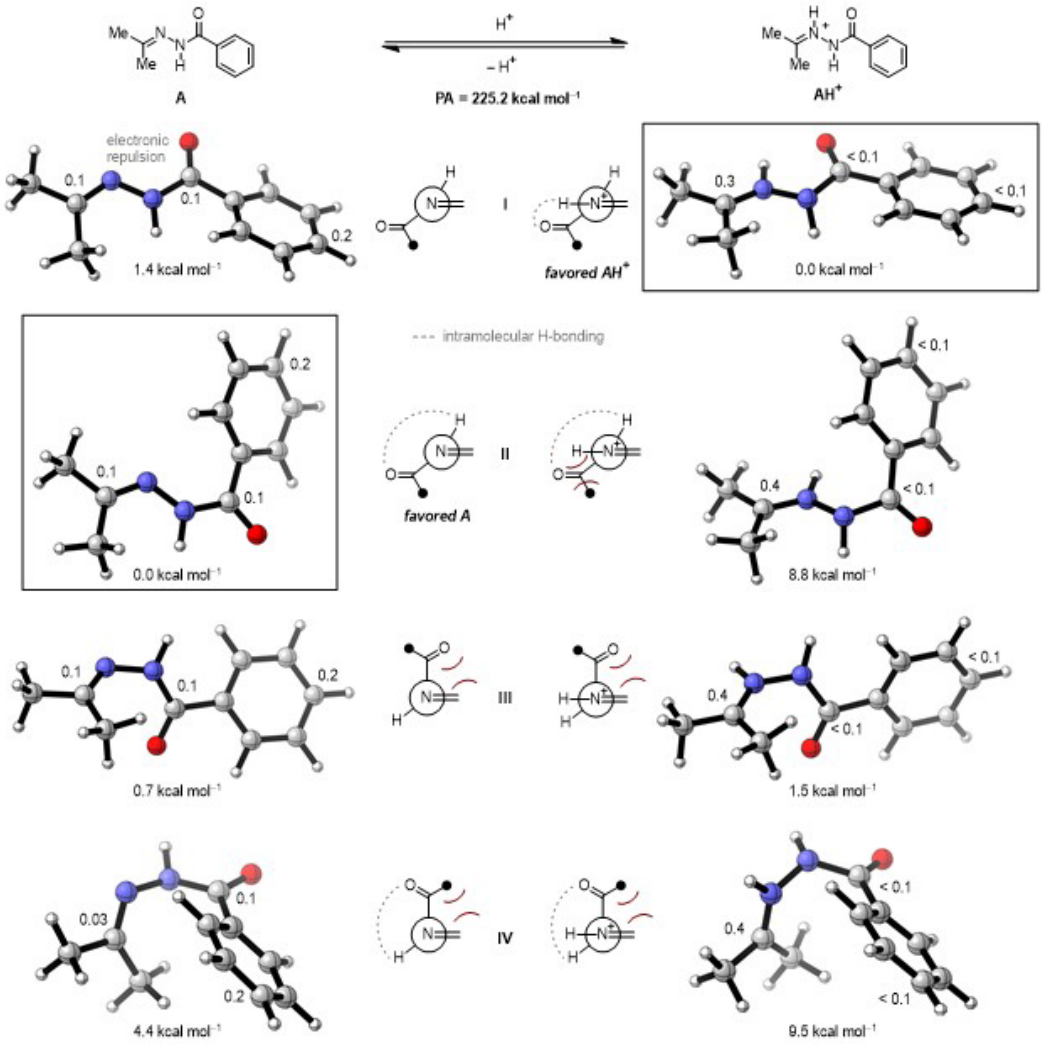


**Figure S6.** Conformational analysis study for the protonation of model substrate alkyl trans-hydrazone resulting from the condensation of acetone and benzohydrazide. Calculated Gibbs free energies at M06-2X/def2-TZVPP//M06-2X/6-31G(d,p) level of theory are presented in kcal $mol^{-1}$ relative to either the most stable neutral (A) or protonated species ($AH^+$). Selected fukui indices (f+) are shown next to electrophilic centers. Proton affinity was calculated using the most favored conformers. Initial guesses for geometry optimized conformers II, III and IV were obtained from I by rotating C-N amide bond, N-N bond, or both, respectively.

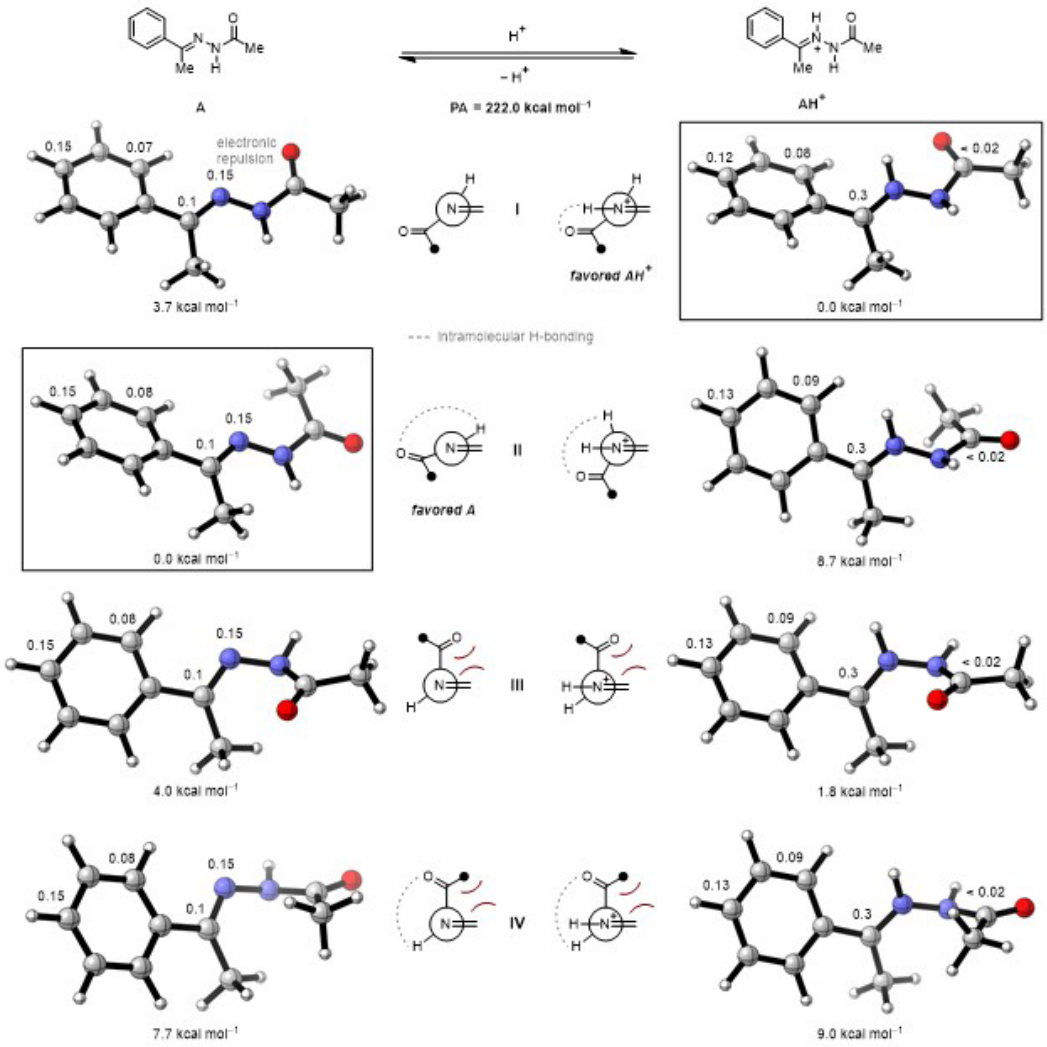


**Figure S7.** Conformational analysis study for the protonation of model substrate aryl trans-hydrazone resulting from the condensation of acetophenone and acetohydrazide. Calculated Gibbs free energies at M06-2X/def2-TZVPP//M06-2X/6-31G(d,p) level of theory are presented in kcal $mol^{-1}$ relative to either the most stable neutral (A) or protonated species ($AH^+$). Selected fukui indices (f+) are shown next to electrophilic centers. Proton affinity was calculated using the most favored conformers. Initial guesses for geometry optimized conformers II, III and IV were obtained from I by rotating C-N amide bond, N-N bond, or both, respectively.

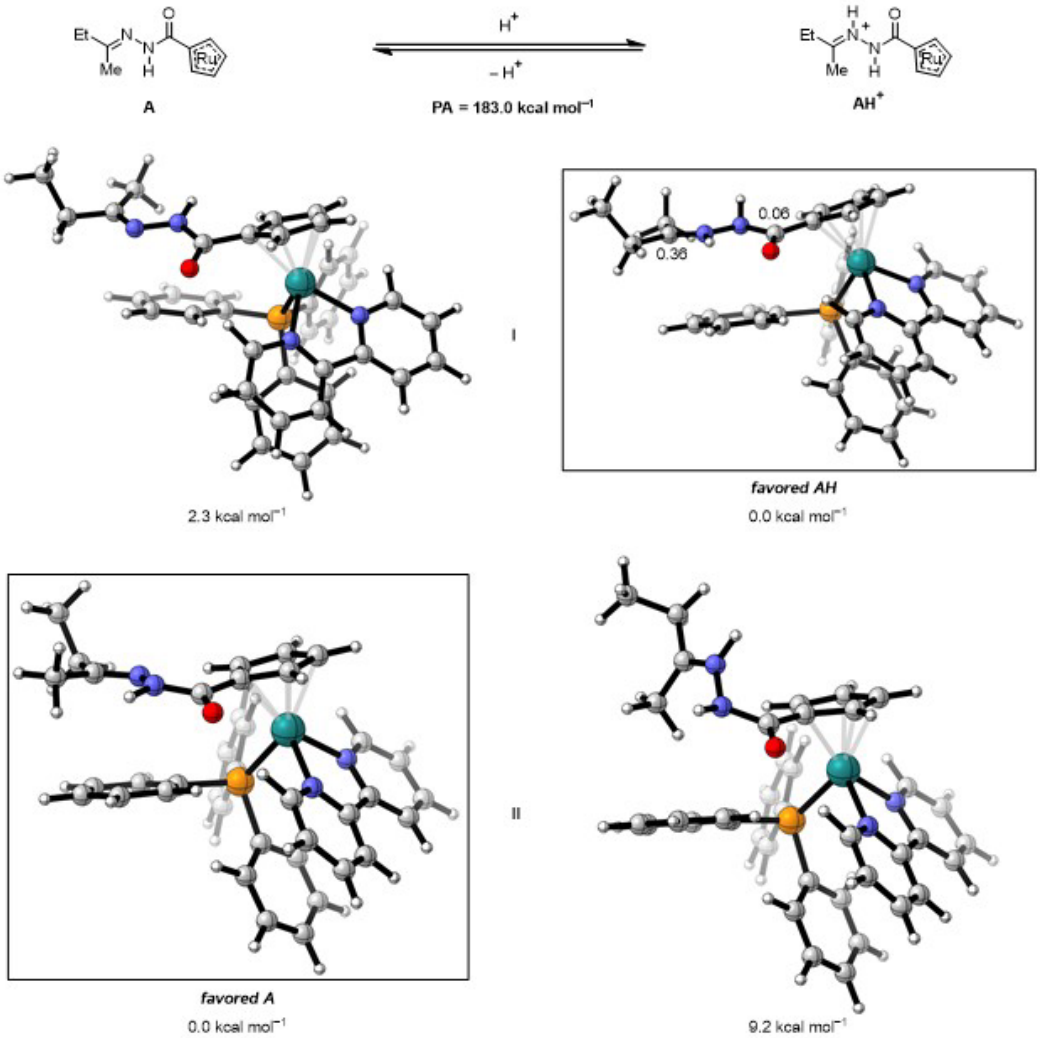


**Figure S8.** Protonation of truncated **RuPC1**. Calculated Gibbs free energies at M06-2X/def2-TZVPP,SDD(Ru)//M06-2X/6-31G(d,p),SDD(Ru) level of theory are presented in kcal $mol^{-1}$ relative to either the most stable neutral (A) or protonated species ($AH^+$). Proton affinity was calculated using the most favored conformers. Selected fukui indices (f+) are shown next to electrophilic centers.

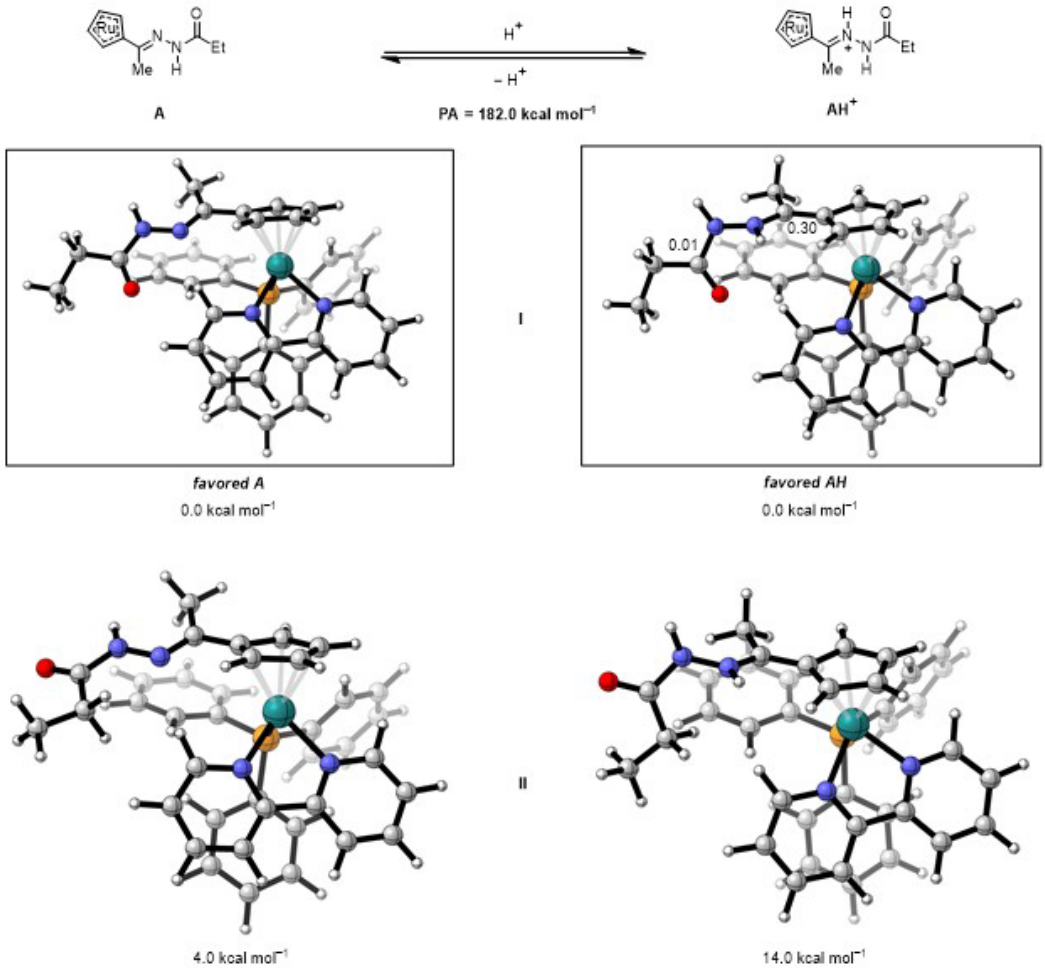


**Figure S9**. Protonation of truncated **RuPC2**. Calculated Gibbs free energies at M06-2X/def2-TZVPP,SDD(Ru)//M06-2X/6-31G(d,p),SDD(Ru) level of theory are presented in kcal $mol^{-1}$ relative to either the most stable neutral (A) or protonated species ($AH^+$). Proton affinity was calculated using the most favored conformers. Selected fukui indices (f+) are shown next to electrophilic centers.

**Table S9.** DFT computer proton affinities (PA) and fukui indices f+ for **RuPC1-2**.

| RuPC | ΔPA (kcal $mol^{-1}$) | $f^+$ ($C_{iminium}$) | $f^+$ ($C_{amide}$) |
|---|---|---|---|
| **1** | 1.0 | 0.36 | 0.06 |
| **2** | 0.0 | 0.30 | 0.01 |

## MD simulations

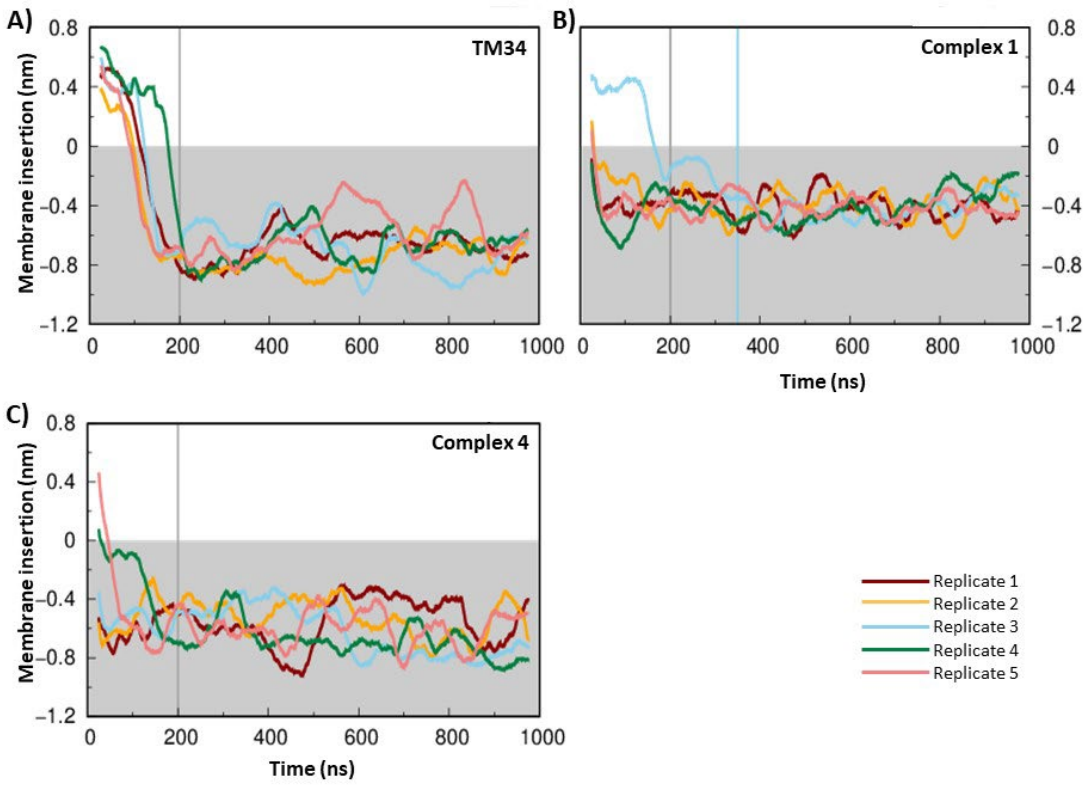


**Figure S10.** Membrane insertion profiles of (**A**) **TM34**, (**B**) complex **1** and (**C**) complex **4** over time plotted with a floating window of 10 ns to reduce local fluctuations. Membrane insertion was calculated using the average position of the phosphorus atoms of the lipid monolayer interacting with the compound as reference, along the membrane normal vector. Membrane is represented by the gray region. The vertical lines illustrate the equilibration times considered. With the exception of replicate 3 of complex **1**, that equilibrated after 350 ns, all replicates were considered equilibrated after 200 ns.

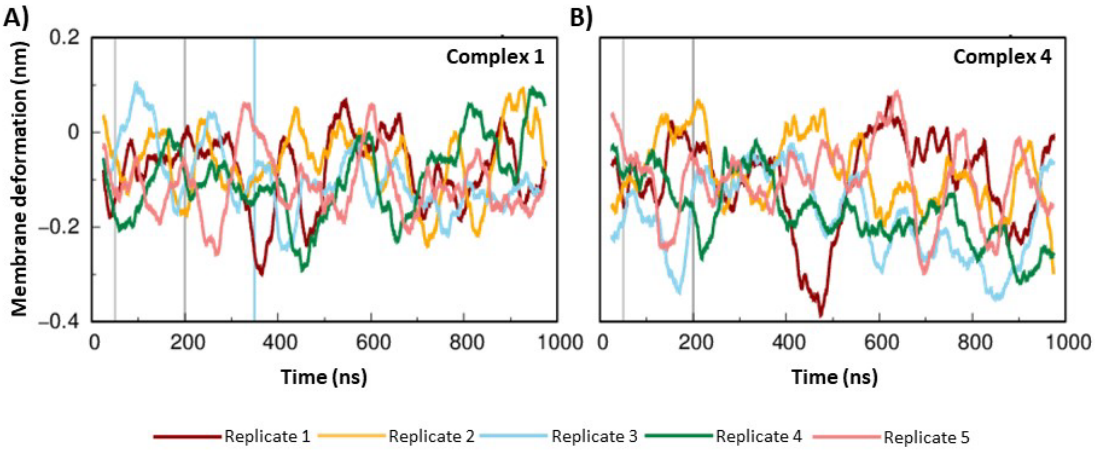


**Figure S11.** Local membrane deformation for (**A**) complex **1** and (**B**) complex **4**. Membrane deformation was calculated with the difference between local monolayer thickness (calculated with the phosphate groups of lipids at <0.5 nm from the compound) and bulk monolayer thickness (calculated with the phosphate groups of lipids at >1.5 nm from the compound). Deformation over time plotted with a floating window of 10 ns to reduce local fluctuations. The vertical lines illustrate the equilibration times considered. The membrane deformation property allowed us to evaluate the membrane integrity along the z axis. These results suggest that the interaction with the compound induces dynamic local deformations in the membrane, which can be positive, with the lipid heads rising above the unperturbed position; or negative, when the lipid head groups are dragged inward/downward. We observed moderate deformation in the local phosphate groups that are probably only stabilizing the compounds in their inserted positions.

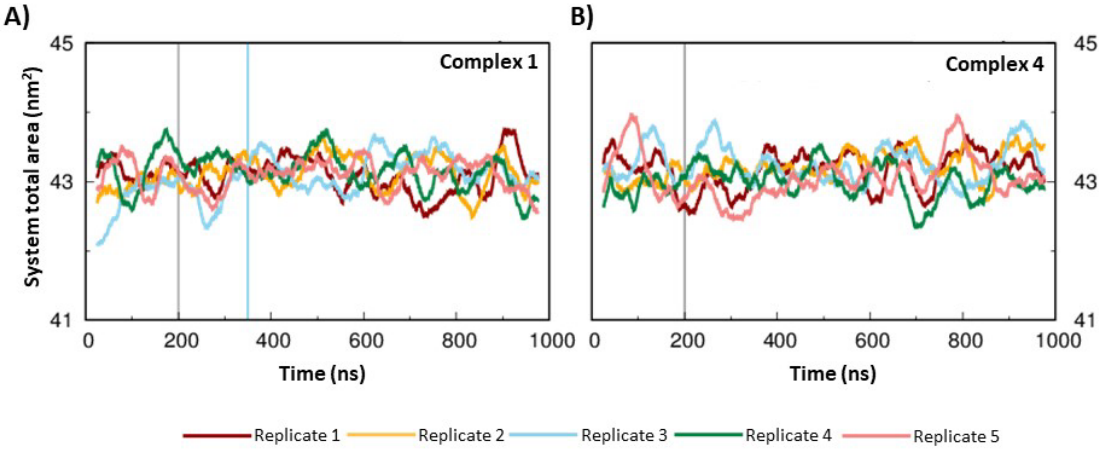


**Figure S12.** Total simulation box in the *xy* area over time of (**A**) complex **1** and (**B**) complex **4**. Plotted with a floating window of 10 ns to reduce local fluctuations. The vertical lines illustrate the equilibration times considered.

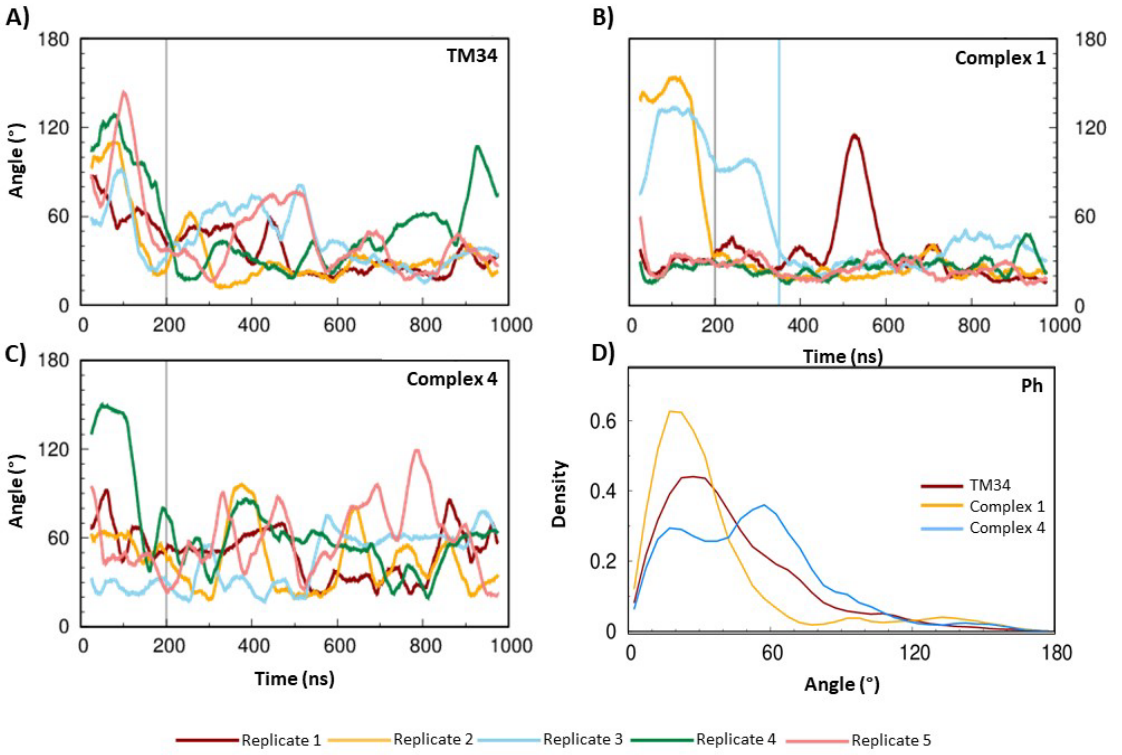


**Figure S13.** Orientation of the triphenylphosphine group of the compounds in study over time. Plotted with a floating window of 10 ns to reduce local fluctuations. The angle vector was defined starting on the ruthenium atom and ending in the phosphorus atom, along the membrane normal vector. The vertical lines illustrate the equilibration times considered. (Bottom right panel) Orientation of the triphenylphosphine group of the compounds in study. Normalized histogram was calculated using the angles from the equilibrated segments of all replicates of each compound. Both complexes show an orientation relative to the membrane normal similar to that of **TM34**, suggesting that functionalization of the Cp ring with a hydrazide or ketone group, does not influence this parameter. The triphenylphosphane (Ph) coligand keeps a strong preference towards the membrane center, while the Cp and bipy coligands are more accessible to the water phase and interact to a lesser extent with the membrane.

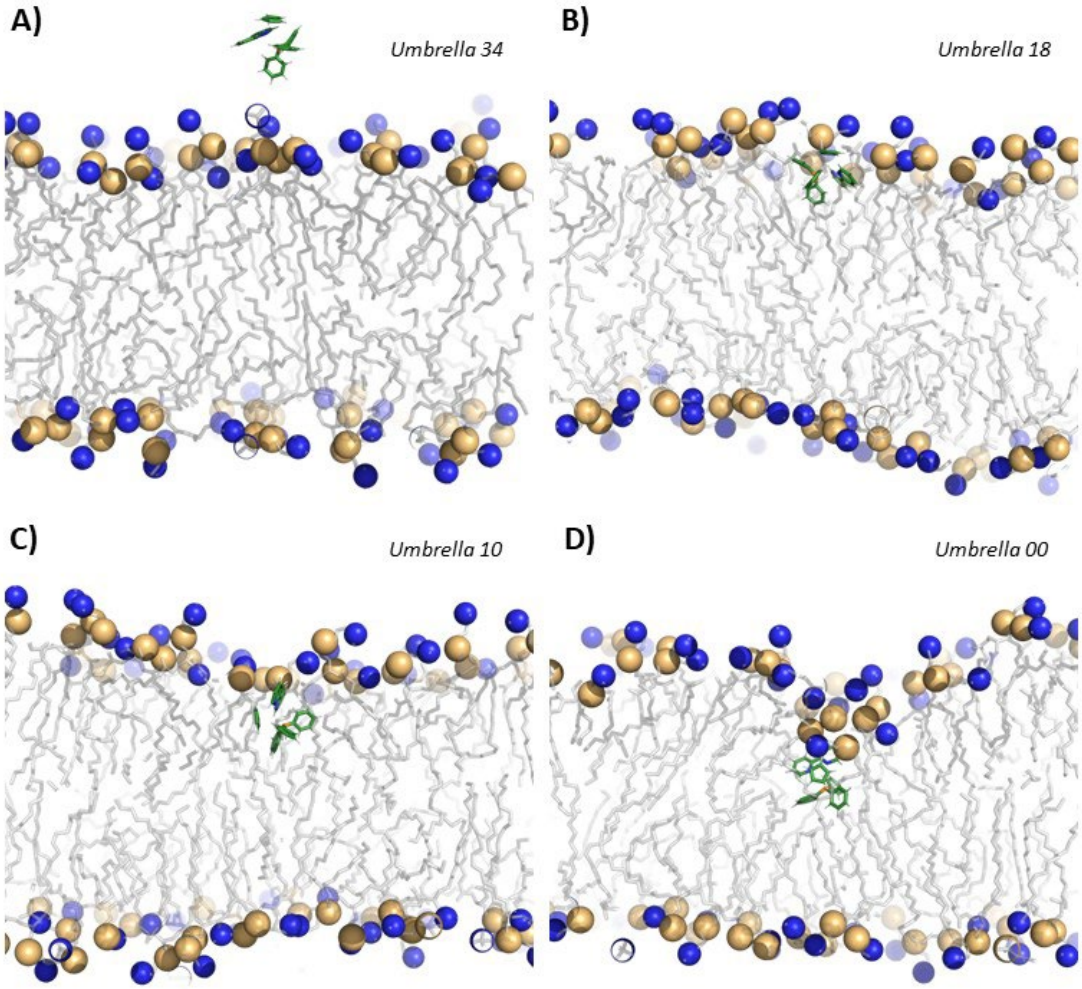


**Figure S14.** Representation of **TM34** conformations illustrating multiple umbrellas where the compound is at different insertion depths. (**A**) Umbrella 34, at 3.4 nm from the membrane center. In this umbrella the compound is in the water phase, not interacting with membrane. (**B**) Umbrella 18, at 1.8 nm from the membrane center. In this umbrella the compound is in interface between the water and membrane phases, interacting with both. (**C**) Umbrella 10, at 1.0 nm from the membrane center. In this umbrella the compound is in the membrane phase, bellow the phosphorous atom's average position. (**D**) Umbrella 00, at 0 nm from the membrane center. In this umbrella the compound is in the center of the membrane. Due to being high energy conformations, some umbrellas near this insertion depth developed inward membrane depressions, suspected to be caused by incomplete water desolvation. The POPC lipid tails are shown with gray sticks with the phosphorus and nitrogen atoms represented as spheres (yellow and blue, respectively). **TM34** is shown as sticks, where the C atoms are colored green. Water molecules were omitted for clarity.

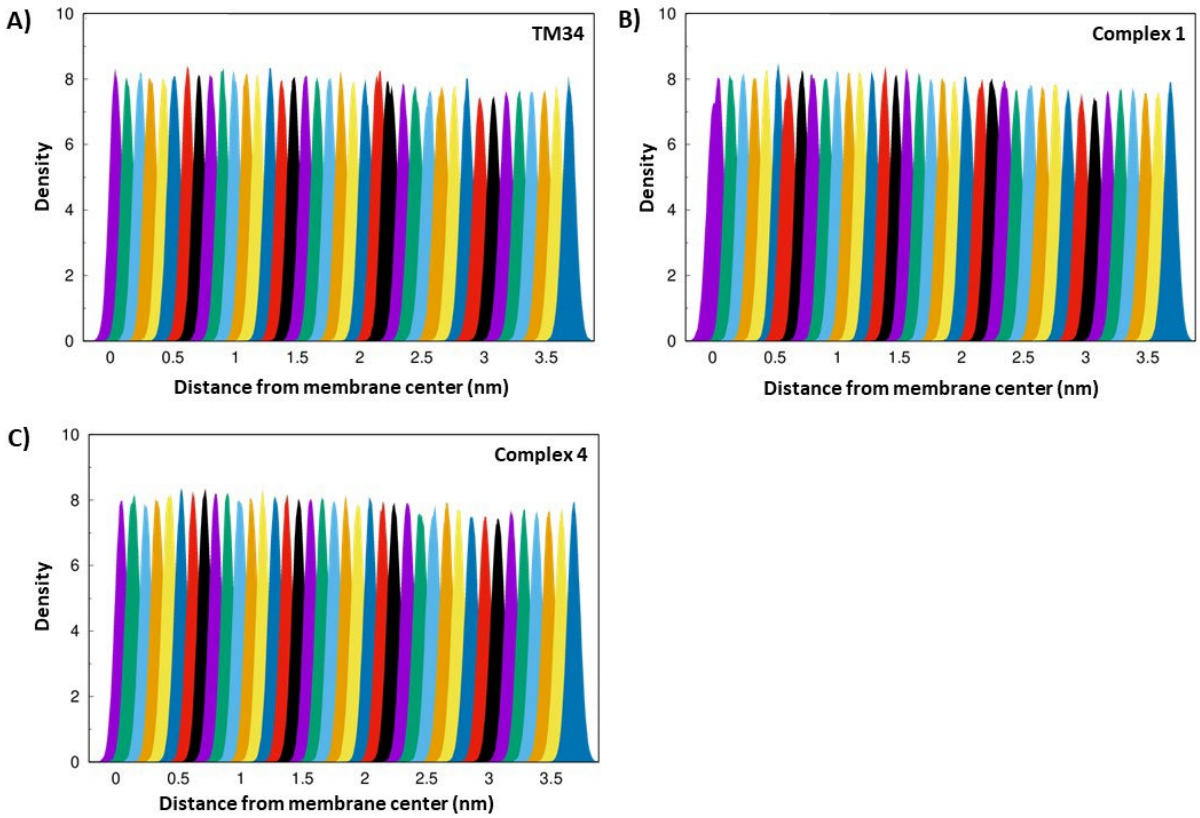


**Figure S15.** Histogram distributions of umbrella positions of (**A**) **TM34**, (**B**) complex **1** and (**C**) complex **4**. Histogram was calculated with the pull-coordinate (pullx) files for all replicates of each compound. The overlap between the sampled distances of each umbrella assures that the entire insertion process was sampled.

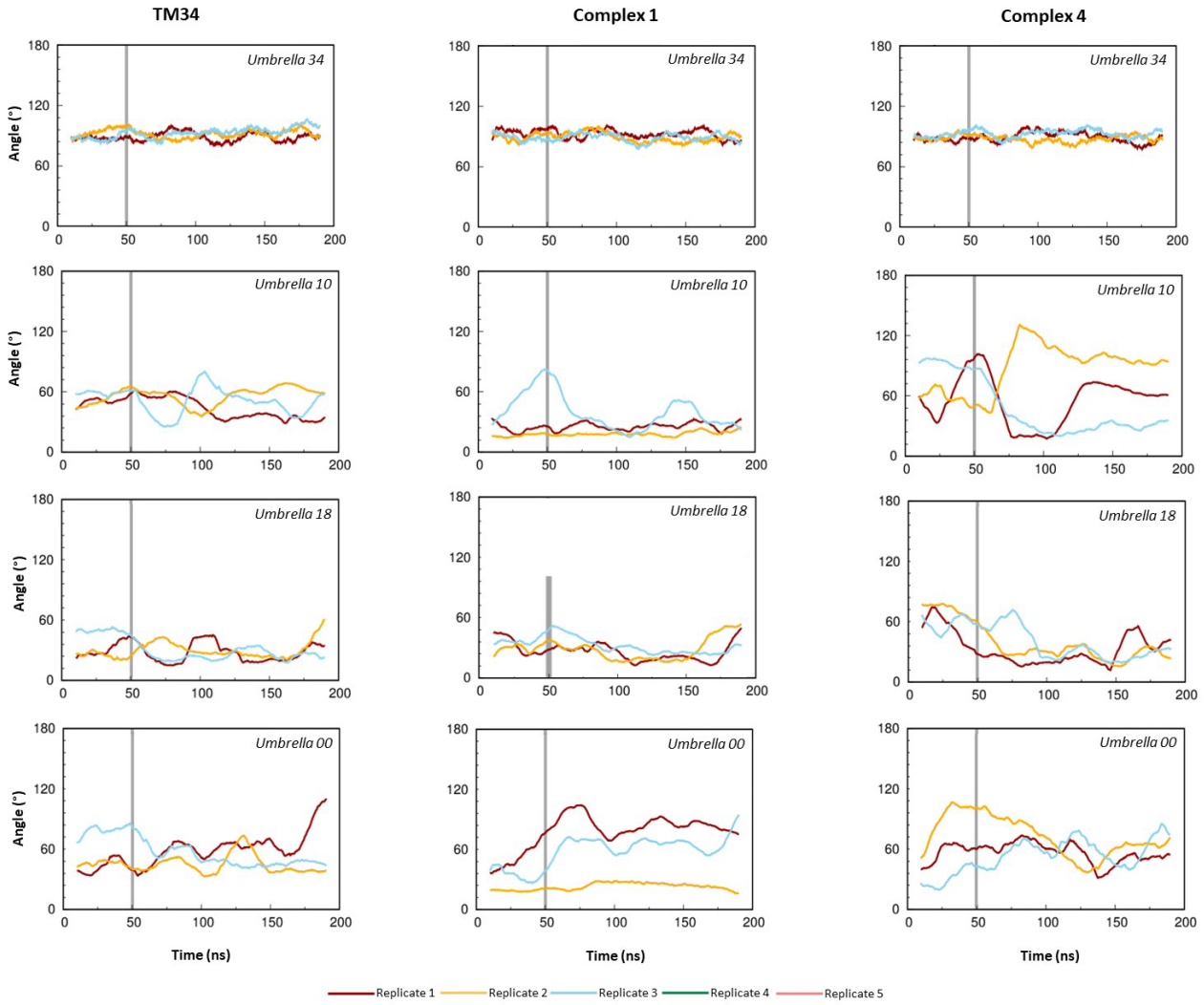


**Figure S16.** Membrane deformation over time for umbrellas at 0.0, 1.0, 1.8 and 3.4 nm from the membrane center for the 3 replicates of **TM34** and complexes **1** and **4**. Average membrane deformation was calculated as the difference between the local membrane thickness (calculated with lipids contained within a circumference of under 0.5 nm from the compound) and bulk membrane thickness (calculated with lipids beyond a circumference of 1.5 nm from the compound) for each of the 3 replicates of each compound. A floating window of 4 ns was used to reduce local fluctuations. The vertical lines illustrate the equilibration time considered. All replicates were considered equilibrated after 50 ns.

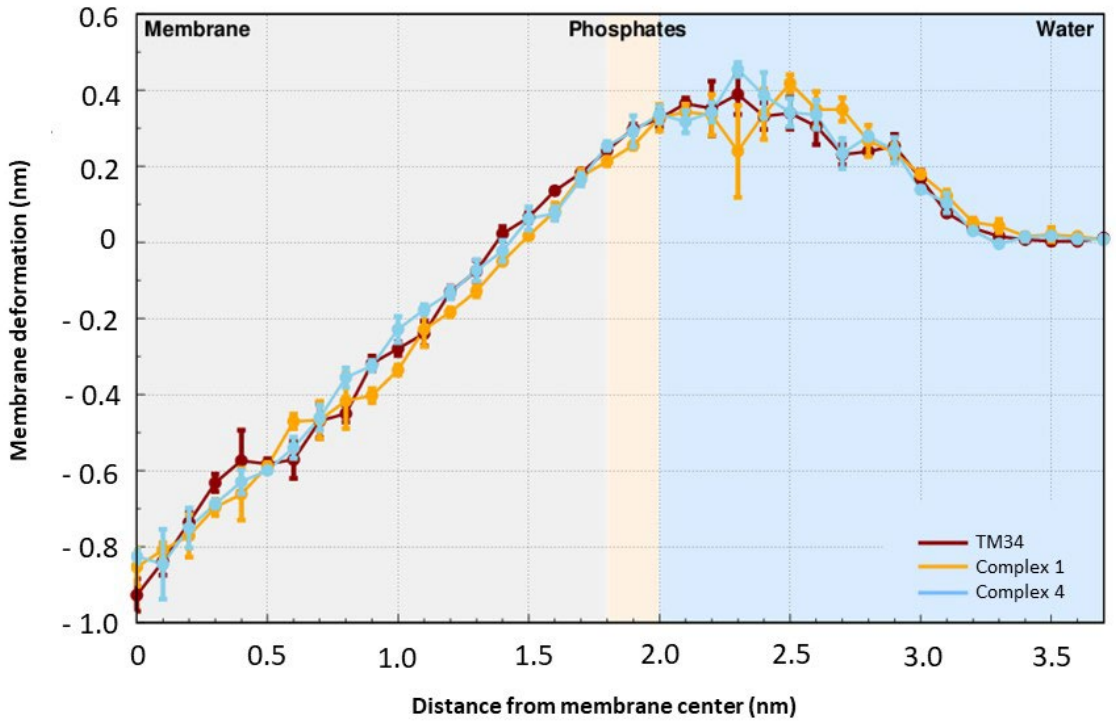


**Figure S17.** Average membrane deformation per umbrella for **TM34** and complexes **1** and **4**. Average membrane deformation was calculated as the difference between the average local membrane thickness (calculated with lipids contained within a circumference of < 0.5 nm from the compound) and average bulk membrane thickness (calculated with lipids beyond a circumference of 1.5 nm from the compound) from the equilibrated segments of all replicates of each compound. Light gray region between 0 and 18 nm represents lipid tails, light pink region between 1.8 and 2.0 nm represents the phosphate group region, and the blue region between 2.0 and 3.7 nm represents the water phase. Average and error bars were calculated with standard error. We observed that when the compounds are away from the membrane (umbrellas >3.2 nm), there is no lipid perturbation, as expected. However, as the compounds start to interact with the closest lipid monolayer, they seem to pull the nearby lipids, inducing the formation of a protuberance in the bilayer (umbrellas 2.0–3.2). When the compounds are adsorbed to the membrane, a similar effect is observed, probably because the lipid heads rise to envelop the hydrophobic groups and allow a better compound intercalation (umbrellas 1.6–2.0). As the compounds insert further into the membrane center, they induce membrane inward depressions that are proportional to the umbrella position and are persistent throughout our simulations' length (umbrellas 0.0–1.4).

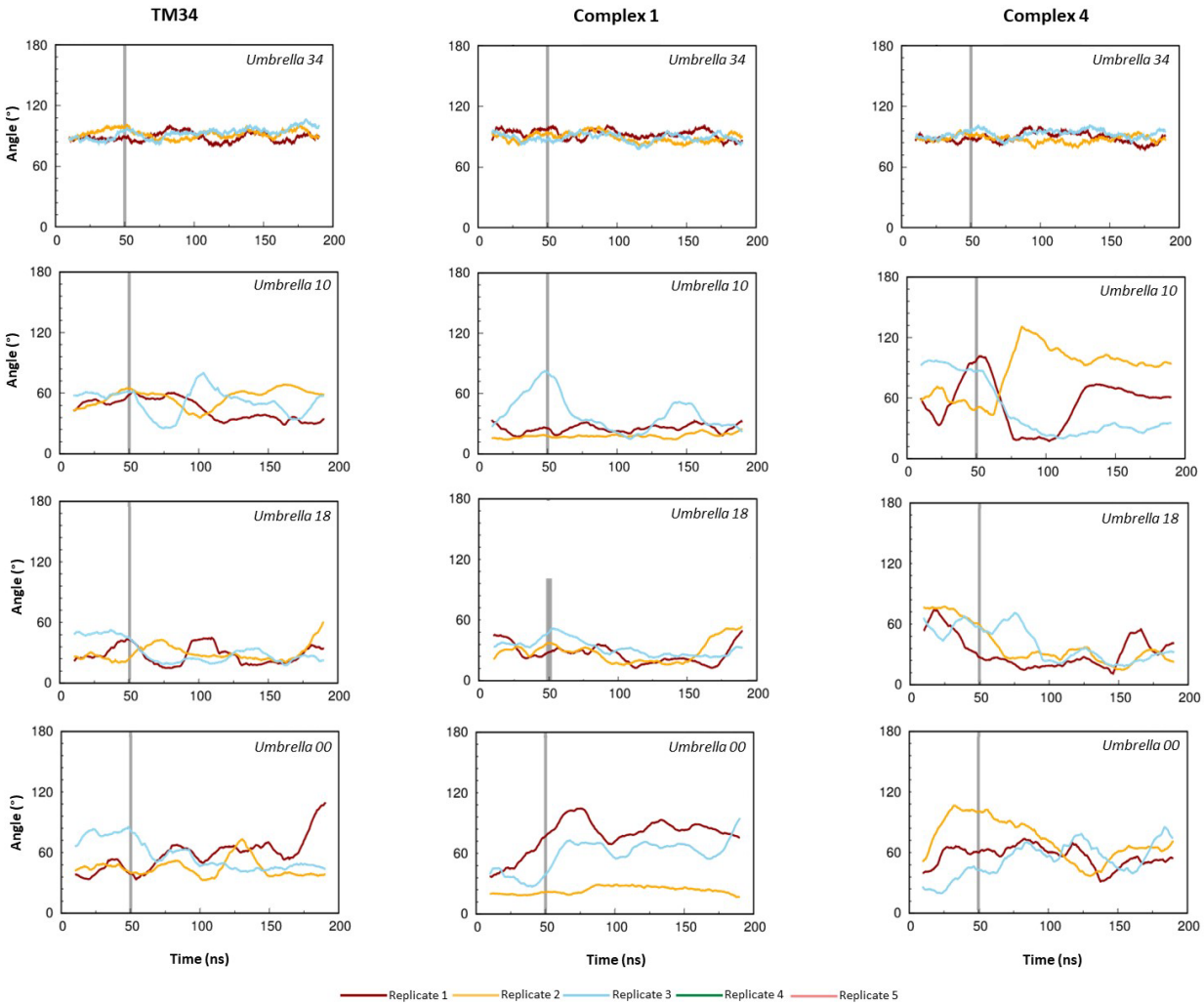


**Figure S18.** Ph angle over time for umbrellas at 0.0, 1.0, 1.8 and 3.4 nm from the membrane center for the 3 replicates of **TM34** and complexes **1** and **4**. A floating window of 4 ns was used to reduce local fluctuations. The vertical lines illustrate the equilibration time considered.

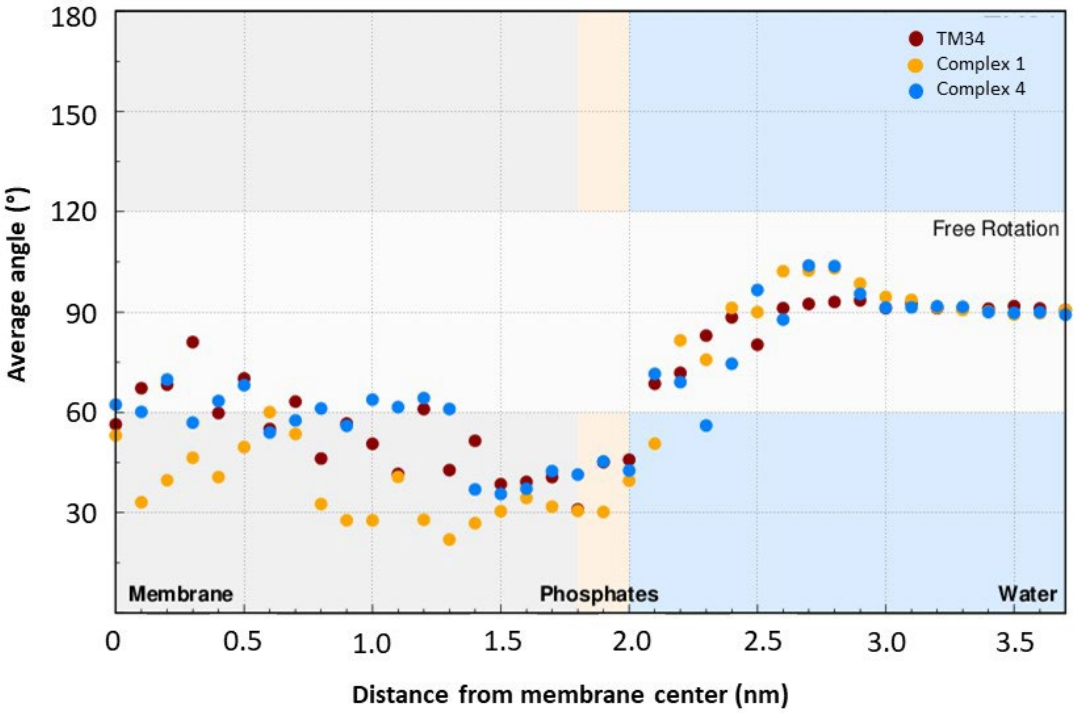


**Figure S19**. Average Ph angle per umbrella for **TM34** and complexes **1** and **4**. Average angles were calculated using the Ph angles from the equilibrated segments of all replicates of each compound. Light gray region between 0 and 18 nm represents lipid tails, light pink region between 1.8 and 2.0 nm represents the phosphate group region, and the blue region between 2.0 and 3.7 nm represents the water phase. White band between 60° and 120° represents increased rotational freedom, where the average angle value may not be representative of the preferred orientation.

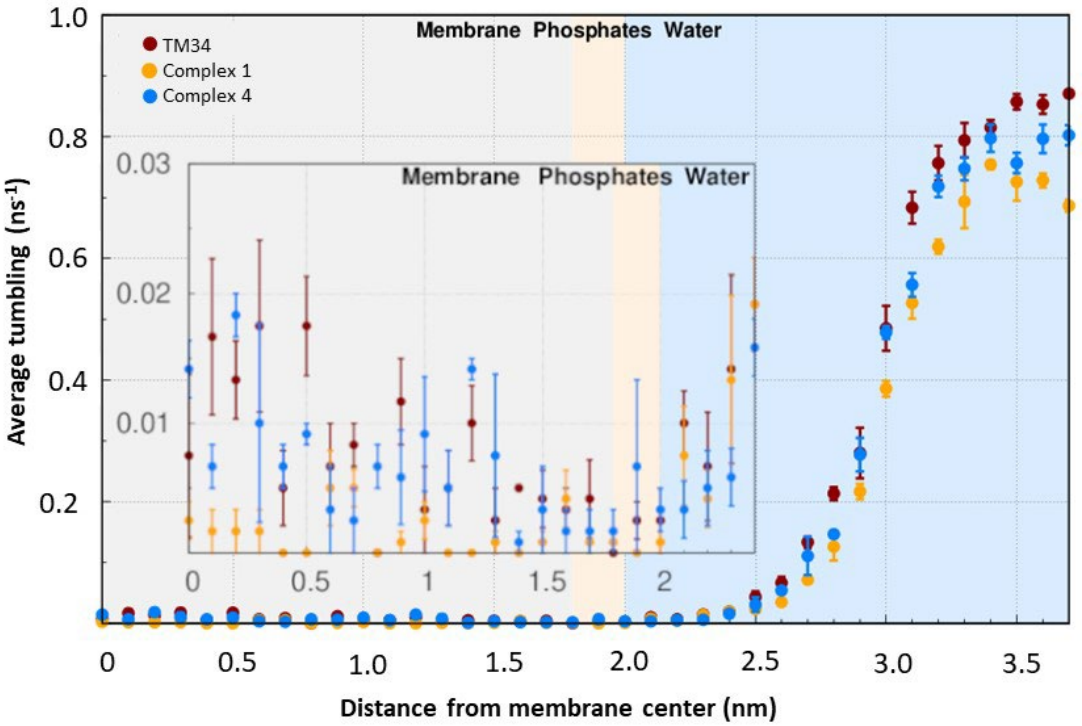


**Figure S20.** Average number of tumbles per ns for each umbrella of **TM34** and complexes **1** and **4**. Inset image contains close-up for umbrellas between 0.0 and 2.4 nm. One tumble was considered when the Ph angle value shifted from 60° (or under) to 120° (or higher), and then back. The values of Ph angle used angle values from the equilibrated segments of all replicates of each compound. Light gray region between 0 and 18 nm represents lipid tails, light pink region between 1.8 and 2.0 nm represents the phosphate group region, and the blue region between 2.0 and 3.7 nm represents the water phase. Average and error bars were calculated with standard error. The tumbling number of each compound nicely captures the loss of conformational freedom of the complexes when they interact with the lipid bilayer. In water, the number of tumbles is ~0.8 $ns^{-1}$, which is limited by their rotational diffusion and will depend only on the size/polarity of the substituted group, as evidenced by **TM34** having higher number of tumbles than any of the two derivatives in most umbrellas (**TM34** should have a slightly higher value than complex **1**). The same principle should apply for when the compounds are within the lipid tails region, although their tumbling counts were significantly smaller (inset).

## NMR Spectra

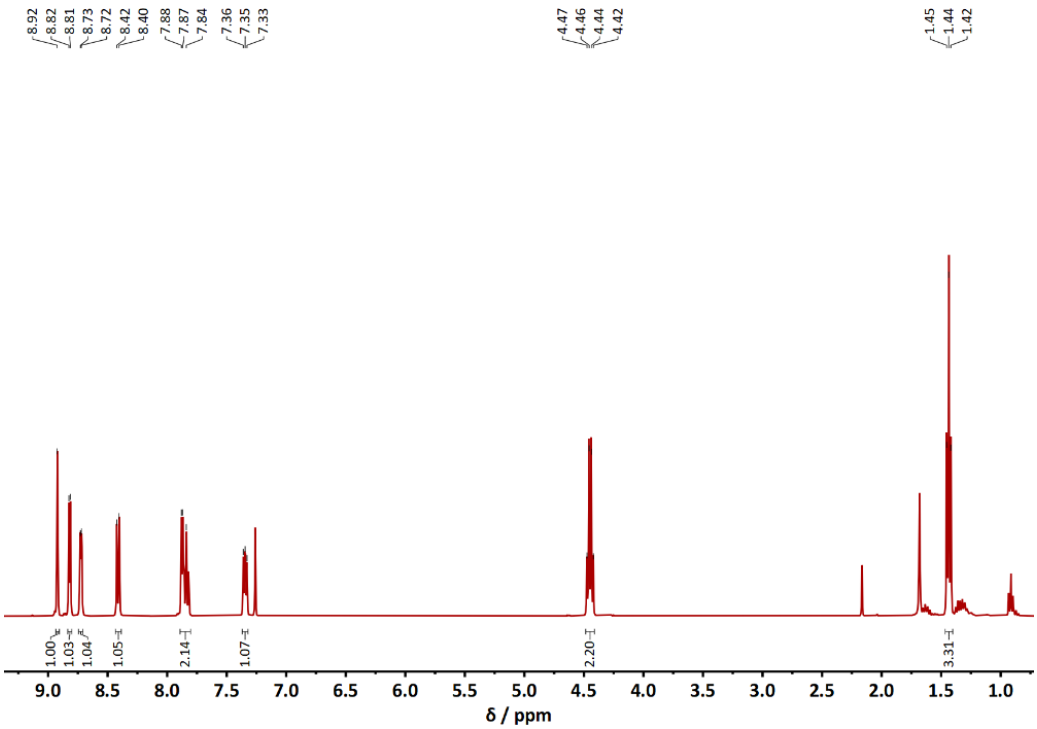


**Figure S21.** $^{1}$H NMR spectrum of ethyl 2,2'-bipyridine-4-carboxylate (**BipyCOOEt**) in $CDCl_3$.

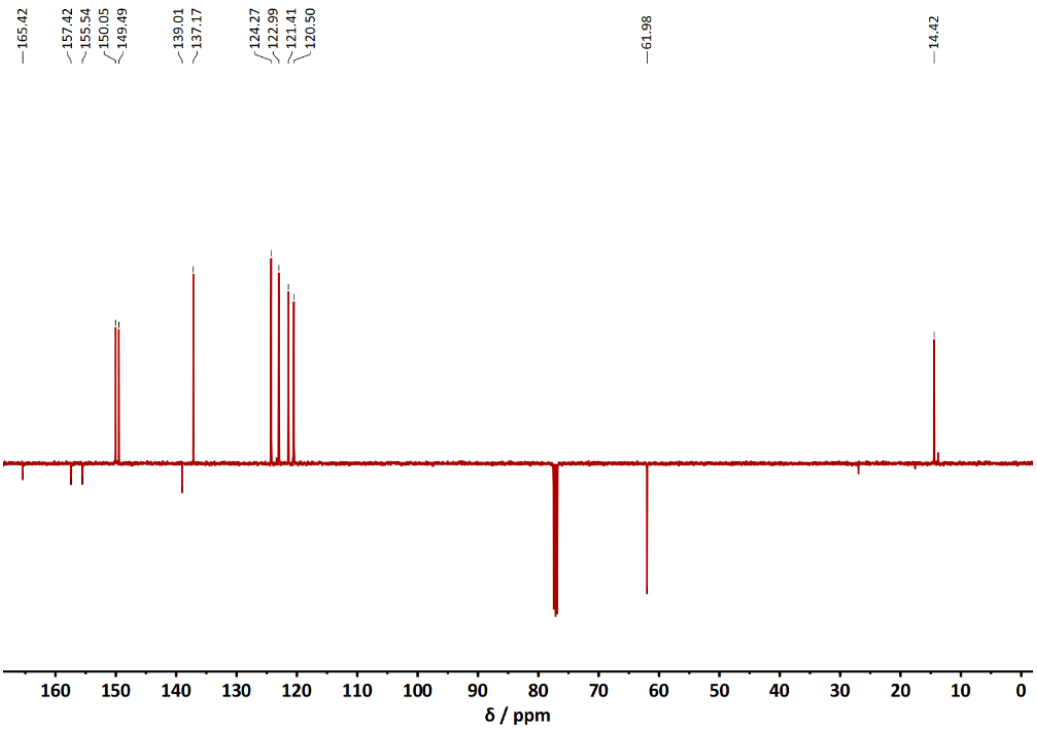


**Figure S22.** APT-$^{13}$C{$^{1}$H} NMR spectrum of ethyl 2,2'-bipyridine-4-carboxylate (**BipyCOOEt**) in $CDCl_3$.

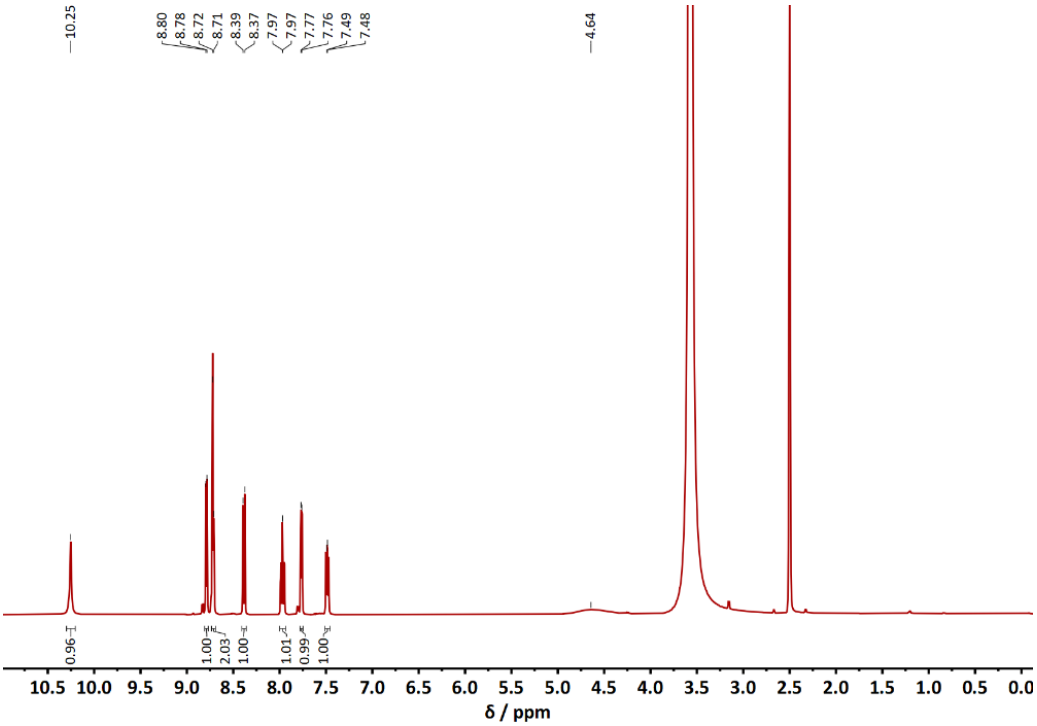


**Figure S23.** $^{1}$H NMR spectrum of 2,2'-bipyridine-4-carbohydrazide (**BipyNHNH$_2$**) in $(CD_3)_2SO$.

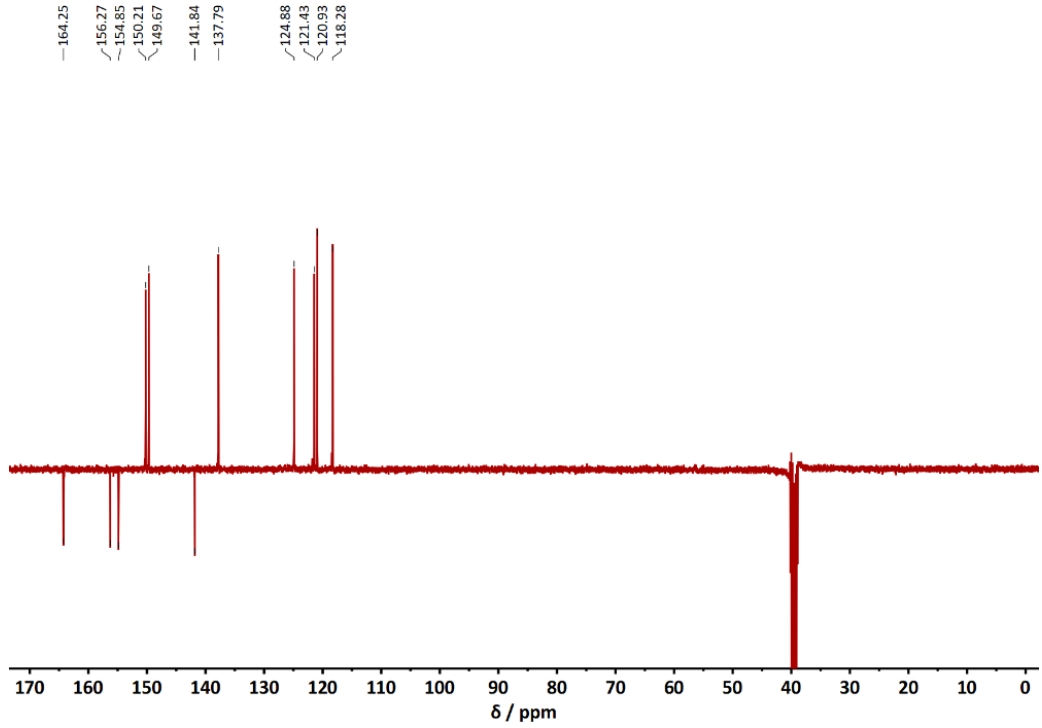


**Figure S24.** APT-$^{13}$C{$^{1}$H} NMR spectrum of 2,2'-bipyridine-4-carbohydrazide (**BipyNHNH$_2$**) in $(CD_3)_2SO$.

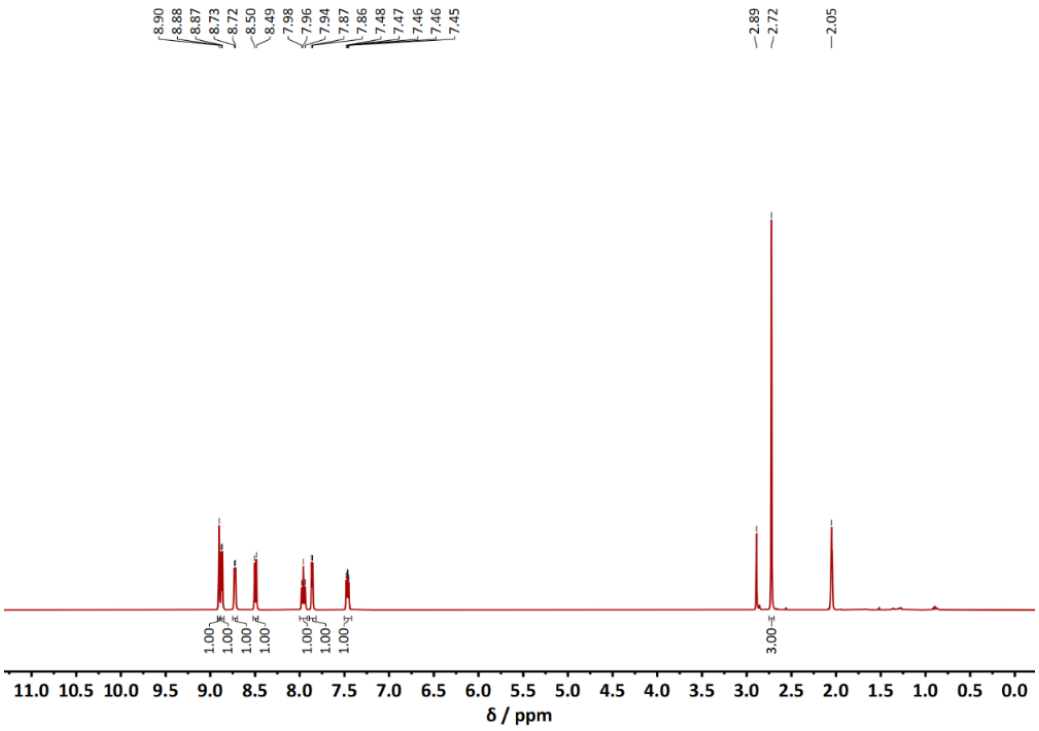


**Figure S25.** $^{1}$H NMR spectrum of 2,2'-bipyridine-4-acetyl (**AcBipy**) in $(CD_3)_2CO$.

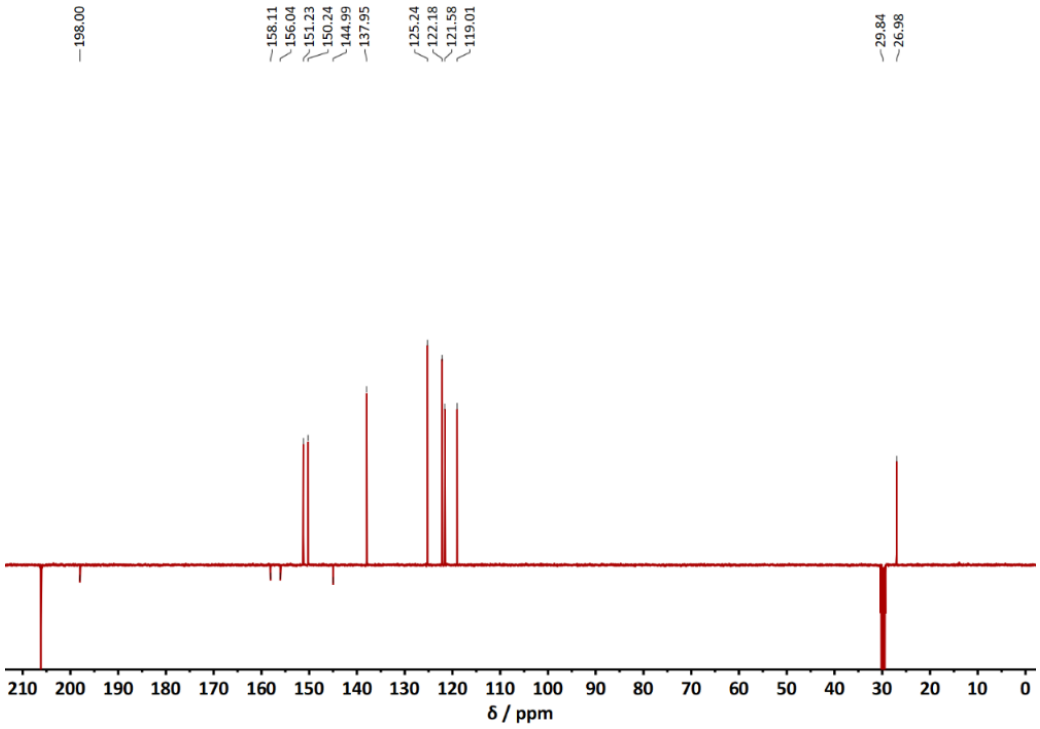


**Figure S26.** APT-$^{13}$C{$^{1}$H} NMR spectrum of 2,2'-bipyridine-4-acetyl (**AcBipy**) in $(CD_3)_2CO$.

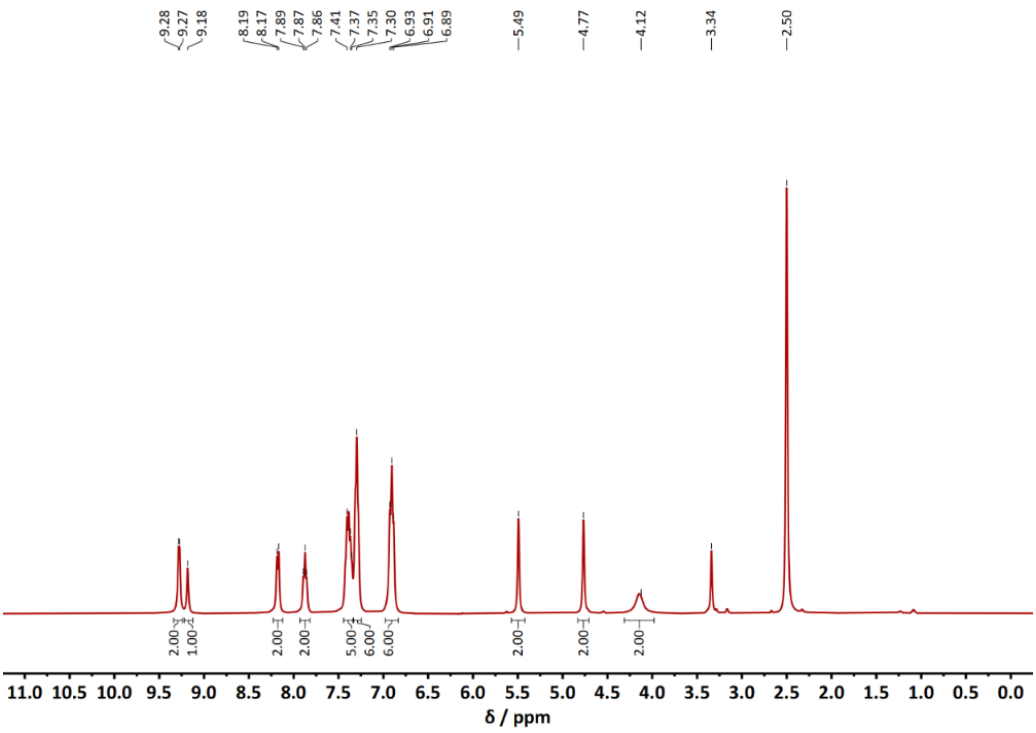


**Figure S27.** $^{1}$H NMR spectrum of [Ru(η$^{5}$-$C_5H_4CONHNH_2$)($PPh_3$)(2,2′-bipy)][$CF_3SO_3$] (**1**) in $(CD_3)_2SO$.

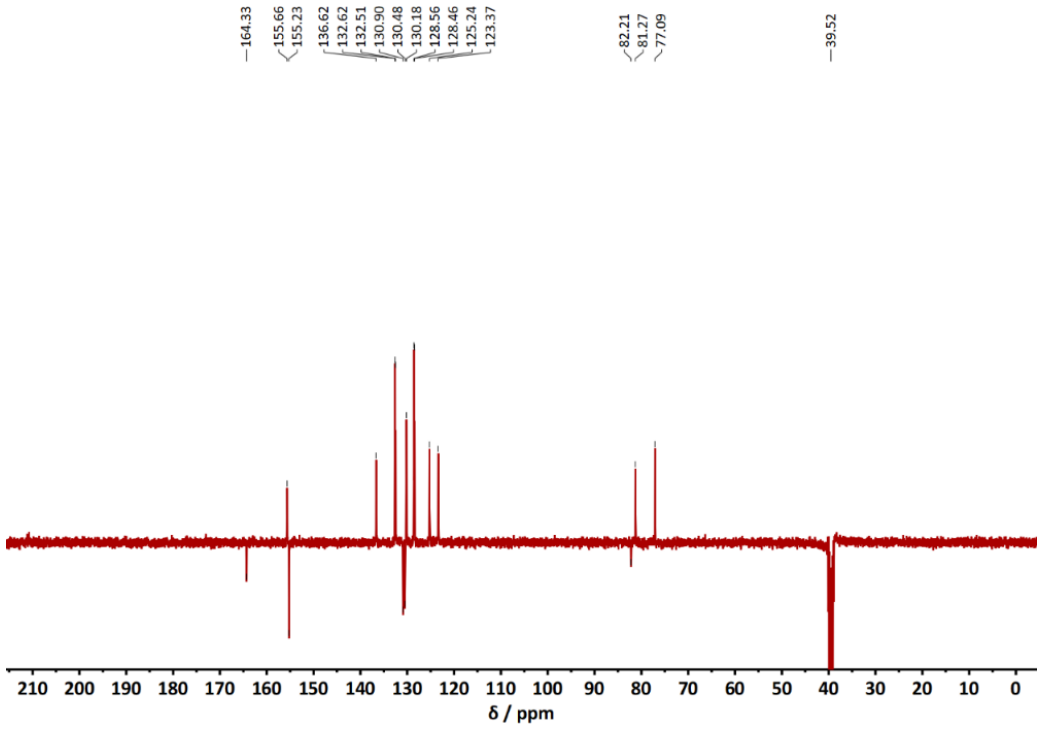


**Figure S28.** APT-$^{13}$C{$^{1}$H} NMR spectrum of [Ru(η$^{5}$-$C_5H_4CONHNH_2$)($PPh_3$)(2,2′-bipy)][$CF_3SO_3$] (**1**) in $(CD_3)_2SO$.

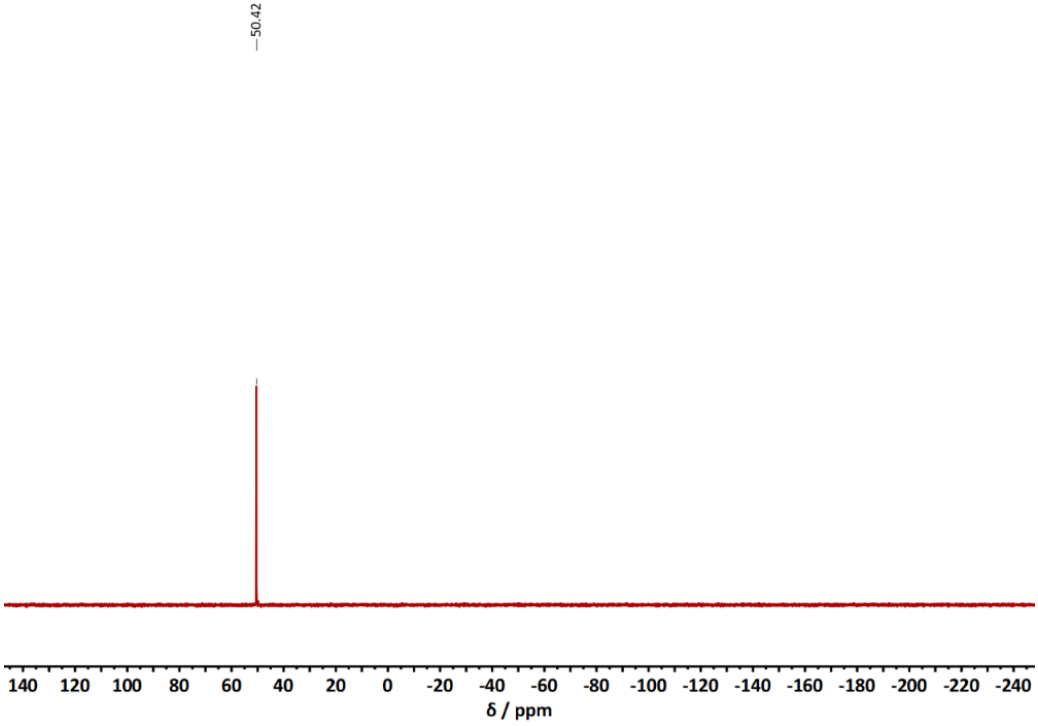


**Figure S29**. $^{31}P\{^{1}H\}$ NMR spectrum of [Ru($\eta^5$-$C_5H_4CONHNH_2$)($PPh_3$)(2,2'-bipy)][$CF_3SO_3$] (**1**) in $(CD_3)_2SO$.

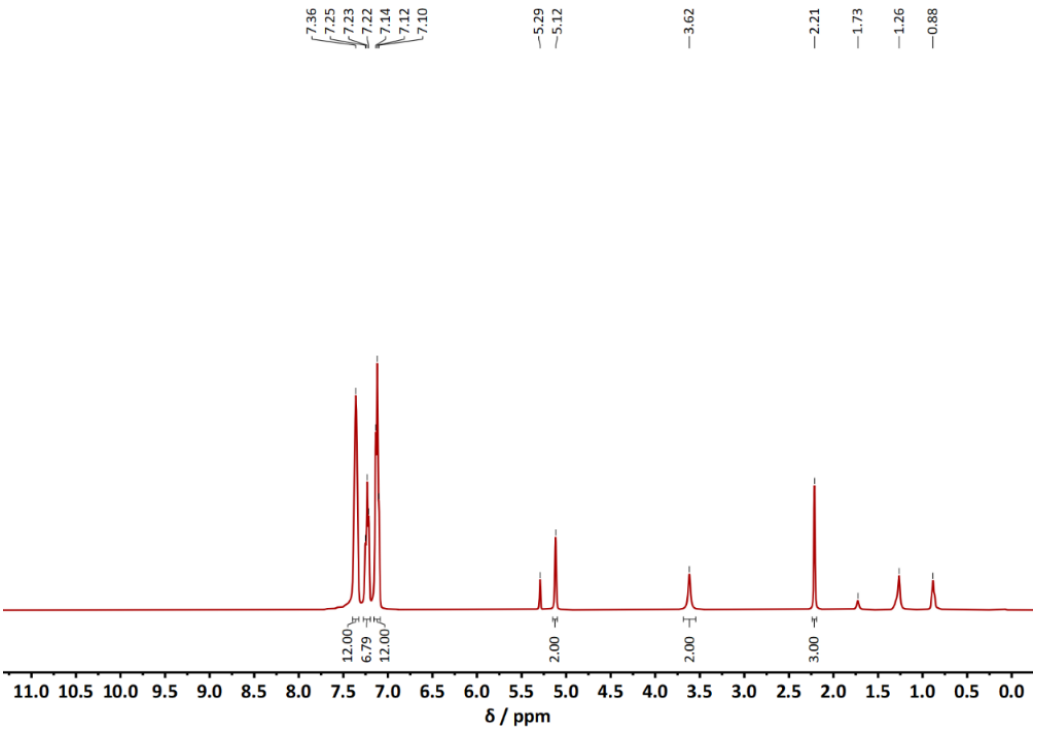


**Figure S30.** $^{1}H$ NMR spectrum of [Ru($\eta^5$-$C_5H_4COCH_3$)($PPh_3$)$_2$Cl] (**3**) in $CDCl_3$.

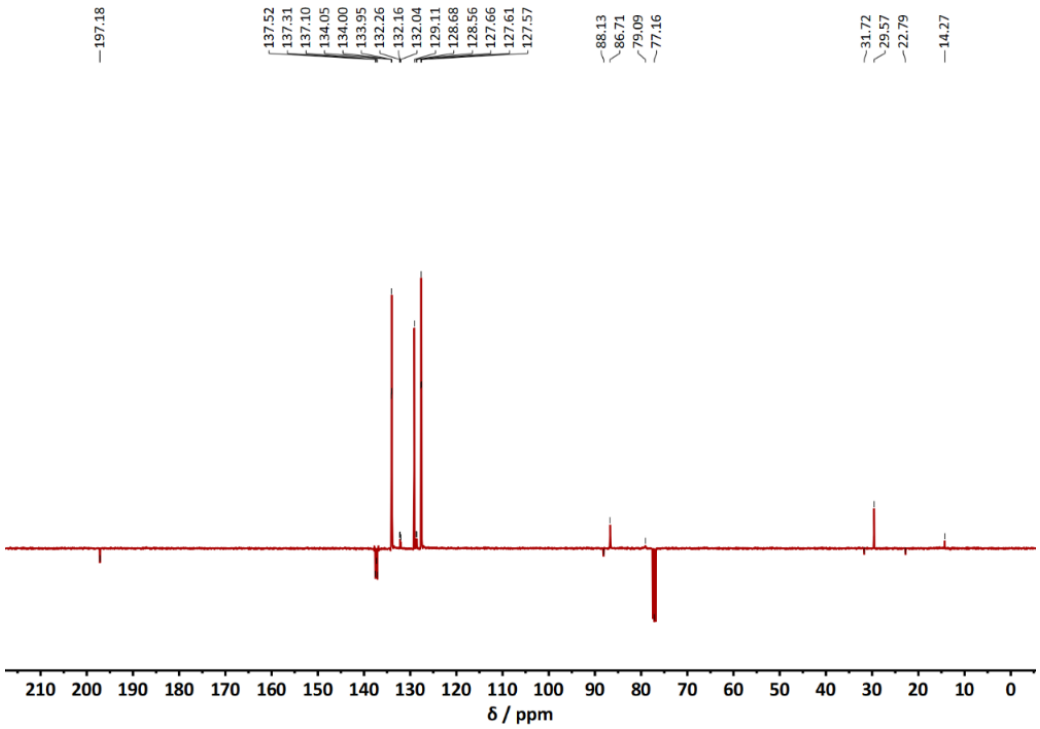


**Figure S31.** APT-$^{13}C\{^{1}H\}$ NMR spectrum of[Ru($\eta^5$-$C_5H_4COCH_3$)$(PPh_3)_2Cl$] (**3**) in $CDCl_3$.

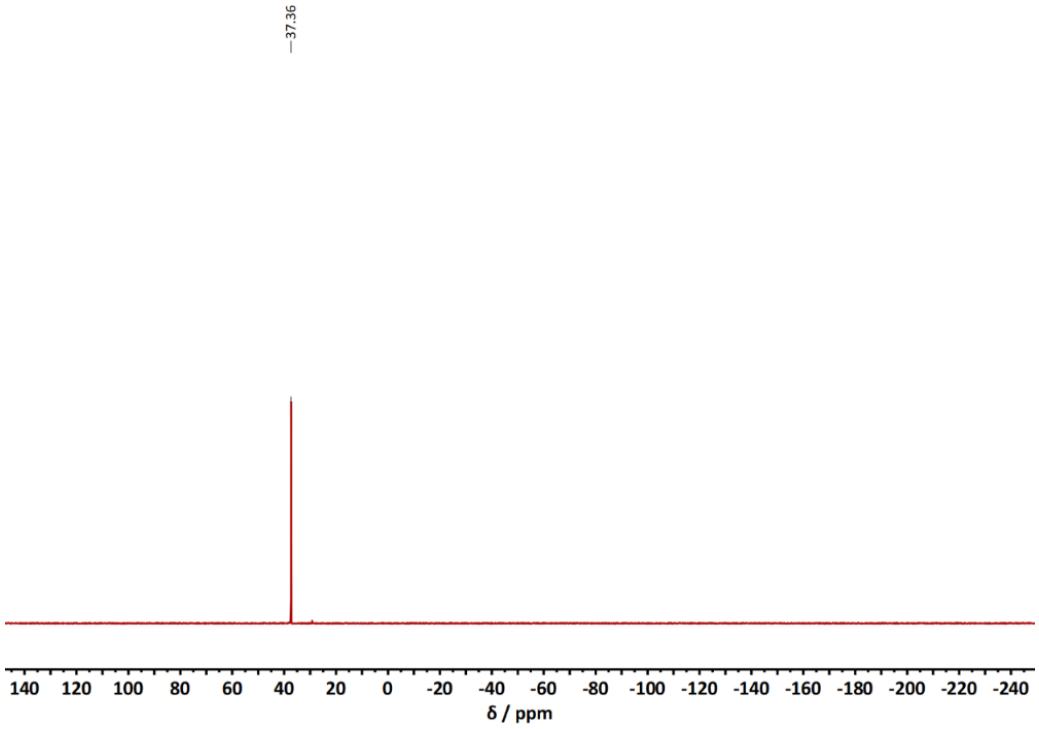


**Figure S32.** $^{31}P\{^{1}H\}$ NMR spectrum of [Ru($\eta^5$-$C_5H_4COCH_3$)$(PPh_3)_2Cl$] (**3**) in $CDCl_3$.

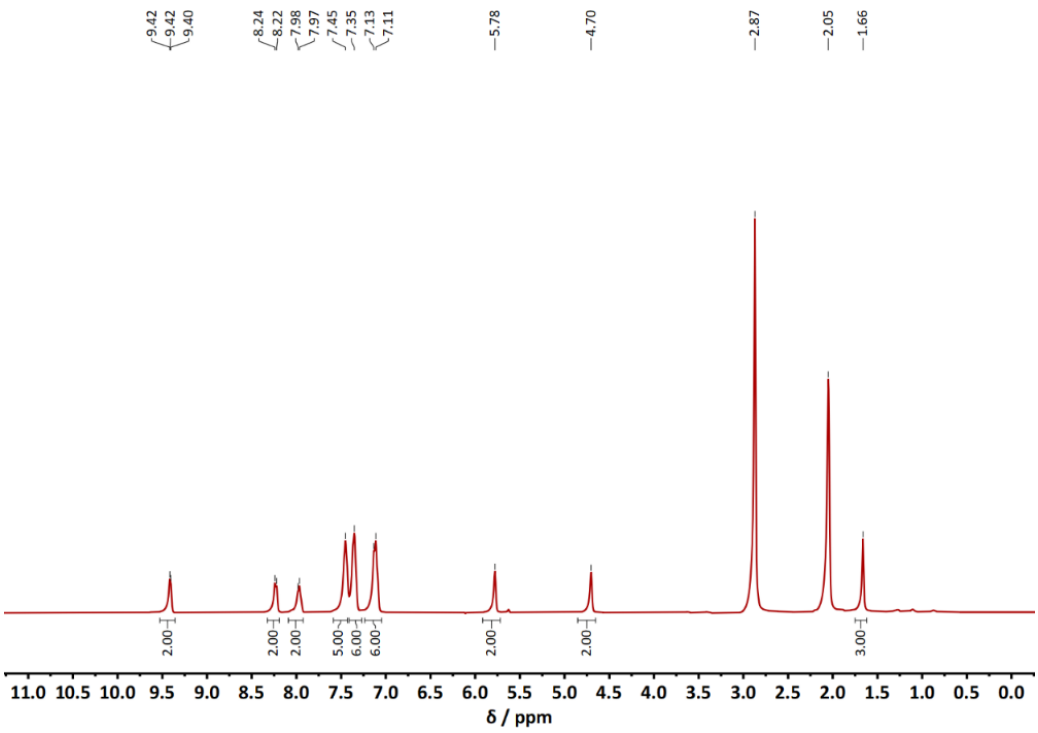


**Figure S33.** $^{1}$H NMR spectrum of [Ru($\eta^5$-$C_5H_4COCH_3$)($PPh_3$)(2,2′-bipy)][$CF_3SO_3$] (**4**) in $(CD_3)_2CO$.

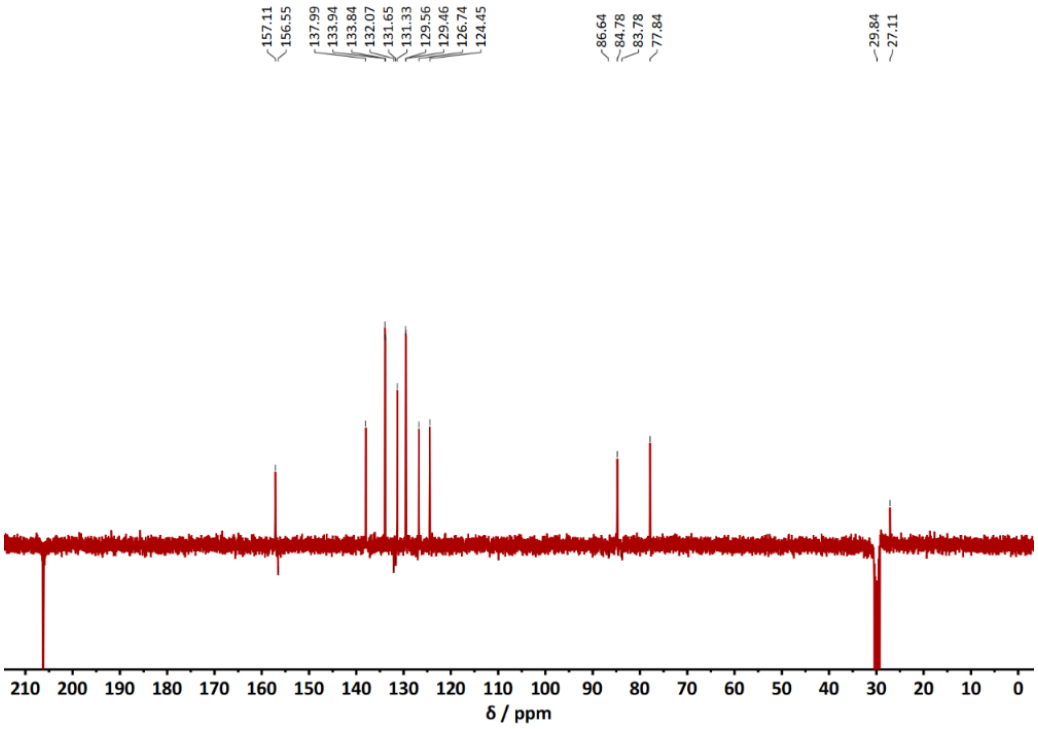


**Figure S34.** APT-$^{13}$C{$^{1}$H} NMR spectrum of [Ru($\eta^5$-$C_5H_4COCH_3$)($PPh_3$)(2,2′-bipy)][$CF_3SO_3$] (**4**) in $(CD_3)_2CO$.

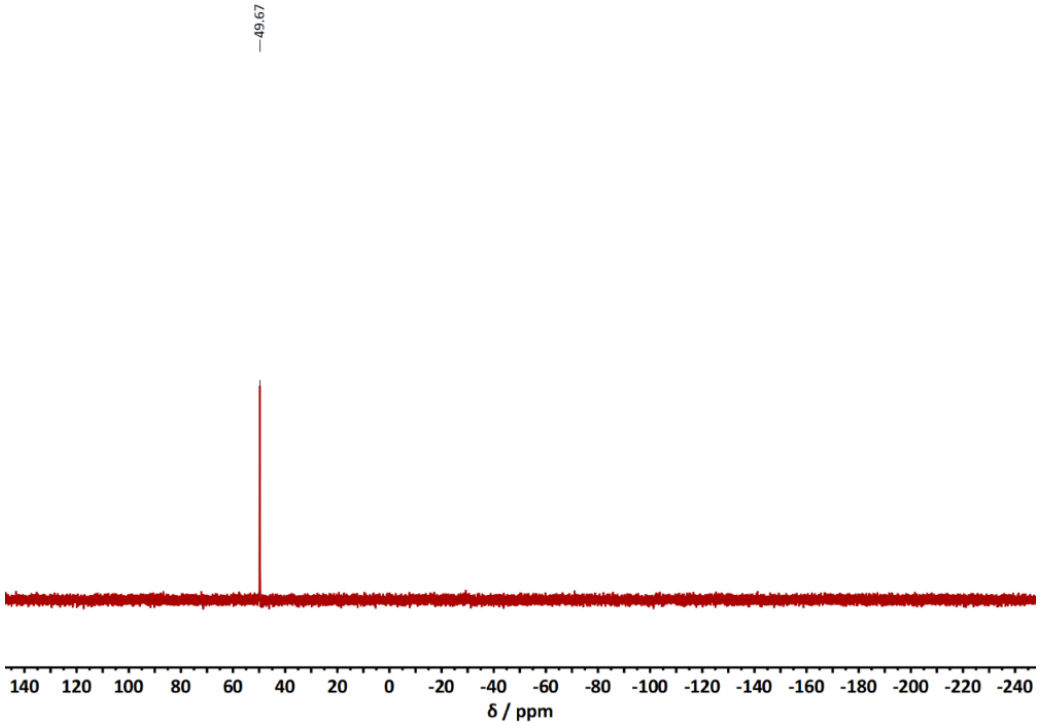


**Figure S35.** $^{31}P\{^{1}H\}$ NMR spectrum of [Ru($\eta^5$-$C_5H_4COCH_3$)($PPh_3$)(2,2'-bipy)][$CF_3SO_3$] (**4**) in $(CD_3)_2CO$

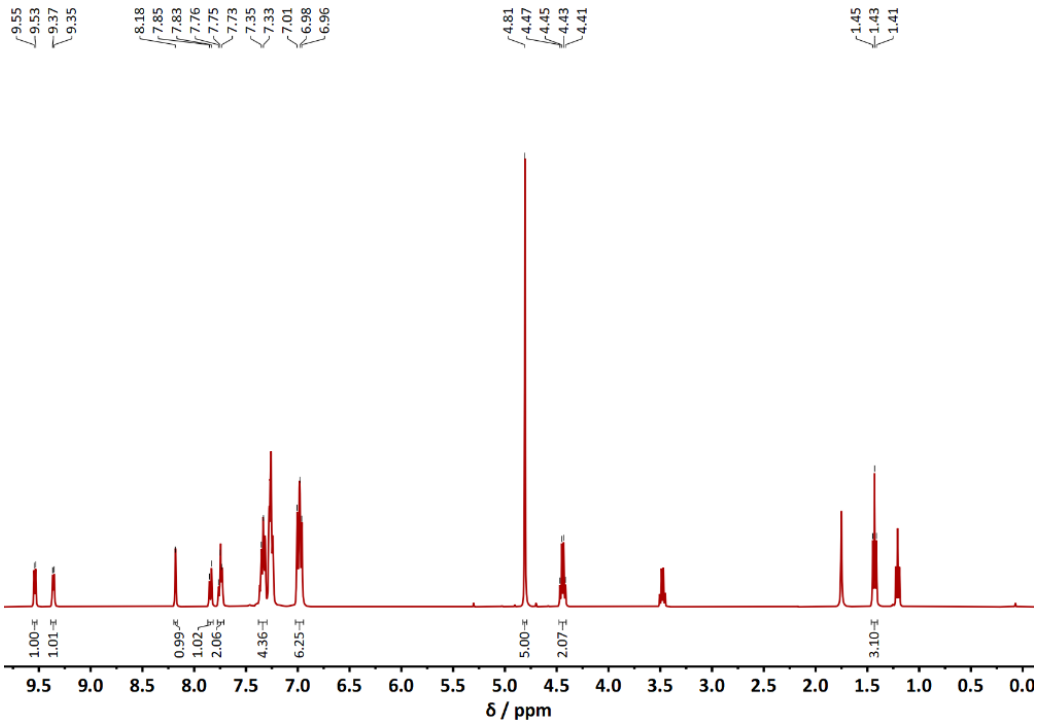


**Figure S36.** $^{1}H$ NMR spectrum of [Ru($\eta^5$-$C_5H_5$)($PPh_3$)(BipyCOOEt)][$CF_3SO_3$] (**5**) in $CDCl_3$.

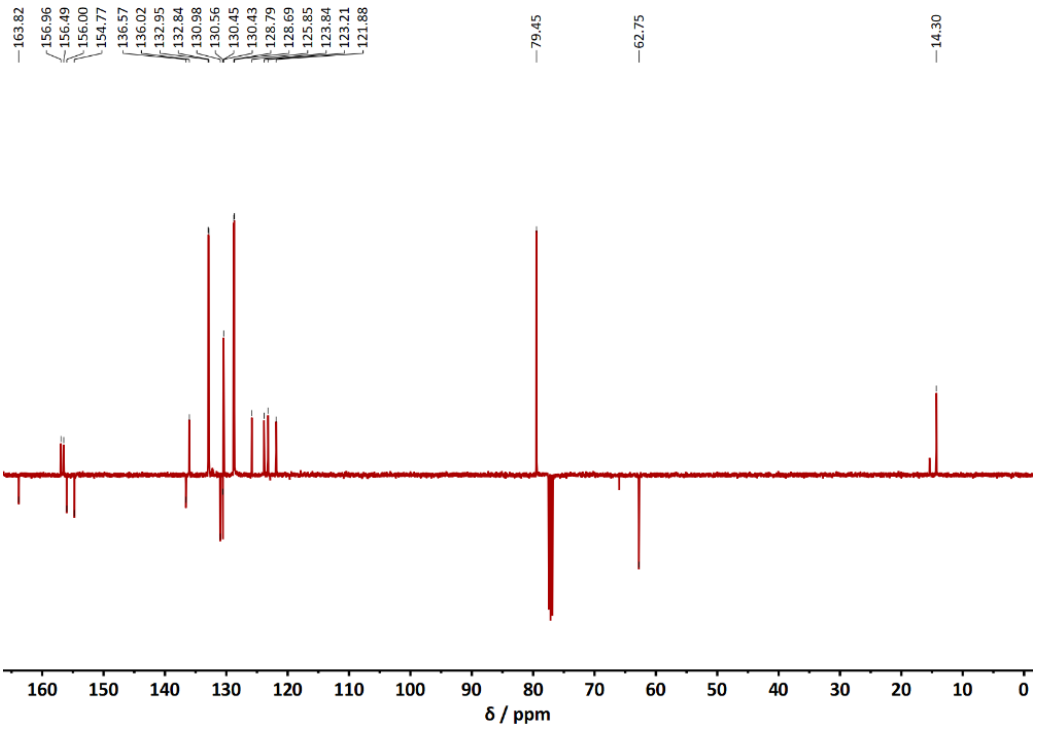


**Figure S37.** APT-$^{13}C\{^{1}H\}$ NMR spectrum of [Ru($\eta^5$-$C_5H_5$)($PPh_3$)(BipyCOOEt)][$CF_3SO_3$] (**5**) in $CDCl_3$.

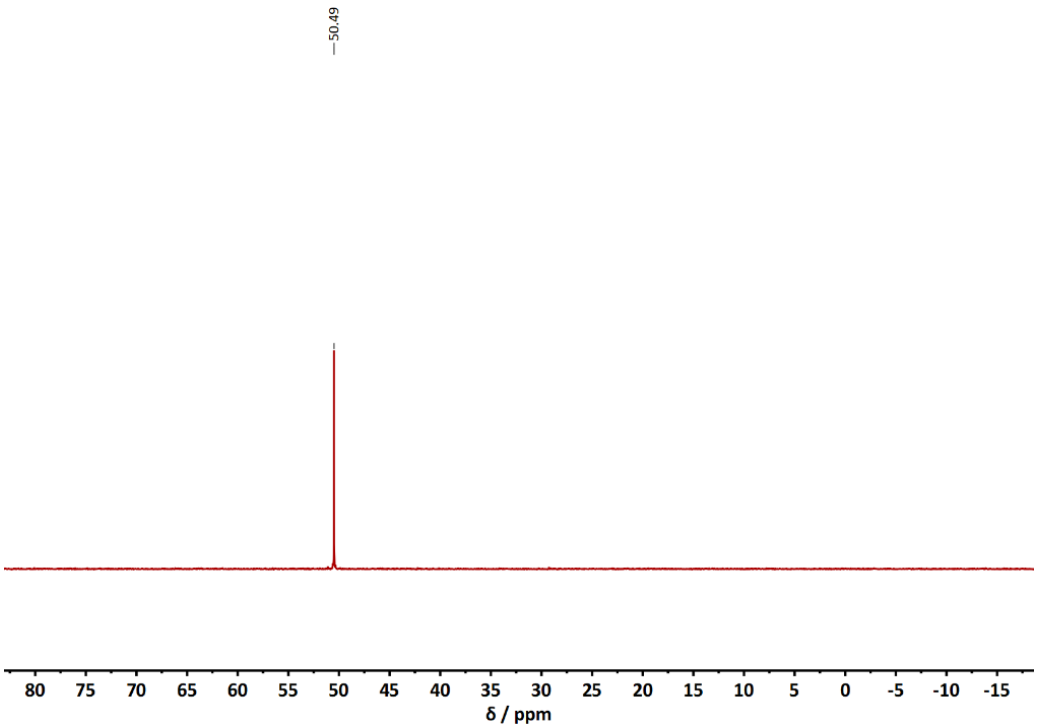


**Figure S38.** $^{31}P\{^{1}H\}$ NMR spectrum of [Ru($\eta^5$-$C_5H_5$)($PPh_3$)(BipyCOOEt)][$CF_3SO_3$] (**5**) in $CDCl_3$.

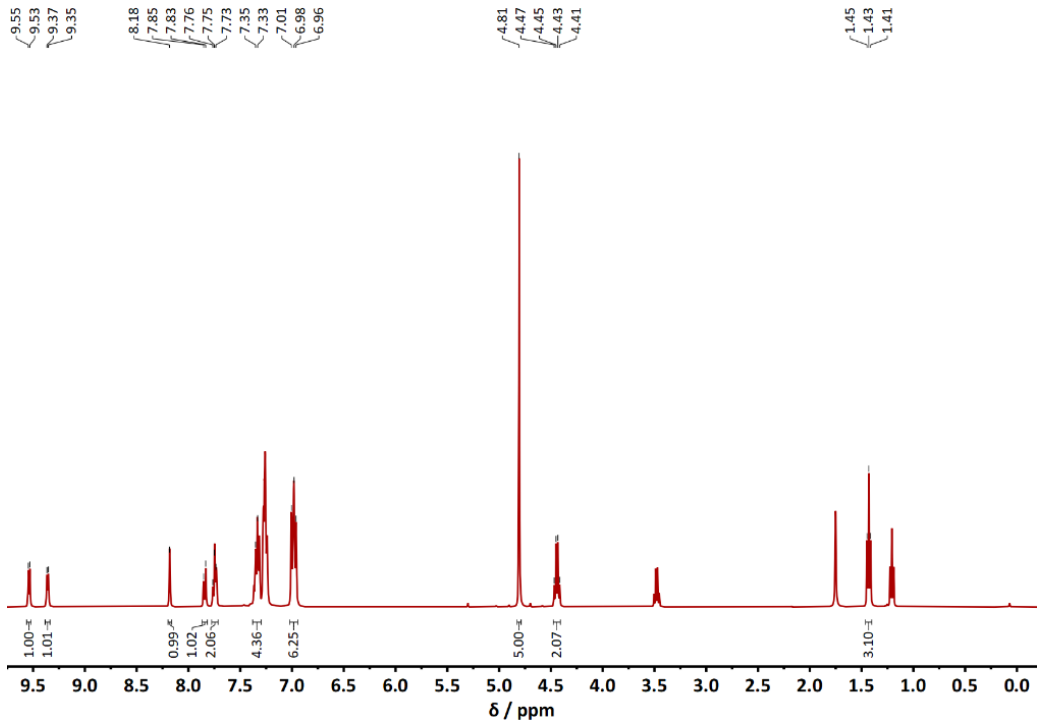


**Figure S39.** $^{1}$H NMR spectrum of [Ru($\eta^5$-$C_5H_5$)($PPh_3$)(BipyCONHNH$_2$)][$CF_3SO_3$] (**6**) in $CDCl_3$.

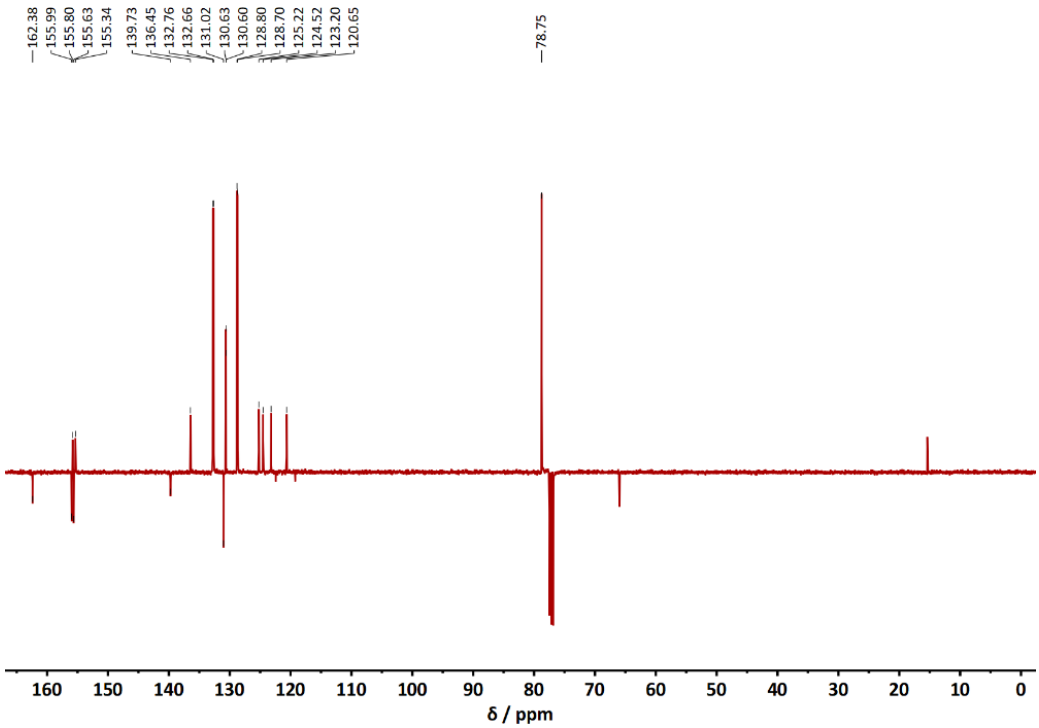


**Figure S40.** APT-$^{13}$C{$^{1}$H} NMR spectrum of [Ru($\eta^5$-$C_5H_5$)($PPh_3$)(BipyCONHNH$_2$)][$CF_3SO_3$] (**6**) in $CDCl_3$.

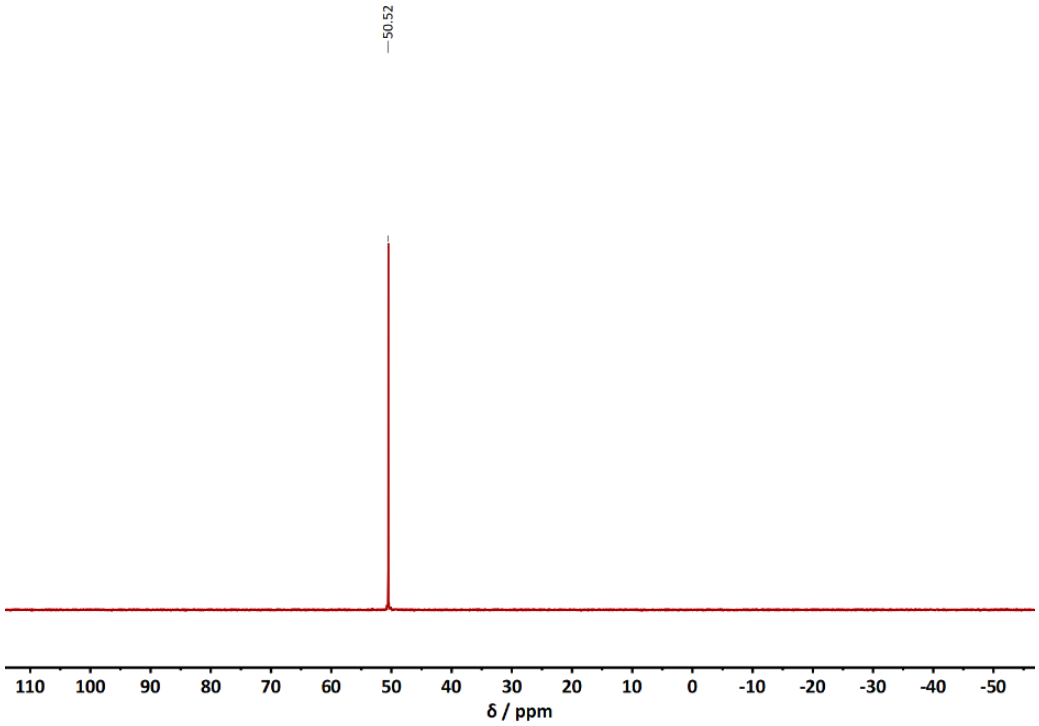


**Figure S41**. $^{31}P\{^{1}H\}$ NMR spectrum of $[Ru(\eta^5\text{-}C_5H_5)(PPh_3)(BipyCONHNH_2)][CF_3SO_3]$ (**6**) in $CDCl_3$.

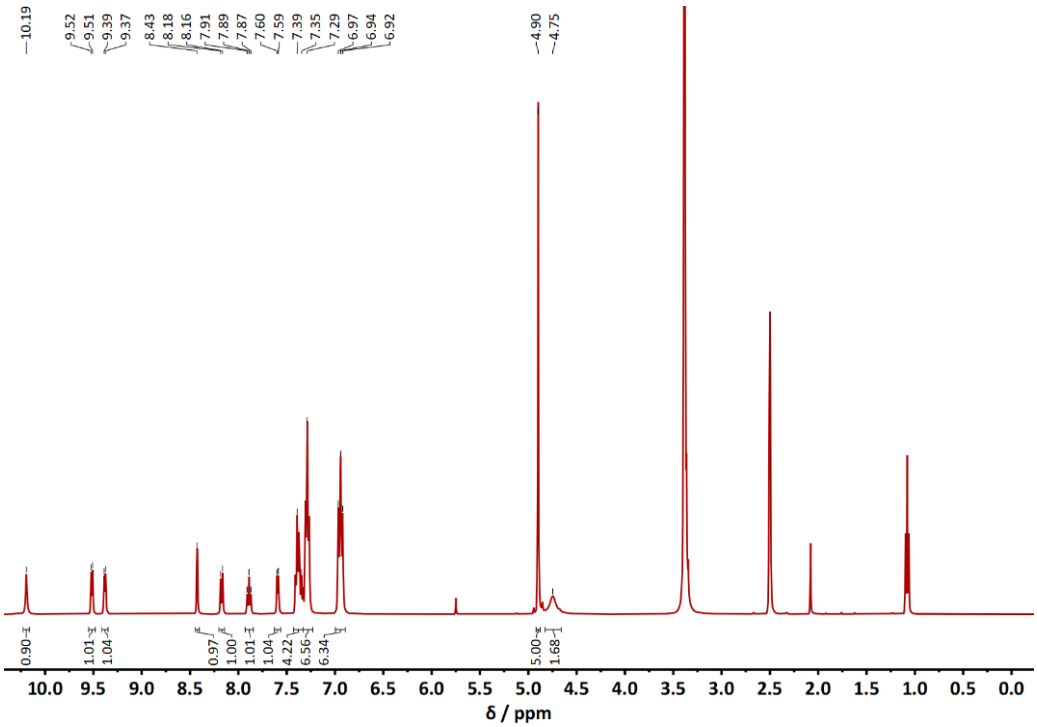


**Figure S42.** $^{1}H$ NMR spectrum of $[Ru(\eta^5\text{-}C_5H_5)(PPh_3)(BipyCONHNH_2)][CF_3SO_3]$ (**6**) in $(CD_3)_2SO$.

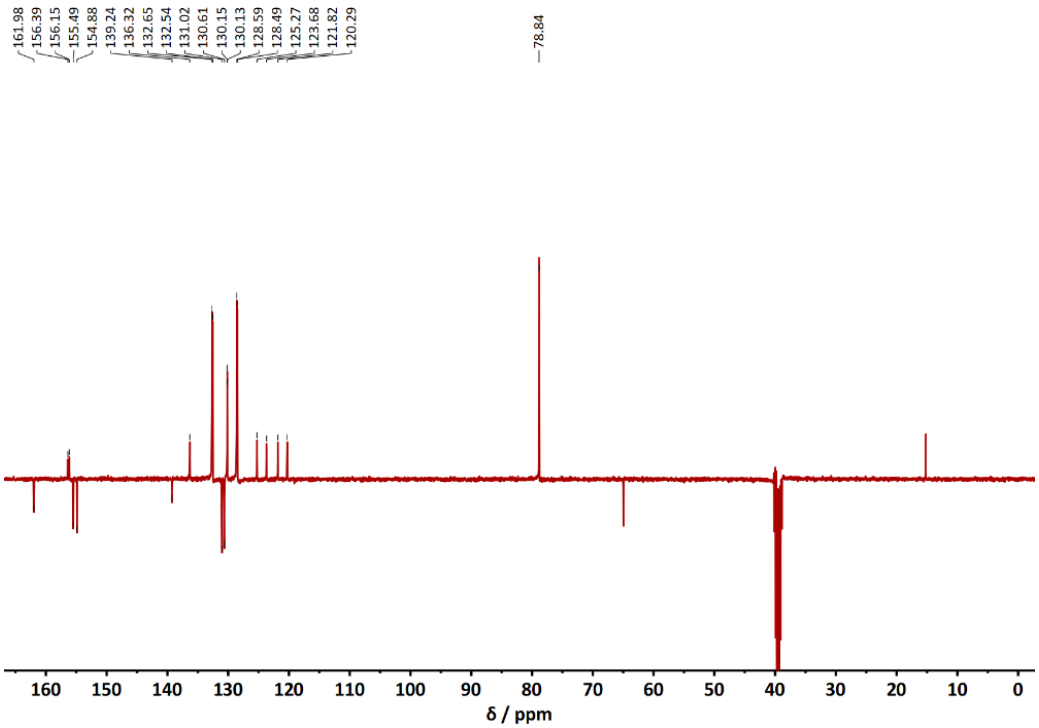


**Figure S43.** APT-$^{13}C\{^{1}H\}$ NMR spectrum $[Ru(\eta^5\text{-}C_5H_5)(PPh_3)(BipyCONHNH_2)][CF_3SO_3]$ (**6**) in $(CD_3)_2SO$.

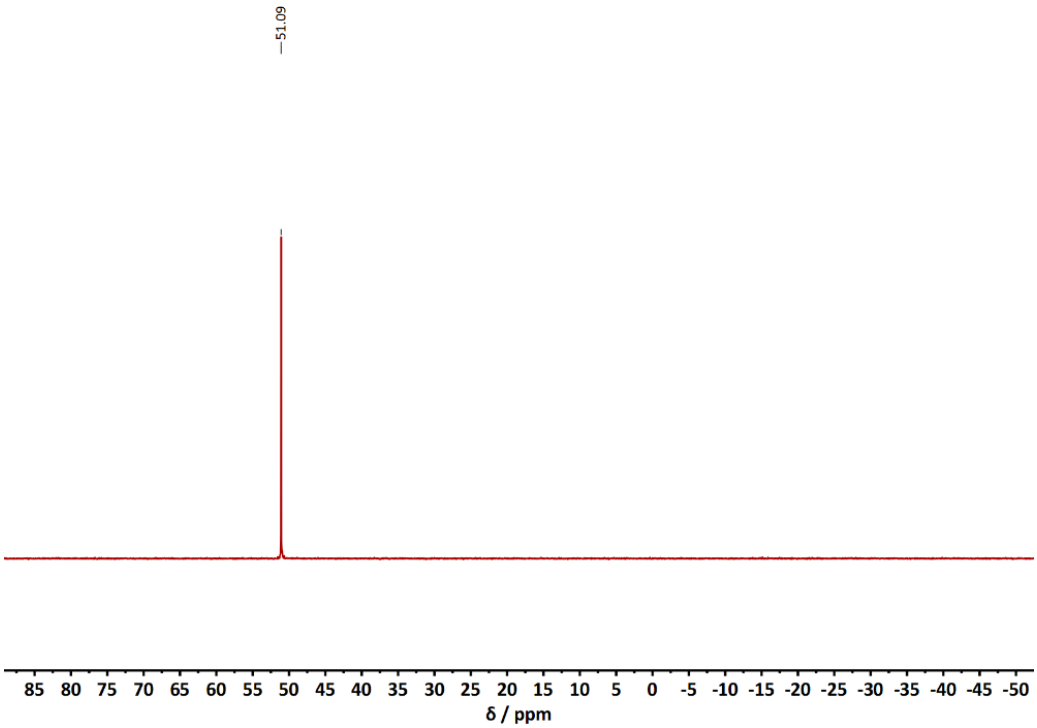


**Figure S44.** $^{31}P\{^{1}H\}$ NMR spectrum of $[Ru(\eta^5\text{-}C_5H_5)(PPh_3)(BipyCONHNH_2)]][CF_3SO_3]$ (**6**) in $(CD_3)_2SO$.

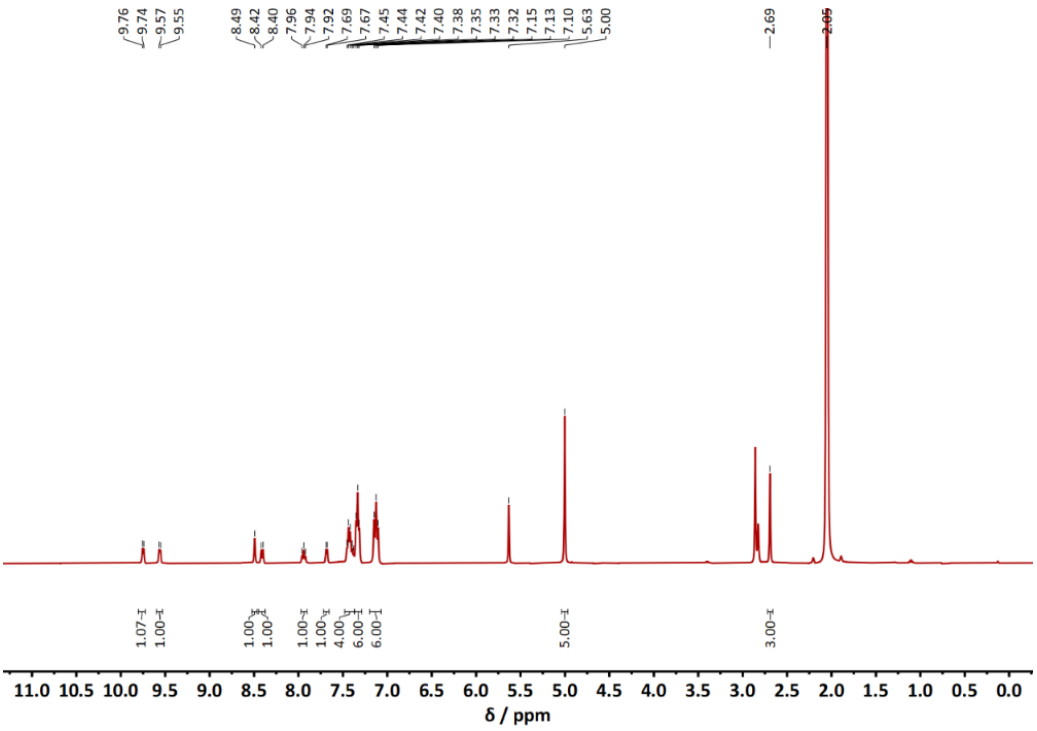


**Figure S45.** $^{1}H$ NMR spectrum of $[Ru(\eta^5\text{-}C_5H_5)(PPh_3)(AcBipy)][CF_3SO_3]$ (**7**) in $(CD_3)_2CO$.

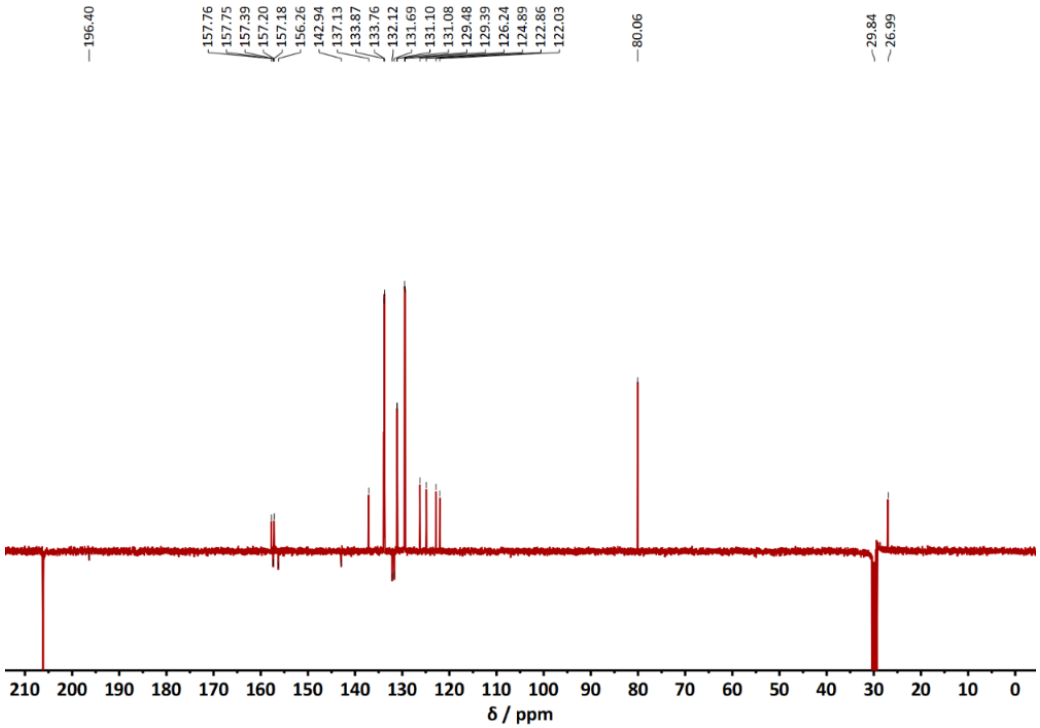


**Figure S46.** APT-$^{13}C\{^{1}H\}$ NMR spectrum of $[Ru(\eta^5\text{-}C_5H_5)(PPh_3)(AcBipy)][CF_3SO_3]$ (**7**) in $(CD_3)_2CO$.

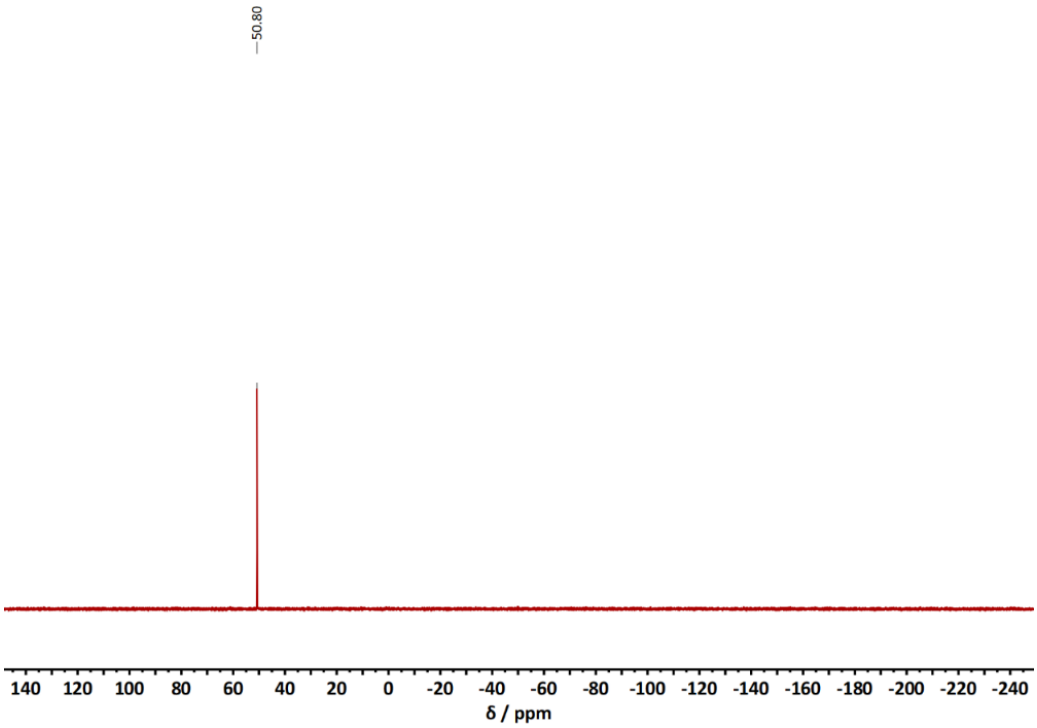


**Figure S47.** $^{31}P\{^{1}H\}$ NMR spectrum of $[Ru(\eta^5\text{-}C_5H_5)(PPh_3)(AcBipy)][CF_3SO_3]$ (**7**) in $(CD_3)_2CO$.

## FT-IR Spectra

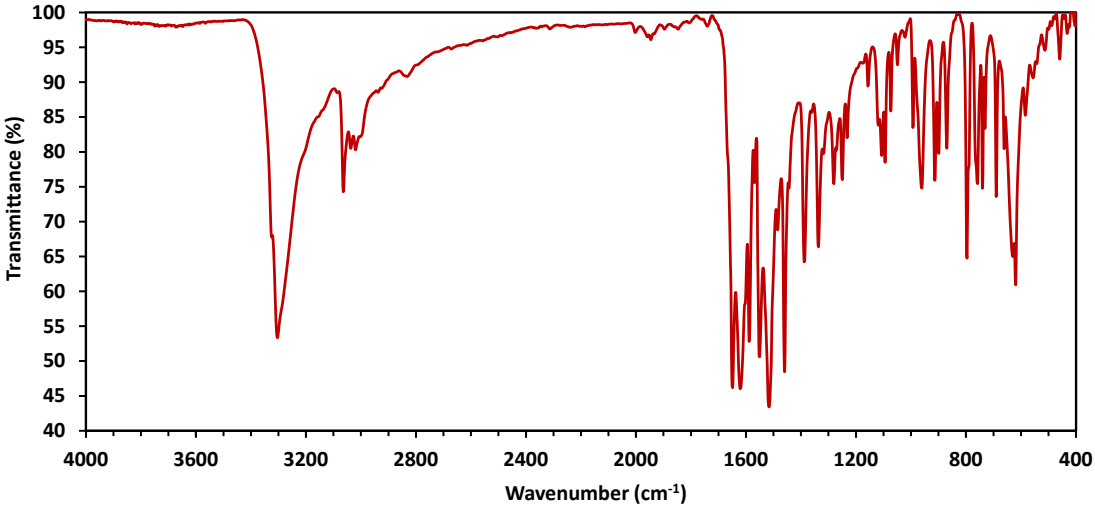


**Figure S48.** FT-IR spectrum of ethyl 2,2'-bipyridine-4-carboxylate (**BipyCONHNH2**) in KBr pellet.

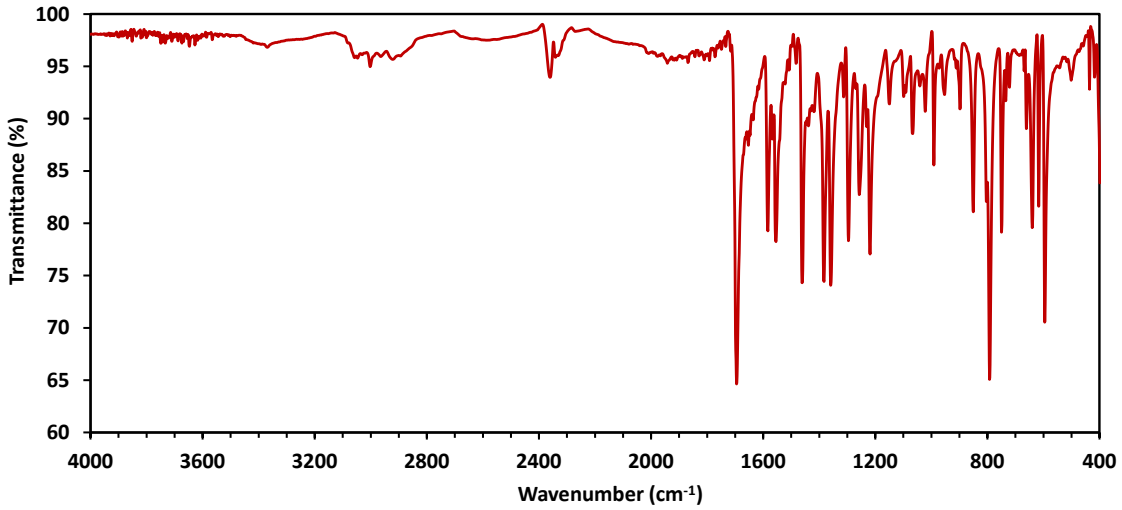


**Figure S49**. FT-IR spectrum of 2,2'-bipyridine-4-acetyl (**AcBipy**) in KBr pellet.

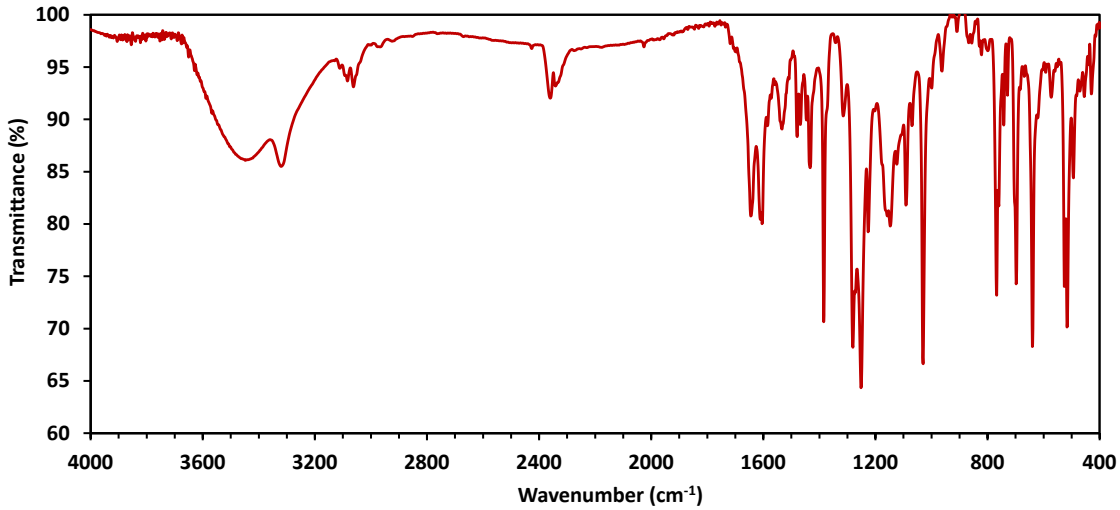


**Figure S50.** FT-IR spectrum of [Ru($\eta^5$-$C_5H_4CONHNH_2$)($PPh_3$)(2,2'-bipy)][$CF_3SO_3$] (**1**) in KBr pellet.

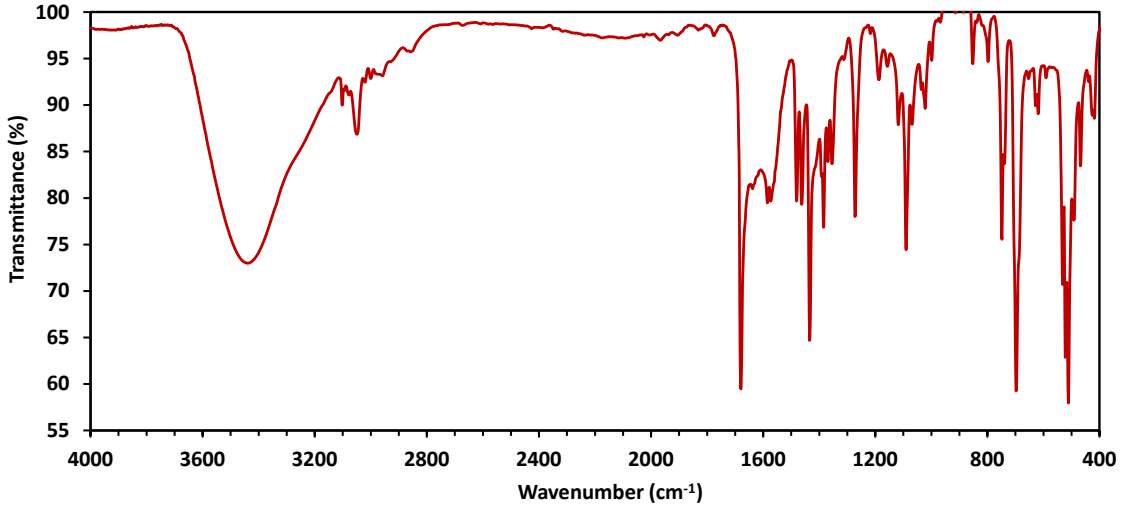


**Figure S51.** FT-IR spectrum of [Ru($\eta^5$-$C_5H_4COCH_3$)($PPh_3$)$_2$Cl] (**3**) in KBr pellet.

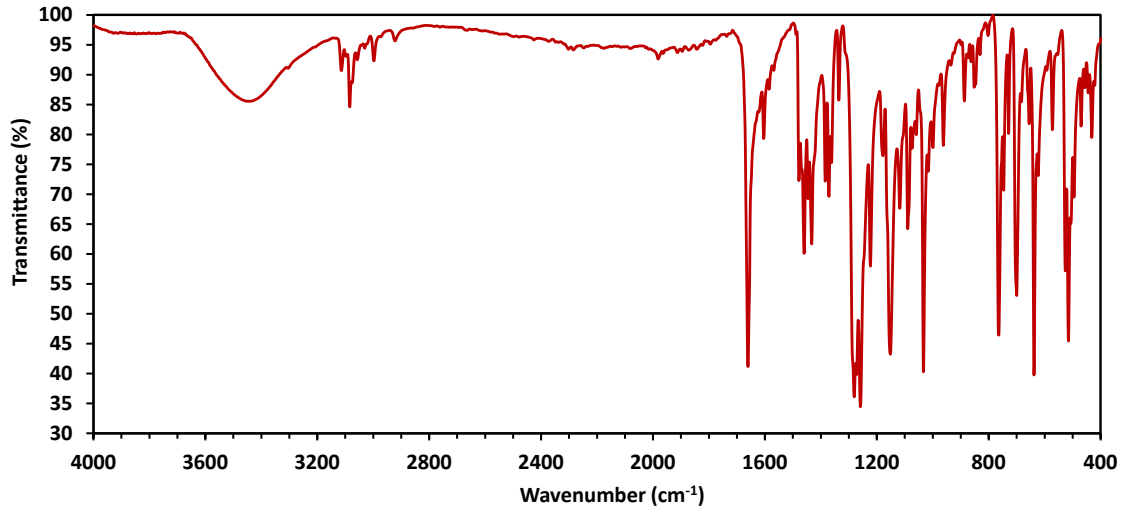


**Figure S52.** FT-IR spectrum of [Ru($\eta^5$-$C_5H_4COCH_3$)($PPh_3$)(2,2'-bipy)][$CF_3SO_3$] (**4**) in KBr pellet.

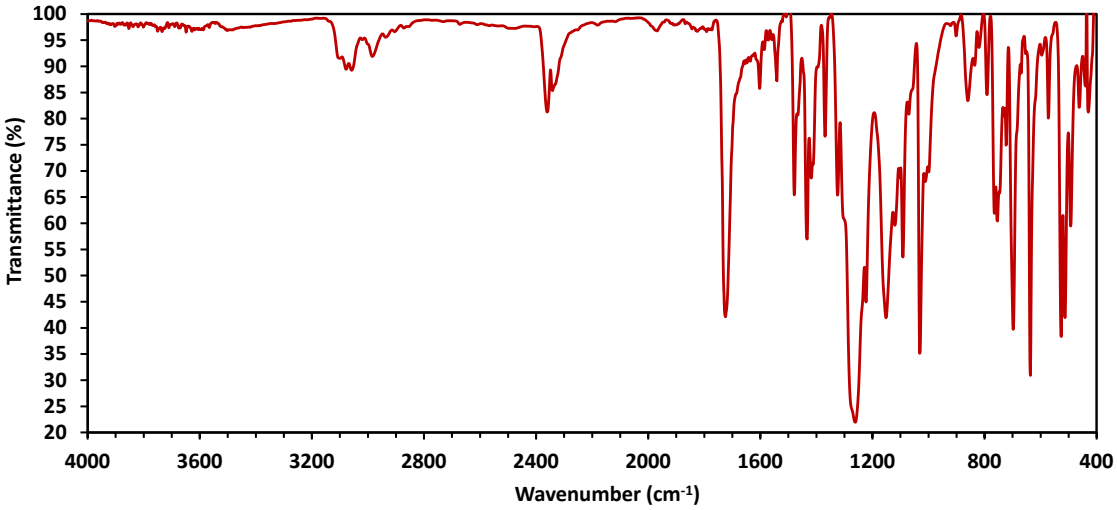


**Figure S53.** FT-IR spectrum of $[Ru(\eta^5\text{-}C_5H_5)(PPh_3)(BipyCOOEt)][CF_3SO_3]$ (**5**) in KBr pellet.

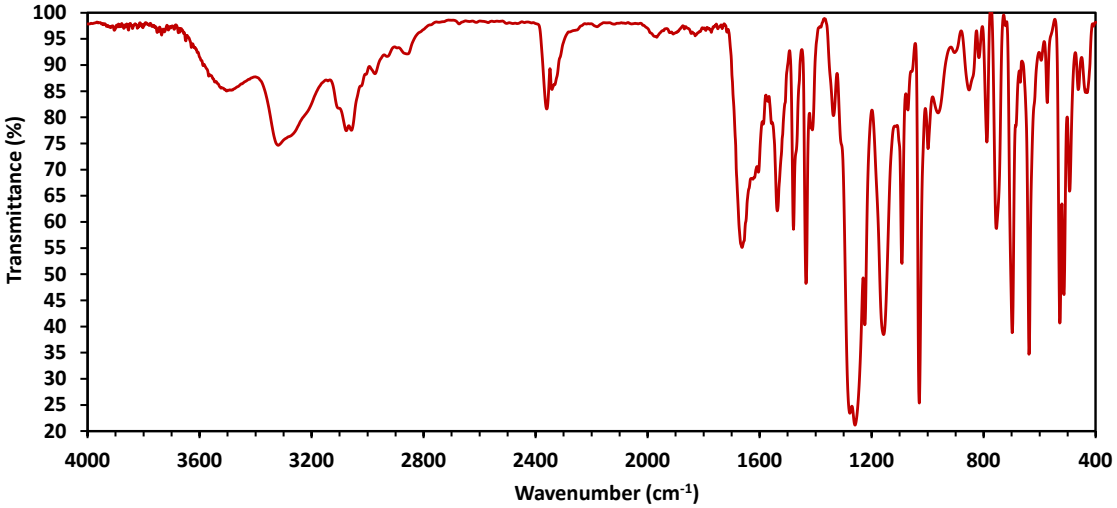


**Figure S54.** FT-IR spectrum of $[Ru(\eta^5\text{-}C_5H_5)(PPh_3)(BipyCONHNH_2)][CF_3SO_3]$ (**6**) in KBr pellet.

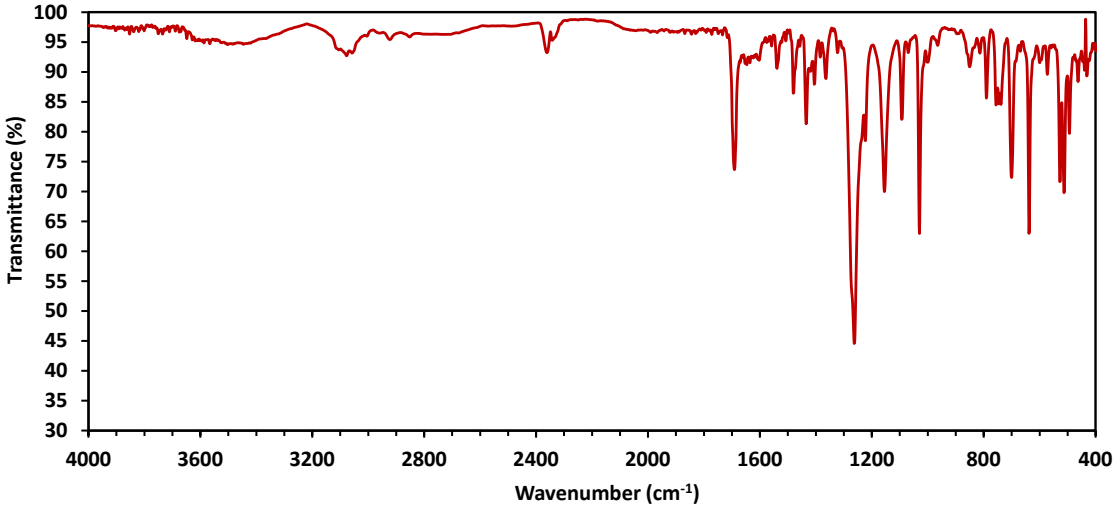


**Figure S55.** FT-IR spectrum of [Ru($\eta^5$-$C_5H_5$)($PPh_3$)(AcBipy)][$CF_3SO_3$] (**7**) in KBr pellet.

## UV-vis Spectra

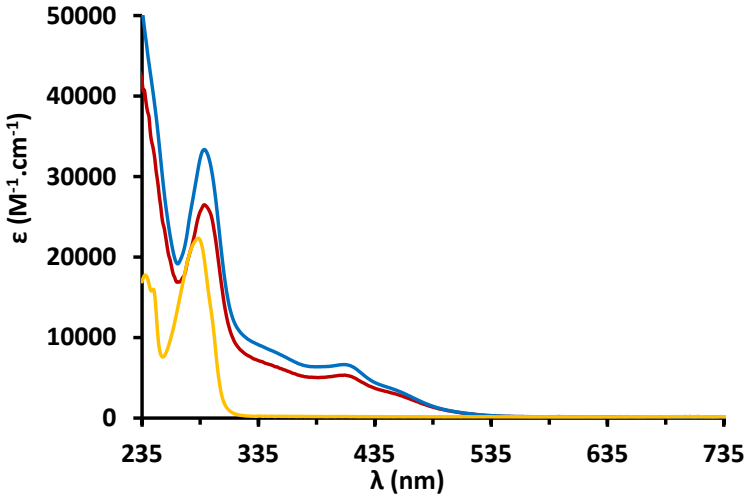


**Figure S56.** UV-vis spectra of [Ru($\eta^5$-$C_5H_4CONHNH_2$)($PPh_3$)(2,2'-bipy)][$CF_3SO_3$] (**1**, —), its precursor [Ru($\eta^5$-$C_5H_4CO_2CH_2CH_3$)($PPh_3$)(2,2'-bipy)][$CF_3SO_3$] (**TM228**, —) and free 2,2'-bipyridine (**2,2'-bipy**, —) in dichloromethane.

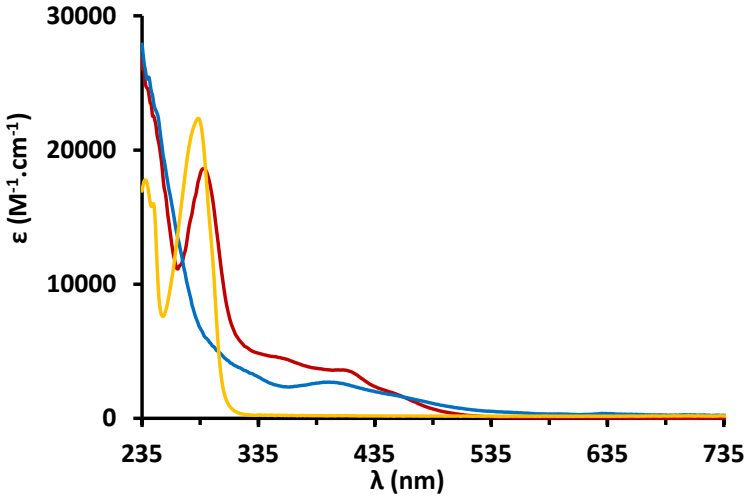


**Figure S57.** UV-vis spectra of [Ru($\eta^5$-$C_5H_4COCH_3$)($PPh_3$)(2,2'-bipy)][$CF_3SO_3$] (**4**, —), its precursor [Ru($\eta^5$-$C_5H_4COCH_3$)($PPh_3$)$_2$Cl] (**3**, —) and free 2,2'-bipyridine (**2,2'-bipy**, —) in dichloromethane.

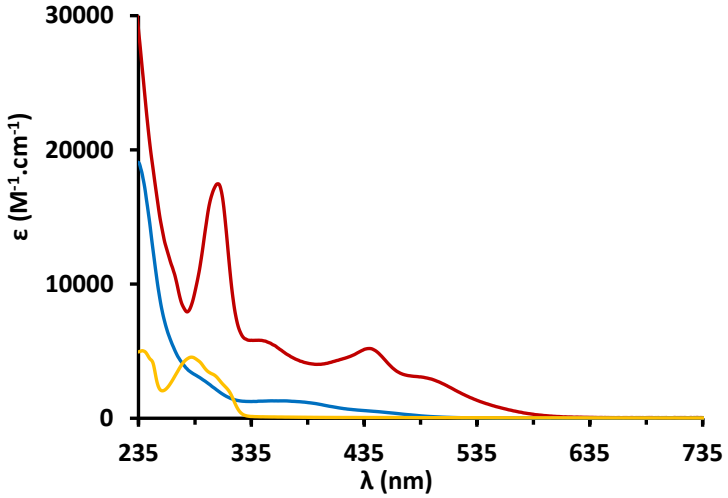


**Figure S58.** UV-vis spectra of [Ru($\eta^5$-$C_5H_5$)($PPh_3$)(BipyCOOEt)][$CF_3SO_3$] (**5**, —), its precursor [Ru($\eta^5$-$C_5H_5$)($PPh_3$)$_2$Cl)][$CF_3SO_3$] ( — ) and free ethyl 2,2'-bipyridine-4-carboxilate (**BipyCOOEt**, —) in dichloromethane.

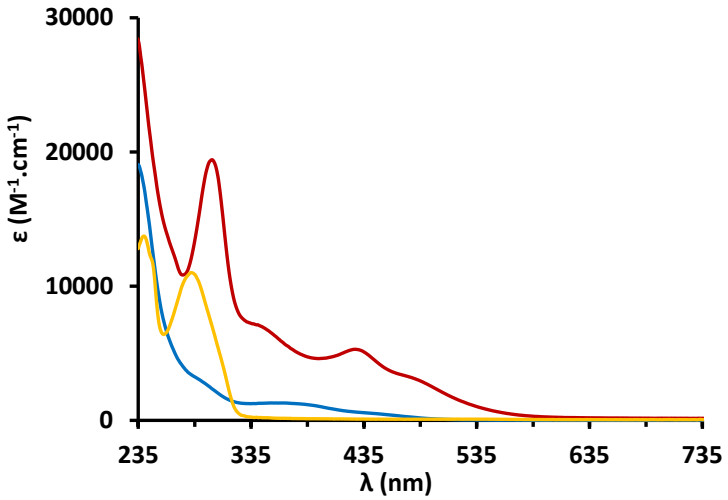


**Figure S59.** UV-vis spectra of $[Ru(\eta^5\text{-}C_5H_5)(PPh_3)(BipyCONHNH_2)][CF_3SO_3]$ (**6**, – –), its precursor $[Ru(\eta^5\text{-}C_5H_5)(PPh_3)_2Cl)][CF_3SO_3]$ (—) and free 2,2'-bipyridine-4-carbohydrazide (**BipyCONHNH$_2$**, —) in dichloromethane.

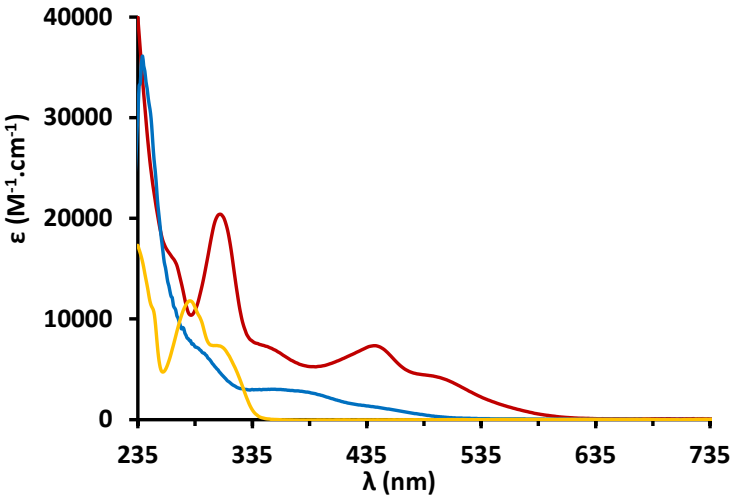


**Figure S60.** UV-vis spectra of $[Ru(\eta^5\text{-}C_5H_5)(PPh_3)(AcBipy)][CF_3SO_3]$ (**7**, —), its precursor $[Ru(\eta^5\text{-}C_5H_5)(PPh_3)_2Cl]$ (—) and free 2,2'-bipyridine-4-acetyl (**AcBipy**, —) in dichloromethane.

## Stability of Ru complexes

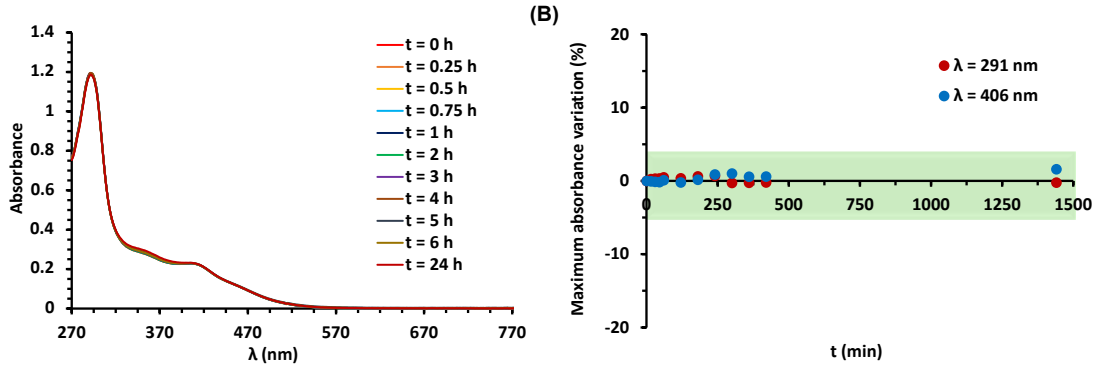


**Figure S61.** Evaluation of the stability of [Ru($\eta^5$-$C_5H_4CONHNH_2$)($PPh_3$)(2,2'-bipy)][$CF_3SO_3$] (**1**) in 100 % DMSO ($5.5\times10^{-5}$ M) over time: **(A)** electronic absorption spectra acquired over 24 h; **(B)** maximum absorbance variation (%) of π→π* (291 nm, ●) and MLCT (406 nm, ●) bands over 24 h.

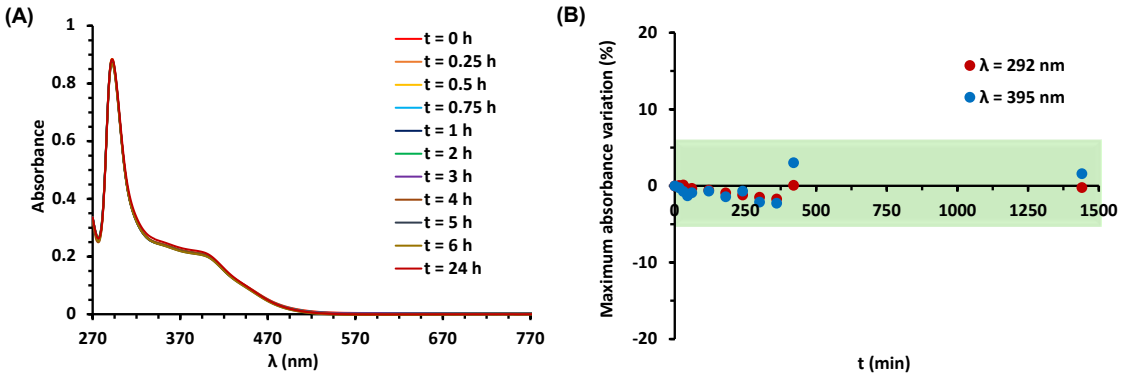


**Figure S62.** Evaluation of the stability of [Ru($\eta^5$-$C_5H_4CONHNH_2$)($PPh_3$)(2,2'-bipy)][$CF_3SO_3$] (**1**) in 95 % DMEM / 5 % DMSO ($5.4\times10^{-5}$ M) over time: **(A)** electronic absorption spectra acquired over 24 h; **(B)** maximum absorbance variation (%) of π→π* (292 nm, ●) and MLCT (395 nm, ●) bands over 24 h.

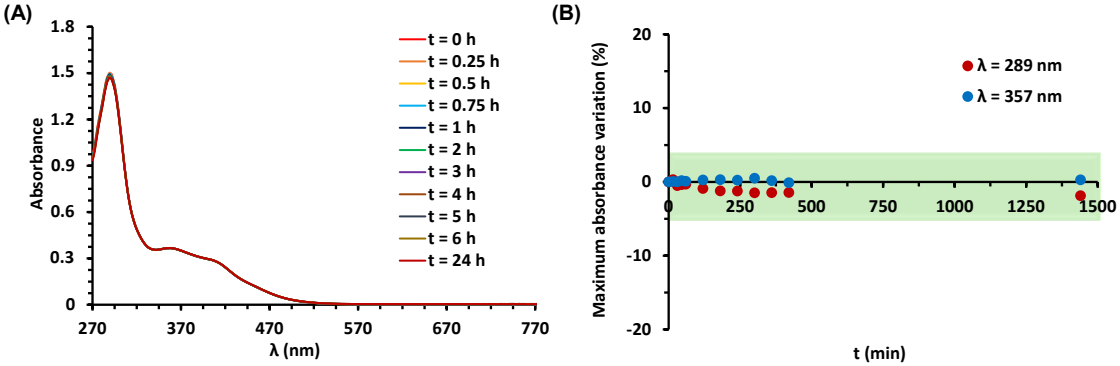


**Figure S63.** Evaluation of the stability of [Ru($\eta^5$-$C_5H_4COCH_3$)($PPh_3$)(2,2'-bipy)][$CF_3SO_3$] (**4**) in 100 % DMSO ($6.2\times10^{-5}$ M) over time: **(A)** electronic absorption spectra acquired over 24 h; **(B)** maximum absorbance variation (%) of π→π* (289 nm, ●) and MLCT (357 nm, ●) bands over 24 h.

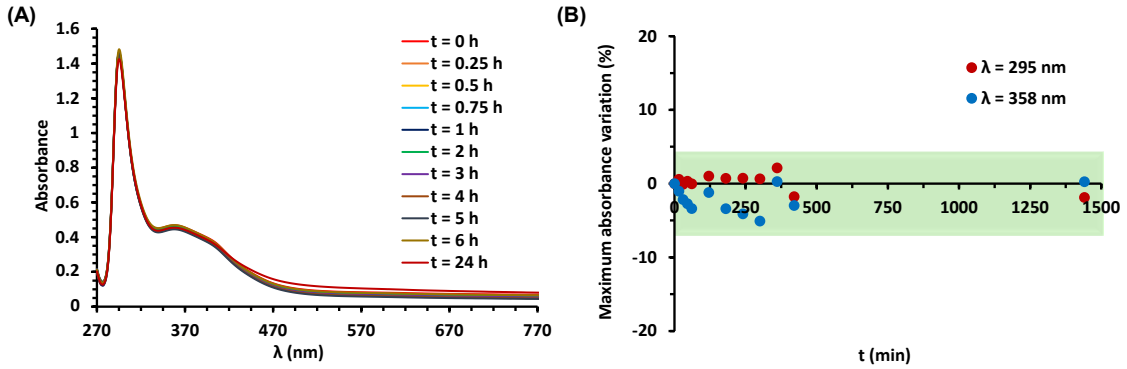


**Figure S64.** Evaluation of the stability of [Ru($\eta^5$-$C_5H_4COCH_3$)($PPh_3$)(2,2'-bipy)][$CF_3SO_3$] (**4**) in 95 % DMEM / 5 % DMSO ($5.8\times10^{-5}$ M) over time: **(A)** electronic absorption spectra acquired over 24 h; **(B)** maximum absorbance variation (%) of π→π* (295 nm, ●) and MLCT (358 nm, ●) bands over 24 h.

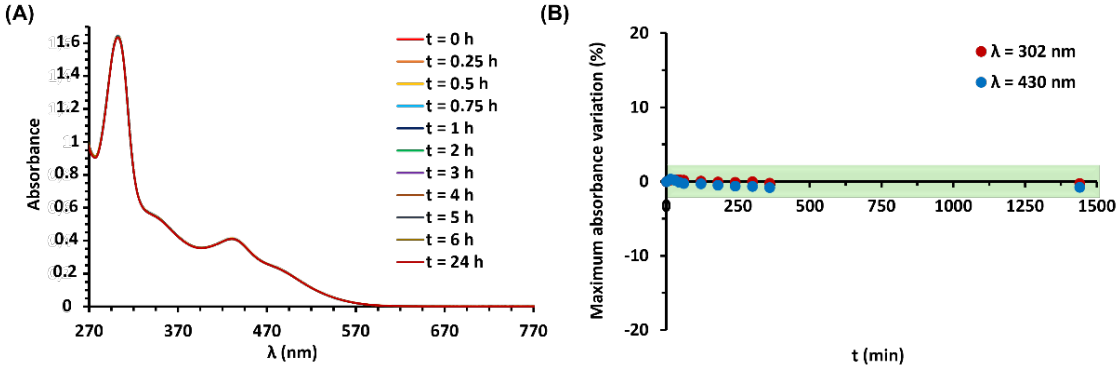


**Figure S65.** Evaluation of the stability of [Ru($\eta^5$-$C_5H_5$)($PPh_3$)(BipyCONHNH$_2$)][$CF_3SO_3$] (**6**) in 100 % DMSO ($6.9\times10^{-5}$ M) over time: **(A)** electronic absorption spectra acquired over 24 h; **(B)** maximum absorbance variation (%) of π→π* (302 nm, ●) and MLCT (430 nm, ●) bands over 24 h.

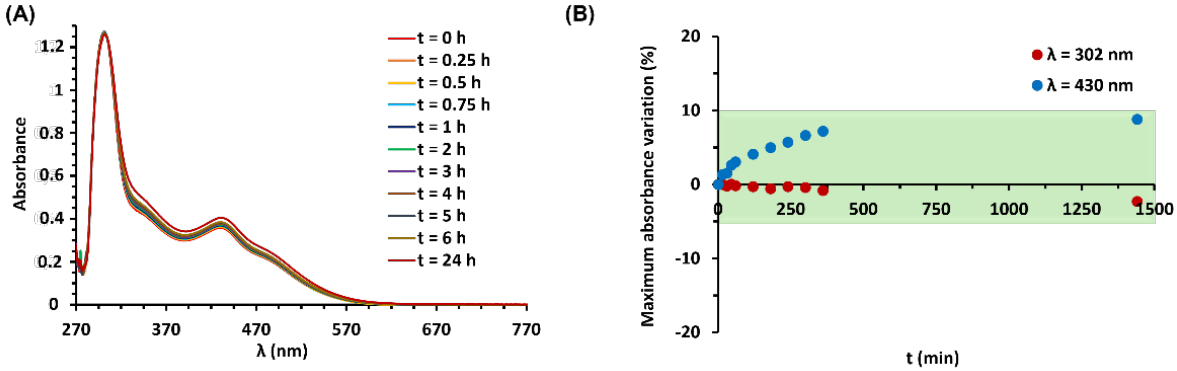


**Figure S66.** Evaluation of the stability of [Ru($\eta^5$-$C_5H_5$)($PPh_3$)(BipyCONHNH$_2$)][$CF_3SO_3$] (**6**) in 95 % DMEM / 5 % DMSO ($7.2\times10^{-5}$ M) over time: **(A)** electronic absorption spectra acquired over 24 h; **(B)** maximum absorbance variation (%) of π→π* (302 nm, ●) and MLCT (430nm, ●) bands over 24 h.

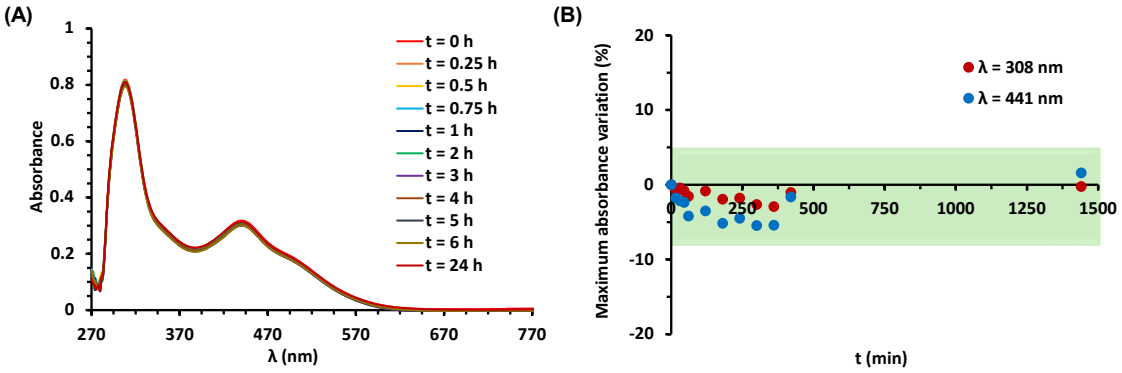


**Figure S67.** Evaluation of the stability of [Ru($\eta^5$-$C_5H_5$)($PPh_3$)(AcBipy)][$CF_3SO_3$] (**7**) in 95 % DMEM / 5 % DMSO ($6.4\times10^{-5}$ M) over time: **(A)** electronic absorption spectra acquired over 24 h; **(B)** maximum absorbance variation (%) of π→π* (308 nm, ●) and MLCT (441 nm, ●) bands over 24 h.

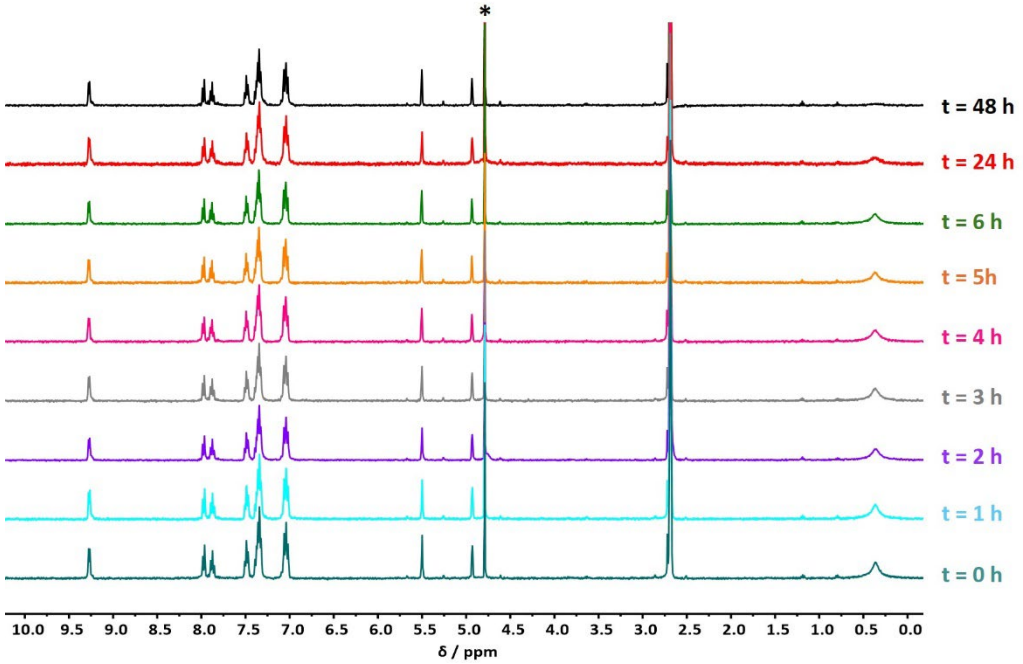


**Figure S68.** Evaluation of the stability of [Ru($\eta^5$-$C_5H_4CONHNH_2$)($PPh_3$)(2,2'-bipy)][$CF_3SO_3$] (**1**) in 80% $D_2O$/20% DMSO-$d_6$ solution over 48 h, by $^1$H NMR. (*water suppression peak)

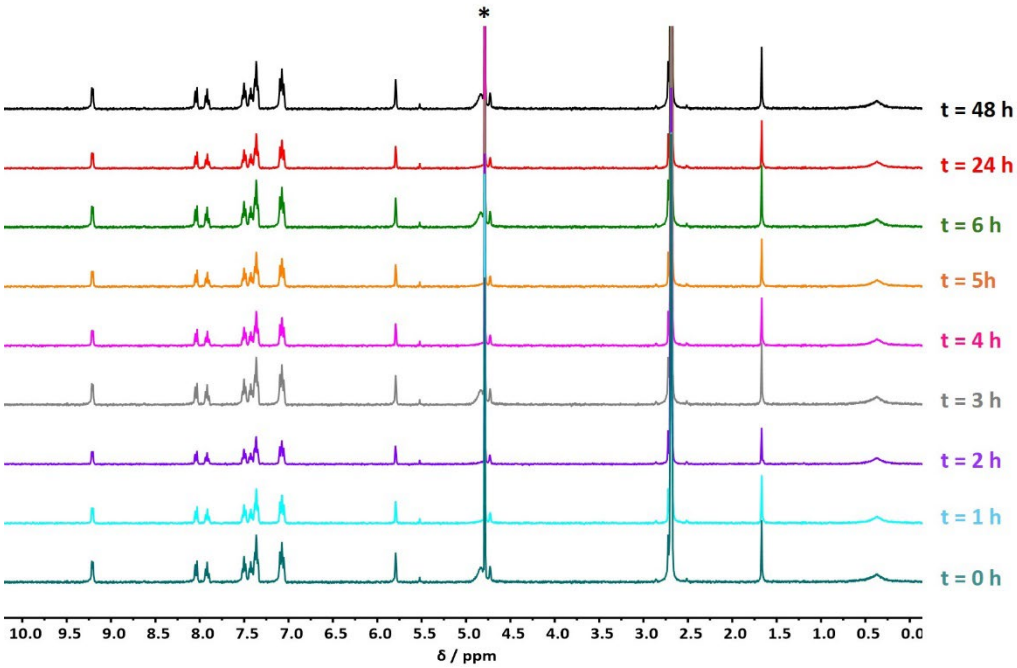


**Figure S69.** Evaluation of the stability of [Ru($\eta^5$-$C_5H_4COCH_3$)($PPh_3$)(2,2'-bipy)][$CF_3SO_3$] (**4**) in 80% $D_2O$/20% DMSO-$d_6$ solution over 48 h, by $^1$H NMR. (*water suppression peak)

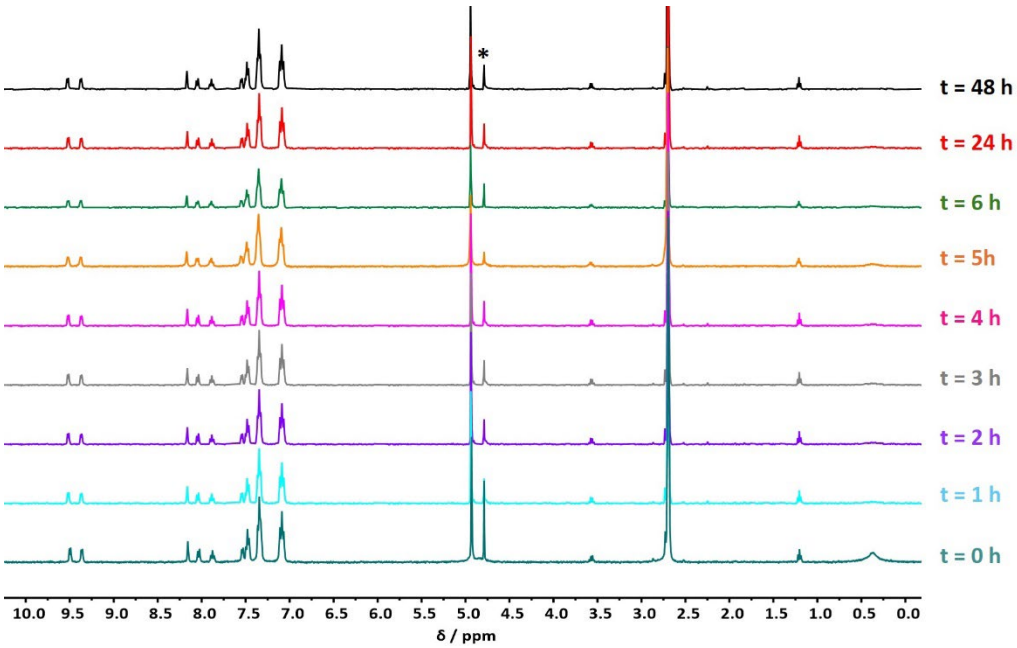


**Figure S70.** Evaluation of the stability of [Ru($\eta^5$-$C_5H_5$)($PPh_3$)(BipyCONHNH$_2$)][$CF_3SO_3$] (**6**) in 80% $D_2O$/20% DMSO-$d_6$ solution over 48 h, by $^1$H NMR. (*water suppression peak)

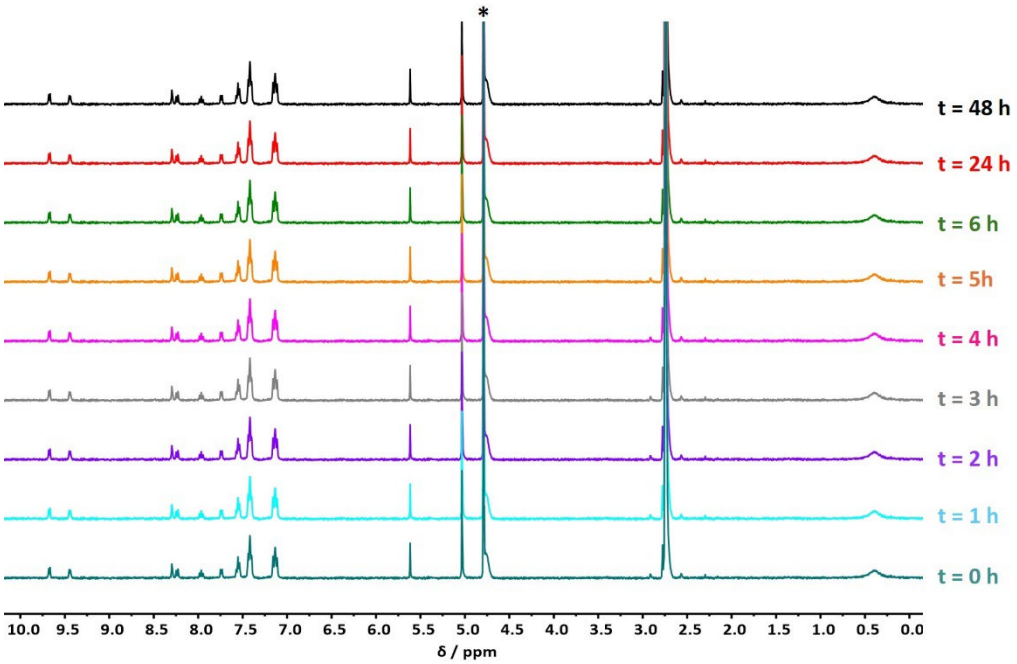


**Figure S71.** Evaluation of the stability of [Ru($\eta^5$-$C_5H_5$)($PPh_3$)(AcBipy)][$CF_3SO_3$] (**7**) in 80% $D_2O$/20% DMSO-$d_6$ solution over 48 h, by $^1H$ NMR. (*water suppression peak)

## RP-HPLC chromatograms

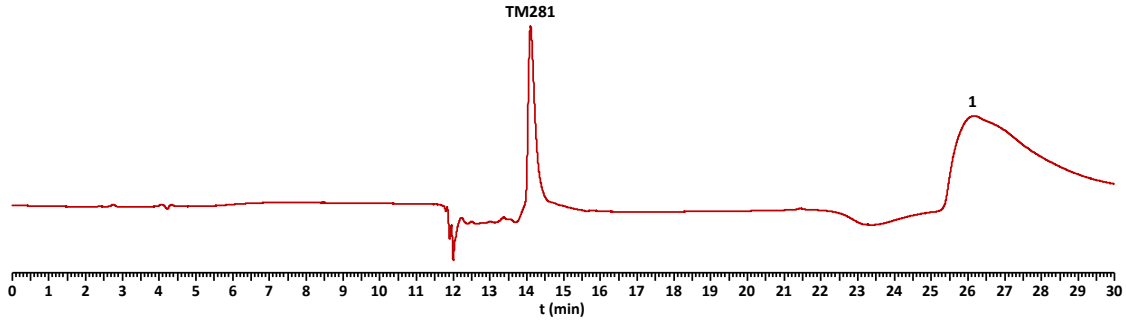


**Figure S72.** Analytical RP-HPLC chromatogram of [Ru($\eta^5$-$C_5H_4CONHNH_2$)($PPh_3$)(Bipy)][$CF_3SO_3$] (**1**) in 90 % phosphate buffer (10 mM in water, pH = 7.4) / 10 % acetonitrile, using method 3 (Table S1). **TM281** = [Ru($\eta^5$-$C_5H_4COOH$)($PPh_3$)(Bipy)][$CF_3SO_3$]

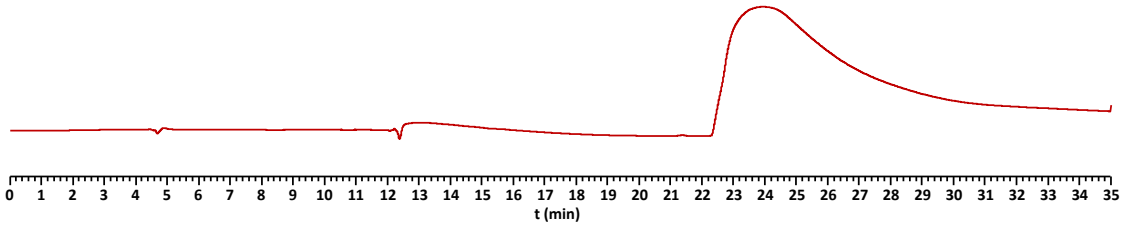


**Figure S73.** Analytical RP-HPLC chromatogram of [Ru($\eta^5$-$C_5H_4COCH_3$)($PPh_3$)(2,2'-bipy)][$CF_3SO_3$] (**4**) in 90 % phosphate buffer (10 mM in water, pH = 7.4) / 10 % acetonitrile, using method 2 (Table S1).

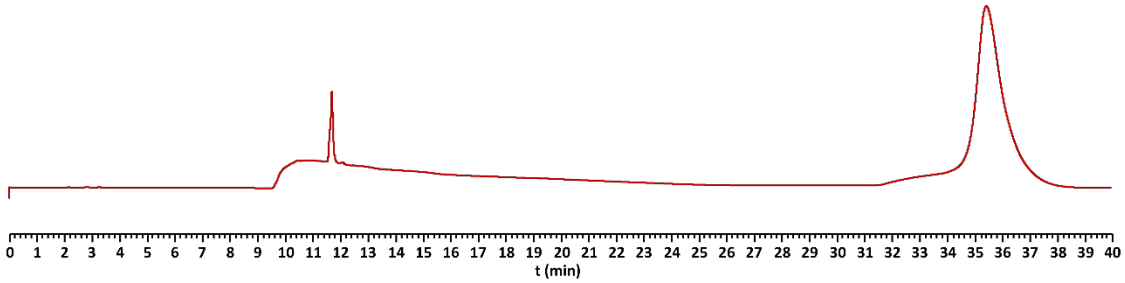


**Figure S74.** Analytical RP-HPLC chromatogram of $[Ru(\eta^5\text{-}C_5H_5)(PPh_3)(BipyCONHNH_2)][CF_3SO_3]$ (**6**) in 90 % phosphate buffer (10 mM in water, pH = 7.4) / 10 % acetonitrile, using method 3 (Table S1).

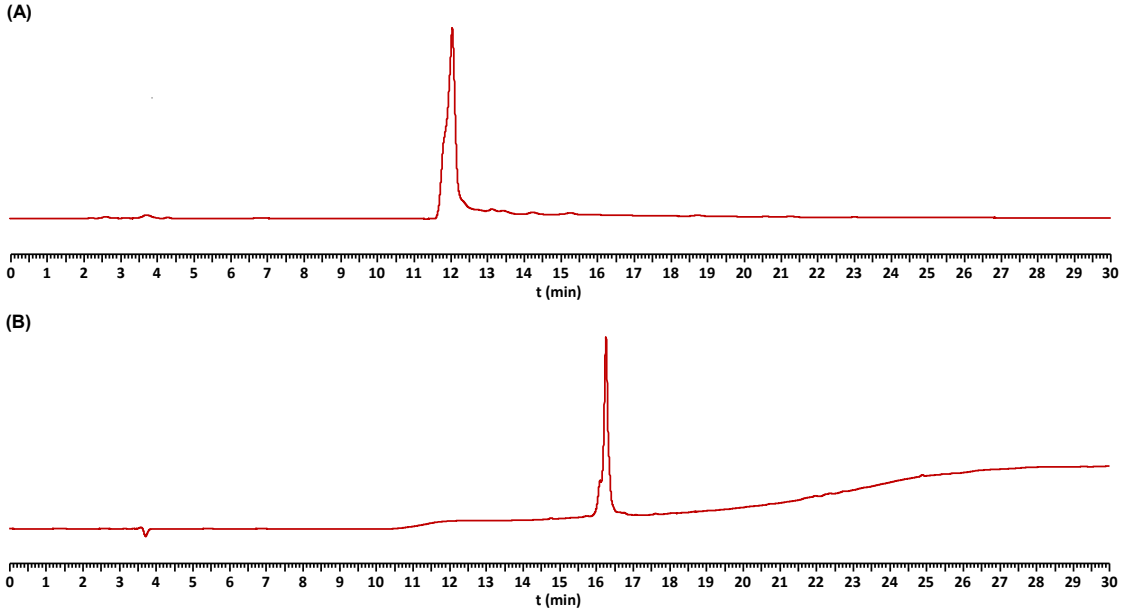


**Figure S75.** Analytical RP-HPLC chromatogram of $CH_3CO(CH_2)_2CONH\text{-}VSPPLTLGQLLS\text{-}CONH_2$ (**P1**) in **(A)** 90 % phosphate buffer (10 mM in water, pH = 7.4) / 10 % acetonitrile, using method 1 (Table S1), or **(B)** 90 % water (with 0.1 % TFA) / 10 % acetonitrile (with 0.1 % TFA), using method 5 (Table S1).

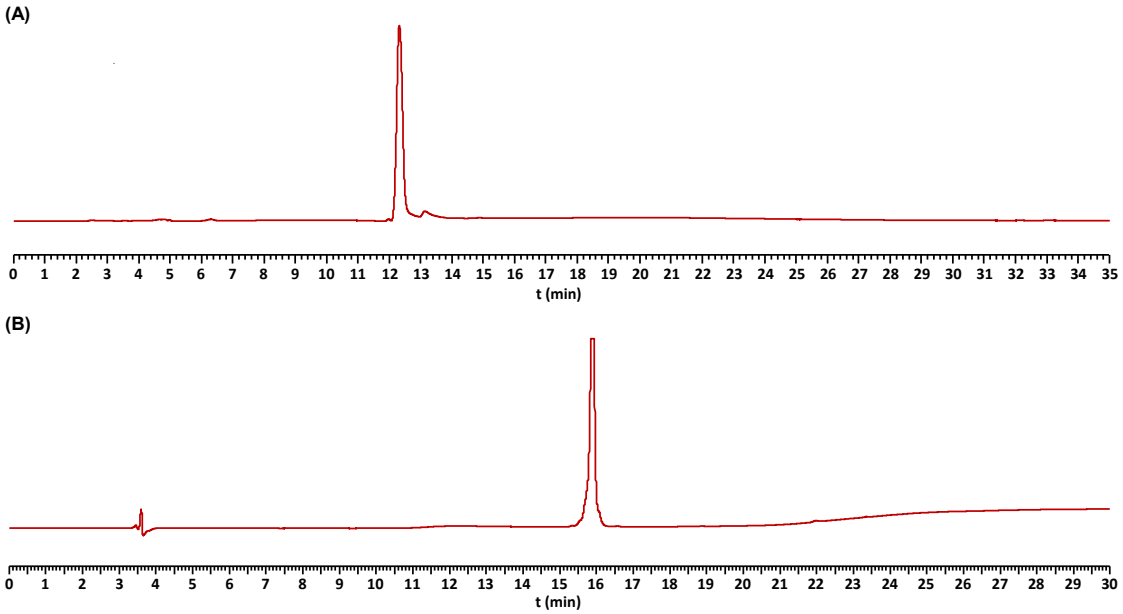


**Figure S76.** Analytical RP-HPLC chromatogram of $NH_2NHCO(CH_2)_2CONH$-VSPPLTLGQLLS-$CONH_2$ (**P2**) in **(A)** 90 % phosphate buffer (10 mM in water, pH = 7.4) / 10 % acetonitrile, using method 2 (Table S1), or **(B)** 90 % water (with 0.1 % TFA) / 10 % acetonitrile (with 0.1 % TFA), using method 5 (Table S1).

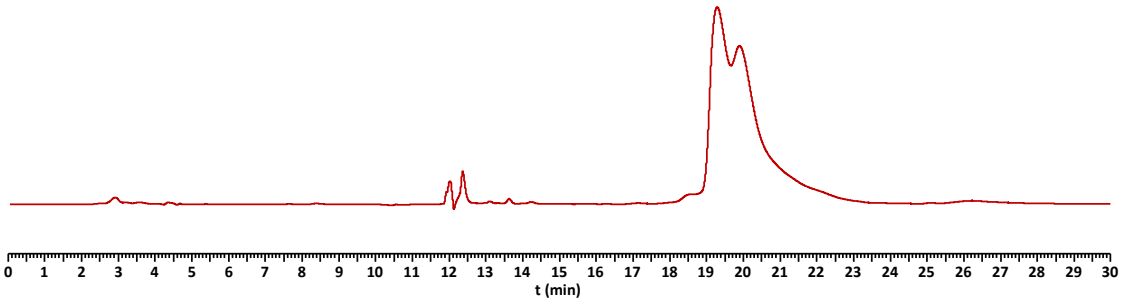


**Figure S77.** Analytical RP-HPLC chromatogram of (E,Z)-[Ru($\eta^5$-$C_5H_4R$)($PPh_3$)(2,2'-bipy)][$CF_3SO_3$], R = $CONHNC(CH_3)(CH_2)_2CONH$-VSPPLTLGQLLS-$CONH_2$ (**RuPC1**) in 90 % phosphate buffer (10 mM in water, pH = 7.4) / 10 % acetonitrile, using method 1 (Table S1).

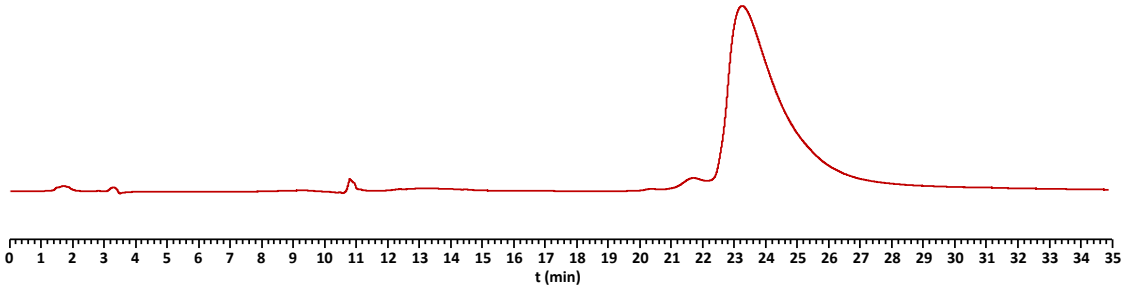


**Figure S78.** Analytical RP-HPLC chromatogram of [Ru($\eta^5$-$C_5H_4R$)($PPh_3$)(2,2'-bipy)][$CF_3SO_3$], R = $C(CH_3)NNHCO(CH_2)_2CONH$-VSPPLTLGQLLS-$CONH_2$ (**RuPC2**) in 90 % phosphate buffer (10 mM in water, pH = 7.4) / 10 % acetonitrile, using method 2 (Table S1).

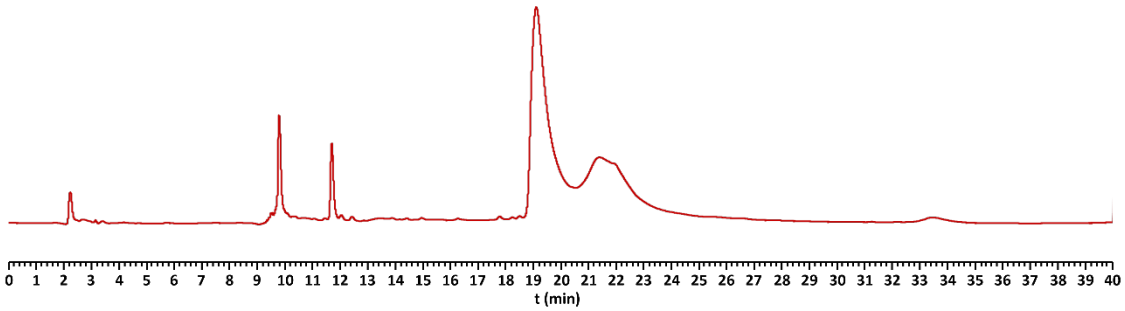


**Figure S79.** Analytical RP-HPLC chromatogram (E,Z)-[Ru($\eta^5$-$C_5H_5$)($PPh_3$)( 2,2'-bipy-R)][$CF_3SO_3$], R = $CONHNC(CH_3)(CH_2)_2CONH$-VSPPLTLGQLLS-$CONH_2$ (**RuPC3**) in 90 % phosphate buffer (10 mM in water, pH = 7.4) / 10 % acetonitrile, using method 3 (Table S1).

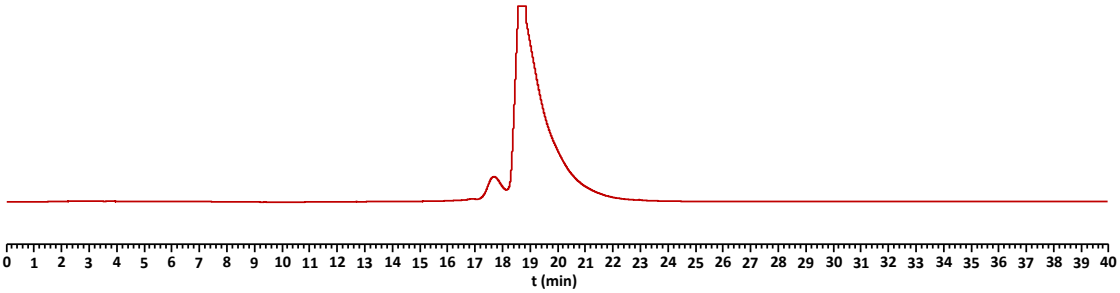


**Figure S80.** Analytical RP-HPLC chromatogram of (E,Z)-[Ru($\eta^5$-$C_5H_5$)($PPh_3$)(2,2'-bipy-R)][$CF_3SO_3$], R = $C(CH_3)NNHCO(CH_2)_2CON(H)$-VSPPLTLGQLLS-$CONH_2$ (**RuPC4**) in 90 % phosphate buffer (10 mM in water, pH = 7.4) / 10 % acetonitrile, using method 11 (Table S1).

## ESI-MS spectra

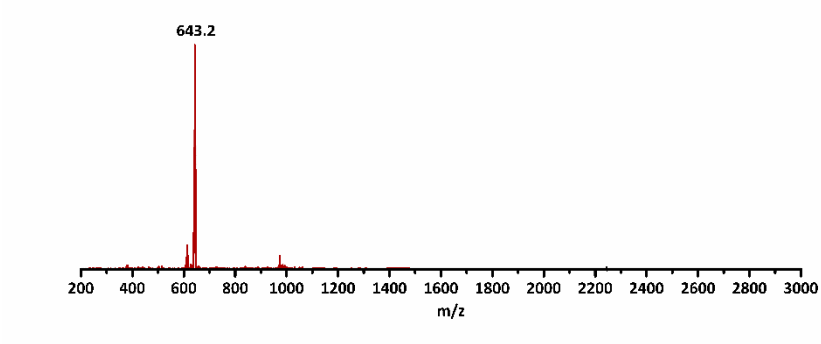


**Figure S81.** ESI-MS spectrum (positive ionization mode) of [Ru($\eta^5$-$C_5H_4CONHNH_2$)($PPh_3$)(2,2'-bipy)][$CF_3SO_3$] (**1**) in acetonitrile.

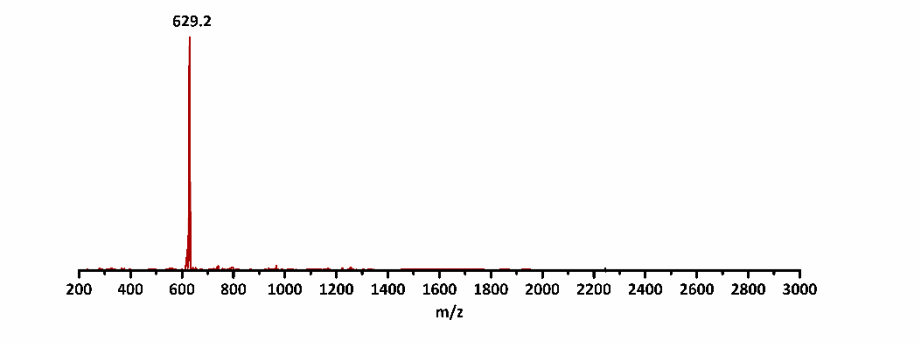


**Figure S82.** ESI-MS spectrum (positive ionization mode) of [Ru($\eta^5$-$C_5H_4COOH$)($PPh_3$)(2,2'-bipy)][$CF_3SO_3$] (**TM281**) in acetonitrile.

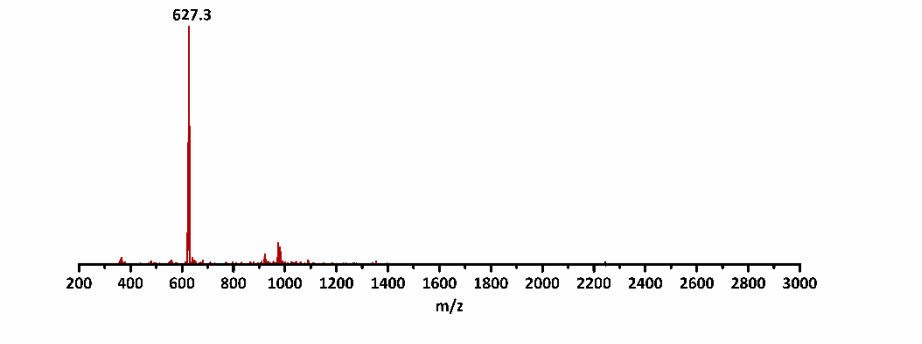


**Figure S83.** ESI-MS spectrum (positive ionization mode) of [Ru($\eta^5$-$C_5H_4COCH_3$)($PPh_3$)(2,2'-bipy)][$CF_3SO_3$] (**4**) in acetonitrile.

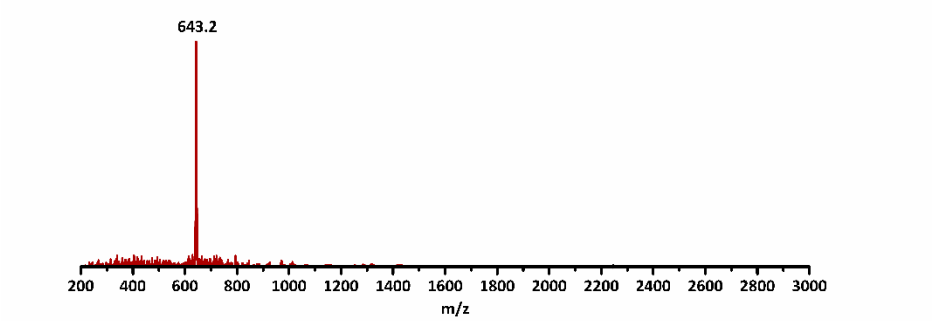


**Figure S84.** ESI-MS spectrum (positive ionization mode) of $[Ru(\eta^5\text{-}C_5H_5)(PPh_3)(BipyCONHNH_2)][CF_3SO_3]$ (**6**) in acetonitrile.

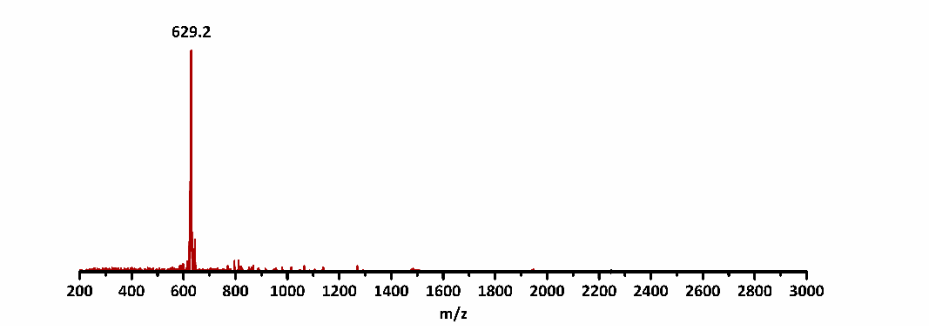


**Figure S85.** ESI-MS spectrum (positive ionization mode) $[Ru(\eta^5\text{-}C_5H_5)(PPh_3)(BipyCOOH)][CF_3SO_3]$ in acetonitrile.

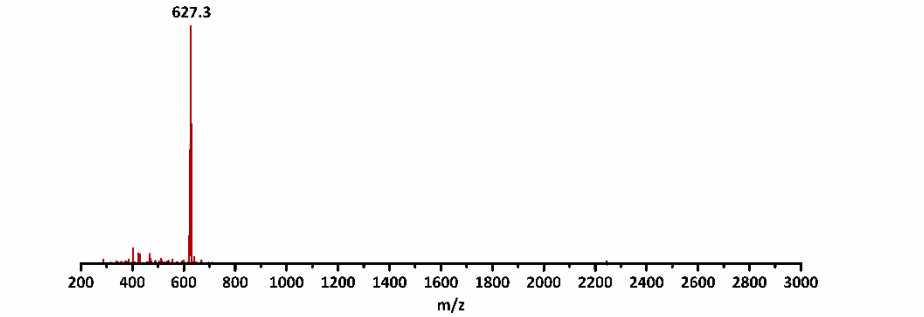


**Figure S86.** ESI-MS spectrum (positive ionization mode) of $[Ru(\eta^5\text{-}C_5H_5)(PPh_3)(AcBipy)][CF_3SO_3]$ (**7**) in acetonitrile.

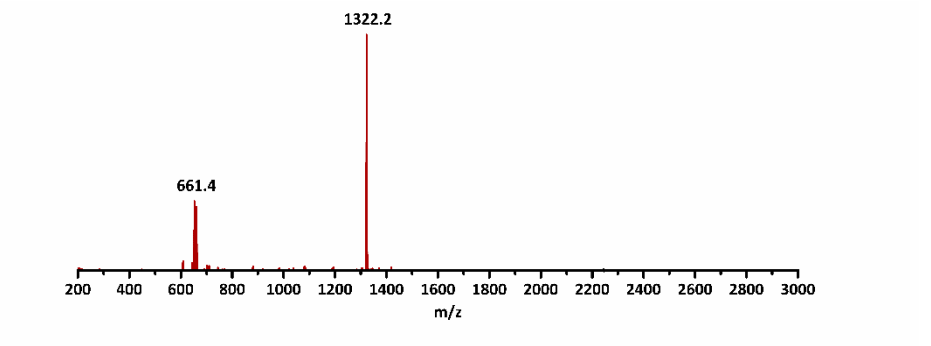


**Figure S87.** ESI-MS spectrum (positive ionization mode) of $CH_3CO(CH_2)_2CONH$-VSPPLTLGQLLS-$CONH_2$ (**P1**) in acetonitrile.

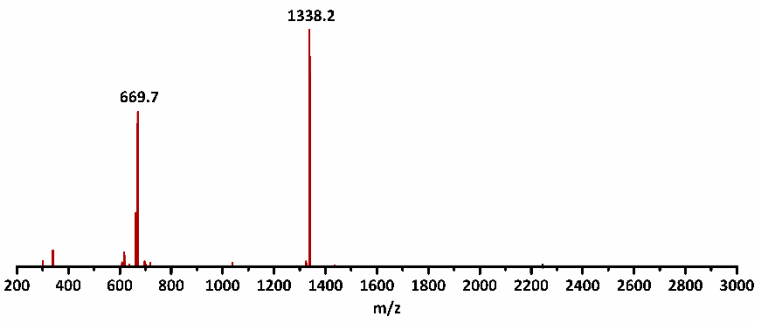


**Figure S88.** ESI-MS spectrum (positive ionization mode) of $NH_2NHCO(CH_2)_2CONH$-VSPPLTLGQLLS-$CONH_2$ (**P2**) in acetonitrile.

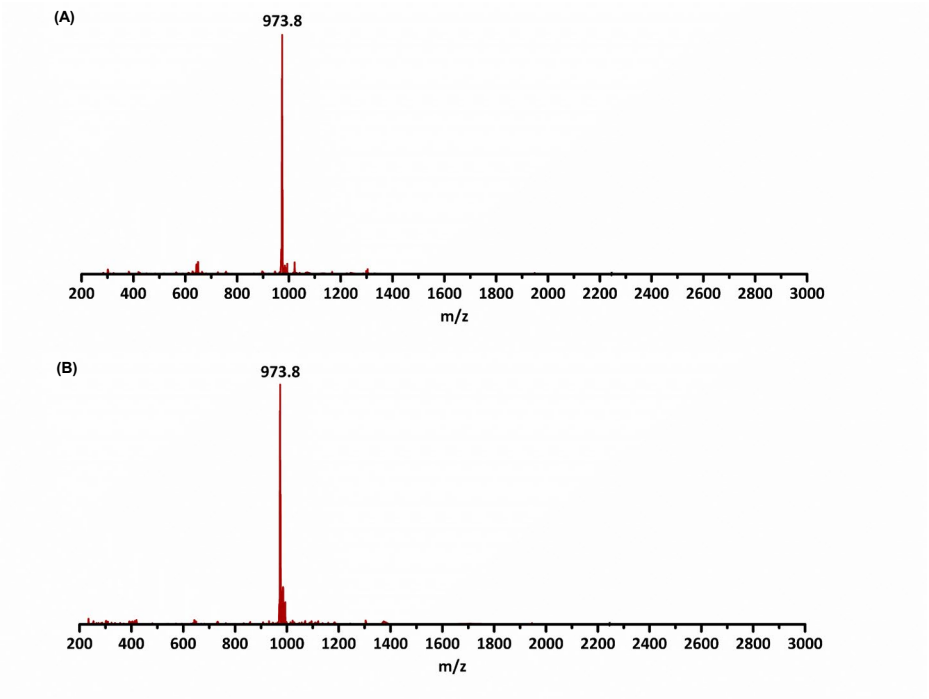


**Figure S89.** ESI-MS spectra (positive ionization mode) of the two isomers, **(A)** and **(B)**, of (E,Z)-[Ru($\eta^5$-$C_5H_4R$)($PPh_3$)(2,2'-bipy)][$CF_3SO_3$], R = $CONHNC(CH_3)(CH_2)_2CONH$-VSPPLTLGQLLS-$CONH_2$ (**RuPC1**) in acetonitrile.

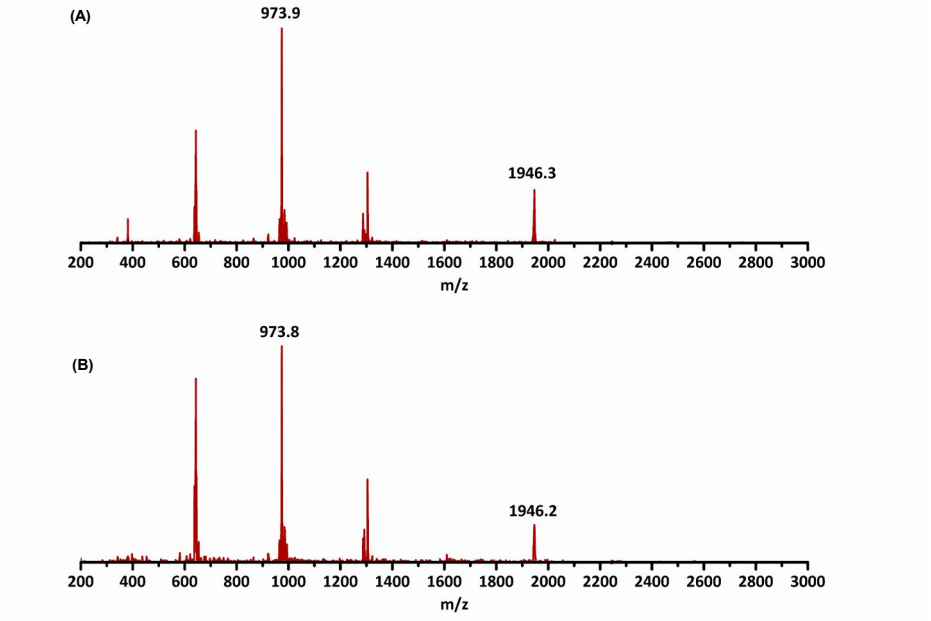


**Figure S90.** ESI-MS spectra (positive ionization mode) of the two isomers, **(A)** and **(B)**, of (E,Z)-[Ru($\eta^5$-$C_5H_5$)($PPh_3$)( 2,2'-bipy-R)][$CF_3SO_3$], R = $CONHNC(CH_3)(CH_2)_2CONH$-VSPPLTLGQLLS-$CONH_2$ (**RuPC3**) in acetonitrile.

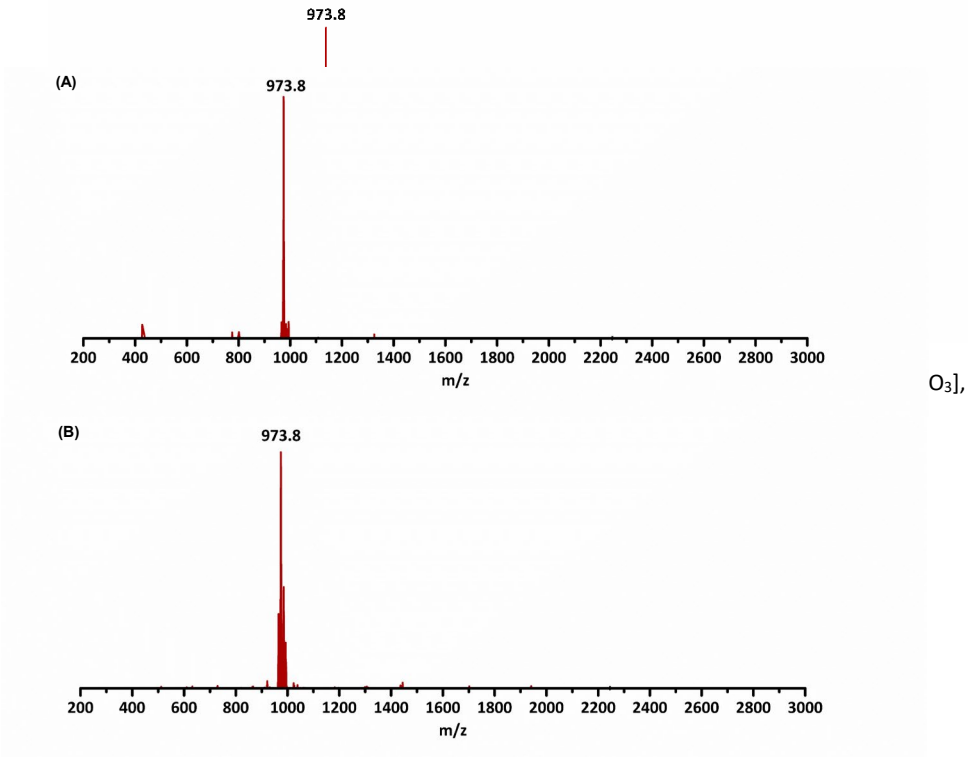


$O_3$],

**Figure S91.** ESI-MS spectrum (positive ionization mode) of the two isomers, **(A)** and **(B)**, of (E,Z)-[Ru($\eta^5$-$C_5H_5$)($PPh_3$)(2,2'-bipy-R)][$CF_3SO_3$], R = $C(CH_3)NNHCO(CH_2)_2CON(H)$-VSPPLTLGQLLS-$CONH_2$ (**RuPC4**) in acetonitrile.

**References**


84 M. I. Bruce, N. J. Windsor, *Aust J Chem* **1977**, *30*, 1601–1604.

85 J. Franco Machado, M. Machuqueiro, F. Marques, M. P. Robalo, M. F. M. Piedade, M. H. Garcia, J. D. G. Correia, T. S. Morais, *Dalton Transactions* **2020**, *49*, 5974–5987.

86 O. Kuleshova, S. Asako, L. Ilies, *ACS Catal* **2021**, *11*, 5968–5973.

87 M. P. Hay, S. Turcotte, J. U. Flanagan, M. Bonnet, D. A. Chan, P. D. Sutphin, P. Nguyen, A. J. Giaccia, W. A. Denny, *J Med Chem* **2010**, *53*, 787–797.

88 N. Mayer, M. Schweiger, E. Fuchs, A. K. Migglautsch, C. Doler, G. F. Grabner, M. Romauch, M. C. Melcher, R. Zechner, R. Zimmermann, R. Breinbauer, *Bioorg Med Chem* **2020**, *28*, 115610.

89 W. P. Hart, D. W. Macomber, M. D. Rausch, *J Am Chem Soc* **1980**, *102*, 1196–1198.

90 APEX2 v2009.3-0. Bruker AXS Inc., Madison, Wisconsin, USA, **2009**.

91 SABADS:Area-detector Absorption Correction, **2004**.

92 G. M. Sheldrick, IUCr, *Acta Crystallogr A* **2007**, *64*, 112–122.

93 G. M. Sheldrick, *Acta Crystallographica Section C* **2015**, *71*, 3–8.

94 L. J. Farrugia, *J. Appl. Cryst* **2012**, *45*, 849–854.

95 A. Berthod, S. Carda-Broch, *J Chromatogr A* **2004**, *1037*, 3–14.

96 F. Merlino, S. Tomassi, A. M. Yousif, A. Messere, L. Marinelli, P. Grieco, E. Novellino, S. Cosconati, S. Di Maro, *Org Lett* **2019**, *21*, 6378–6382.

97 R. D. M. Silva, J. F. Machado, K. Gonçalves, F. M. Lucas, S. Batista, R. Melo, T. S. Morais, J. D. G. Correia, *Molecules* **2021**, *26*, 7349.

98 E. Kaiser, R. L. Colescott, C. D. Bossinger, P. I. Cook, *Anal Biochem* **1970**, *34*, 595–598.

99 B. Chaves-Arquero, J. M. Pérez-Cañadillas, M. A. Jiménez, *Chemistry – A European Journal* **2020**, *26*, 5970–5981.

100 W. Lee, M. Tonelli, J. L. Markley, *Bioinformatics* **2015**, *31*, 1325–1327.

101 K. Wüthrich, M. Billeter, W. Braun, *J Mol Biol* **1984**, *180*, 715–740.

102 B. Chaves-Arquero, J. M. Pérez-Cañadillas, M. A. Jiménez, *Chemistry – A European Journal* **2020**, *26*, 5970–5981.

103 M. J. Frisch, G. W. Trucks, H. B. Schlegel, G. E. Scuseria, M. a. Robb, J. R. Cheeseman, G. Scalmani, V. Barone, G. a. Petersson, H. Nakatsuji, X. Li, M. Caricato, a. V Marenich, J. Bloino, B. G. Janesko, R. Gomperts, B. Mennucci, H. P. Hratchian, J. V Ortiz, a. F. Izmaylov, J. L. Sonnenberg, Williams, F. Ding, F. Lipparini, F. Egidi, J. Goings, B. Peng, A. Petrone, T. Henderson, D. Ranasinghe, V. G. Zakrzewski, J. Gao, N. Rega, G. Zheng, W. Liang, M. Hada, M. Ehara, K. Toyota, R. Fukuda, J. Hasegawa, M. Ishida, T. Nakajima, Y.

Honda, O. Kitao, H. Nakai, T. Vreven, K. Throssell, J. a. Montgomery Jr., J. E. Peralta, F. Ogliaro, M. J. Bearpark, J. J. Heyd, E. N. Brothers, K. N. Kudin, V. N. Staroverov, T. a. Keith, R. Kobayashi, J. Normand, K. Raghavachari, a. P. Rendell, J. C. Burant, S. S. Iyengar, J. Tomasi, M. Cossi, J. M. Millam, M. Klene, C. Adamo, R. Cammi, J. W. Ochterski, R. L. Martin, K. Morokuma, O. Farkas, J. B. Foresman, D. J. Fox, **2019**, Gaussian 09, Gaussian, Inc., Wallingford CT.

104 "CYLview Visualization Software," can be found under http://www.cylview.org/, **n.d.**

105 Y. Zhao, D. G. Truhlar, *Theor Chem Acc* **2008**, *120*, 215–241.

106 L. Schrödinger, *The PyMOL Molecular Graphics System, Version 2.4.* **2020**, https://pymol.org/2/.

107 K. B. Koziara, M. Stroet, A. K. Malde, A. E. Mark, *J Comput Aided Mol Des* **2014**, *28*, 221–233.

108 S. H. Vosk0, S. A. And, L. W. Ilk, M. Nusair, *Can J Phys* **1980**, *58*, 1200–1211.

109 A. D. Becke, *J Chem Phys* **1993**, *98*, 5648–5652.

110 C. Lee, W. Yang, R. G. Parr, *Phys Rev B* **1988**, *37*, 785.

111 P. C. Hariharan, J. A. Pople, *Theor Chim Acta* **1973**, *28*, 213–222.

112 M. Dolg, ; U Wedig, ; H Stoll, ; H Preuss, M. Oolg, U. Wedig, H. Stoll, H. Preuss, *J Chem Phys* **1987**, *86*, 866–872.

113 Lindahl, Abraham, Hess, van der Spoel, **2021**, DOI 10.5281/ZENODO.4457591.

114 N. Schmid, A. P. Eichenberger, A. Choutko, S. Riniker, M. Winger, A. E. Mark, W. F. Van Gunsteren, *European Biophysics Journal* **2011**, *40*, 843–856.

115 J. Hermans, H. J. C. Berendsen, W. F. Van Gunsteren, J. P. M. Postma, *Biopolymers* **1984**, *23*, 1513–1518.

116 M. Parrinello, A. Rahman, *J Appl Phys* **1981**, *52*, 7182–7190.

117 S. Nosé, M. L. Klein, *Mol Phys* **2006**, *50*, 1055–1076.

118 G. Bussi, D. Donadio, M. Parrinello, *J Chem Phys* **2007**, *126*, DOI 10.1063/1.2408420.

119 P. R. Magalhães, P. B. P. S. Reis, D. Vila-Viçosa, M. MacHuqueiro, B. L. Victor, *J Chem Inf Model* **2022**, *62*, 3034–3042.

120 B. Hess, *J Chem Theory Comput* **2008**, *4*, 116–122.

121 S. Miyamoto, P. A. Kollman, *J Comput Chem* **1992**, *13*, 952–962.

122 J. Kästner, *Wiley Interdiscip Rev Comput Mol Sci* **2011**, *1*, 932–942.

123 *MembIT Inser. Thick. Anal. Syst. with lipid bilayers* **2022**, https://github.com/mms-fcul/MembIT.

124 S. Kumar, J. M. Rosenberg, D. Bouzida, R. H. Swendsen, P. A. Kollman, *J Comput Chem* **1992**, *13*, 1011–1021.

125 R. M. Venable, A. Krämer, R. W. Pastor, *Chem Rev* **2019**, *119*, 5954.

126 C. J. Dickson, V. Hornak, R. A. Pearlstein, J. S. Duca, *J Am Chem Soc* **2017**, *139*, 442–452.

127 C. F. de Faria, T. Moreira, P. Lopes, H. Costa, J. R. Krewall, C. M. Barton, S. Santos, D. Goodwin, D. Machado, M. Viveiros, M. Machuqueiro, F. Martins, *Biomed Pharmacother* **2021**, *144*, DOI 10.1016/J.BIOPHA.2021.112362.

128 P. T. Borges, D. Silva, T. F. D. Silva, V. Brissos, M. Cañellas, M. F. Lucas, L. Masgrau, E. P. Melo, M. Machuqueiro, C. Frazão, L. O. Martins, *Comput Struct Biotechnol J* **2022**, *20*, 3899.

129 T. F. D. Silva, D. Vila-Viçosa, M. Machuqueiro, *J Chem Theory Comput* **2021**, *17*, 3830–3840.

130 J. Racine, *Journal of Applied Econometrics* **2006**, *21*, 133–141.